

TKK Dissertations 130  
Espoo 2008

**PARTIAL DISCHARGE DETECTION FOR CONDITION  
MONITORING OF COVERED-CONDUCTOR OVERHEAD  
DISTRIBUTION NETWORKS USING ROGOWSKI COIL**

Doctoral Dissertation

**Ghulam Murtaza Hashmi**



**Helsinki University of Technology  
Faculty of Electronics, Communications and Automation  
Department of Electrical Engineering**

TKK Dissertations 130  
Espoo 2008

**PARTIAL DISCHARGE DETECTION FOR CONDITION  
MONITORING OF COVERED-CONDUCTOR OVERHEAD  
DISTRIBUTION NETWORKS USING ROGOWSKI COIL**

Doctoral Dissertation

**Ghulam Murtaza Hashmi**

Dissertation for the degree of Doctor of Science in Technology to be presented with due permission of the Faculty of Electronics, Communications and Automation for public examination and debate in Auditorium S4 at Helsinki University of Technology (Espoo, Finland) on the 22nd of August, 2008, at 12 noon.

**Helsinki University of Technology  
Faculty of Electronics, Communications and Automation  
Department of Electrical Engineering**

**Teknillinen korkeakoulu  
Elektroniikan, tietoliikenteen ja automaation tiedekunta  
Sähkötekniikan laitos**

Distribution:

Helsinki University of Technology  
Faculty of Electronics, Communications and Automation  
Department of Electrical Engineering  
P.O. Box 3000  
FI - 02015 TKK  
FINLAND  
URL: <http://powersystems.tkk.fi/eng/>  
Tel. +358-9-451 5833  
Fax +358-9-451 5012  
E-mail: [murtaza.hashmi@tkk.fi](mailto:murtaza.hashmi@tkk.fi)

© 2008 Ghulam Murtaza Hashmi

ISBN 978-951-22-9446-6  
ISBN 978-951-22-9447-3 (PDF)  
ISSN 1795-2239  
ISSN 1795-4584 (PDF)  
URL: <http://lib.tkk.fi/Diss/2008/isbn9789512294473/>

TKK-DISS-2493

Picaset Oy  
Helsinki 2008



ABSTRACT OF DOCTORAL DISSERTATION		HELSINKI UNIVERSITY OF TECHNOLOGY P.O. BOX 1000, FI-02015 TKK <a href="http://www.tkk.fi">http://www.tkk.fi</a>	
Author Ghulam Murtaza Hashmi			
Name of the dissertation Partial Discharge Detection for Condition Monitoring of Covered-Conductor Overhead Distribution Networks using Rogowski Coil			
Manuscript submitted February 2008		Manuscript revised June 2008	
Date of the defense August 22, 2008			
<input checked="" type="checkbox"/> Monograph		<input type="checkbox"/> Article dissertation (summary + original articles)	
Faculty	Faculty of Electronics, Communications and Automation		
Department	Department of Electrical Engineering		
Field of research	Power Systems		
Opponent(s)	Prof. Akihiro Ametani and Prof. Dr. Ömer Usta		
Supervisor	Prof. Matti Lehtonen		
Instructor	Prof. Matti Lehtonen		
Abstract			
<p>Partial discharge (PD) is a small electrical avalanche caused by locally disrupted electric fields in dielectric materials, and is known to be one of the major factors which accelerate the degradation of electrical insulation. This thesis deals with a relatively new and challenging application of conducting on-line high frequency PD measurements for the monitoring of falling trees on covered-conductor (CC) overhead distribution lines.</p> <p>A measuring test set-up was arranged in the high voltage laboratory for real-time analysis. A pine tree was leaned against a 20 kV energized conductor and PDs were measured at different locations on the CC line using a Rogowski coil. The time domain reflectometry (TDR) measurement technique is presented to extract the frequency-dependent wave propagation characteristics (attenuation, phase constant, and propagation velocity) of CC overhead distribution lines. The theoretical modeling of the CC line based on its geometry is presented using two-wire transmission line theory and its frequency-dependent line characteristics are derived. The theoretical model is verified experimentally using TDR measurements taken on a certain length of the line.</p> <p>The entire single-phase on-line PD monitoring system including CC line and Rogowski coil is simulated in the electromagnetic transient program-alternative transient program (EMTP-ATP) simulation environment for detecting falling trees on CC overhead distribution lines. The model is confirmed by the measurement results taken in the laboratory. The model can be used to estimate the length of the CC line at which the PDs due to falling trees can be detected, thus deciding the number and positioning of the sensors over a particular length of the CC line. Moreover, the challenges in on-line condition monitoring of falling trees on CC lines using wireless sensors are also discussed. The wavelet transform technique is applied as a powerful tool to de-noise on-line PD signals, which are completely buried by electromagnetic interference.</p> <p>Automatic detection of falling trees will reduce visual inspection work after storms and it will improve the reliability and safety of the distribution system. The system can be planned to be integrated into the distribution automation system to reduce the overall costs of CC lines.</p>			
Keywords	Partial discharge, covered-conductor, distribution lines, Rogowski coil, time domain reflectometry, attenuation, EMTP-ATP, wavelet transform		
ISBN (printed)	978-951-22-9446-6	ISSN (printed)	1795-2239
ISBN (pdf)	978-951-22-9447-3	ISSN (pdf)	1795-4584
Language	English	Number of pages	xiv + 134 p.
Publisher	Helsinki University of Technology, Faculty of Electronics, Communications and Automation		
Print distribution	Helsinki University of Technology, Faculty of Electronics, Communications and Automation		
<input checked="" type="checkbox"/> The dissertation can be read at <a href="http://lib.tkk.fi/Diss/2008/isbn9789512294473/">http://lib.tkk.fi/Diss/2008/isbn9789512294473/</a>			



## Acknowledgements

The research work related to this thesis has been carried out at the Power Systems and High Voltage (HV) Laboratory, Helsinki University of Technology (TKK) during February 2005-March 2008. This work would have been impossible without the help and guidance of several people, whose contribution I would like to acknowledge.

First of all, I would like to express my deepest gratitude to my supervisor Prof. Matti Lehtonen, for accepting and giving me this wonderful research project. His supervision both helped me to channel and specify the discussed ideas and at the same time provided much appreciated freedom and support to explore new ways and concepts. His endless drive for new and better results is highly appreciated. I am very thankful to Lt. Gen. (R) Muhammad Akram Khan, Vice Chancellor, University of Engineering and Technology (UET), Lahore, Pakistan for granting me study leave to pursue doctoral research at TKK. Special thanks to Prof. Dr. Suhail A. Qureshi at UET for help and generous cooperation to deal with administrative affairs.

I wish to thank present and former members of the Power Systems and HV Laboratory at TKK for wonderful cooperation and providing a pleasant working environment. I am grateful to Mikael Nordman for his guidance and very inspiring discussions that have always been a source of encouragement. Thanks to Nagy Elkalashy and Abdelsalam Elhaffar at TKK for their valuable discussions and contributions to this work and helping with EMTP-ATP issues. I thank Petri Hyvönen for the interesting discussions on diagnostics and PD measurements. I also thank Veli-Matti Niiranen for his readiness to rectify problems related to measuring instruments. Many thanks to Hannu Kokkola for arranging testing facilities at the laboratory. Special thanks to Uupa Laakkonen and Pirjo Heine for being extremely helpful in academic and other financial matters. I also acknowledge the language corrections made by Bridget Emery and John Millar.

I am very grateful to the pre-examiners of this doctoral dissertation, Prof. Abdel-Maksoud Taalab and Prof. Dr. Ömer Usta, for their valuable comments and corrections.

Any research work conducted is not possible without financial assistance. The financial support from the Power Systems and HV Laboratory at TKK, Fortumin Säätiö, Higher Education Commission (HEC) in Pakistan, Emil Aaltosen Säätiö, and the Graduate School of Electrical Engineering (GSEE) are gratefully acknowledged.

Finally and most significantly, my deepest gratitude goes to my beloved dear mother, who bore immense difficulties to educate her children at the highest level (may Allah keep her soul in eternal peace). Many thanks to my wife Faiqa, who has been a pillar of support and comfort during this hard time. The affection and love of my son Irtaza and especially daughter Sajal are deeply appreciated. They have brought happiness and joy to my life and made this task much easier. Many thanks to my father, sisters and brother, whose love, though from the distance, has supported me throughout this time.

Ghulam Murtaza Hashmi  
Espoo, August 2008.



## List of Publications

The author has published the following articles during his research work:

- [1] G. M. Hashmi, M. Nordman, and M. Lehtonen, "A Partial Discharge Detection Concept for Wireless Sensors in Covered-Conductors Distribution System", *Europe's Premier Conference on Electrical Insulation (INSUCON2006)*, Birmingham, UK, May 24-26, 2006.
- [2] G. M. Hashmi, M. Nordman, and M. Lehtonen, "Determination of the Wave Propagation Characteristics of Covered-Conductors Distribution System for On-line Partial Discharge Detection", *Modern Electric Power Systems (MEPS06) Conference*, Wroclaw, Poland, September 6-8, 2006.
- [3] G. M. Hashmi, M. Lehtonen, and M. Nordman, "Application of Wavelet Transform to De-noise Partial Discharge Signals in Covered-Conductor Distribution Networks", *XVI-th International Conference on Electromagnetic Disturbances (EMD06)*, Kaunas, Lithuania, September 27-29, 2006.
- [4] G. M. Hashmi, R. Papazyan, and M. Lehtonen, "Comparing Wave Propagation Characteristics of MV XLPE Cable and Covered-Conductor Overhead Line using Time Domain Reflectometry Technique" *IEEE International Conference on Electrical Engineering (ICEE07)*, University of Engineering and Technology (UET), Lahore, Pakistan, April 11-12, 2007.
- [5] G. M. Hashmi, M. Lehtonen, and A. Elhaffar, "Modeling of Rogowski Coil for On-line PD Monitoring in Covered-Conductor Overhead Distribution Networks", *19<sup>th</sup> International Conference on Electricity Distribution (CIRED07)*, Vienna, Austria, May 21-24, 2007.
- [6] G. M. Hashmi and M. Lehtonen, "On-line PD Measuring System Modeling and Experimental Verification for Covered-Conductor Overhead Distribution Lines", *IEEE Mediterranean Conference on Control and Automation (MED07)*, Athens, Greece, June 27-29, 2007.
- [7] G. M. Hashmi and M. Lehtonen, "Covered-Conductor Overhead Distribution Line Modeling and Experimental Verification for Determining its Line Characteristics", *IEEE PES PowerAfrica2007 Conference and Exposition*, Johannesburg, South Africa, July 16-20, 2007.
- [8] G. M. Hashmi and M. Lehtonen, "On-line PD Detection for Condition Monitoring of Covered-Conductor Overhead Distribution Networks – A Literature Survey", *IEEE International Conference on Electrical Engineering (ICEE08)*, University of Engineering and Technology (UET), Lahore, Pakistan, March 25-26, 2008.
- [9] G. M. Hashmi and M. Lehtonen, "Effects of Rogowski Coil and Covered-Conductor Parameters on the Performance of PD Measurements in Overhead Distribution Networks", *16<sup>th</sup> Power Systems Computation Conference (PSCC08)*, Glasgow, UK, July 14-18, 2008.



## List of Symbols

Symbol	Description	Units
$\omega$	Angular velocity of signal	rad/s
$\alpha$	Attenuation constant	Np/m
$\beta$	Phase constant	rad/s
$\gamma$	Propagation constant	1/m
$\Gamma$	Reflection coefficient	-
$\mu_0$	Permeability of free space	H/m
$\mu_{al}$	Permeability of aluminum	H/m
$\sigma_{air}$	Conductivity of air	1/ $\Omega$ m
$\sigma_{al}$	Conductivity of aluminum	1/ $\Omega$ m
$\rho_{al}$	Resistivity of aluminum	$\Omega$ m
$\rho_c$	Resistivity of copper	$\Omega$ m
$\epsilon_c$	Permittivity of conductor insulating material	F/m
$\sigma_g$	Ground conductivity	1/ $\Omega$ m
$\epsilon_0$	Permittivity of free space (or air)	F/m
$ q_1(t) $	Absolute value of charge at point P <sub>1</sub>	C
$ q_2(t) $	Absolute value of charge at point P <sub>2</sub>	C
$ q_c(t) $	Absolute value of actual charge produced by pulse calibrator	C
$ q_T(t) $	Absolute value of charge at point P <sub>T</sub>	C
$\epsilon_{rc}$	Relative permittivity of conductor insulating material	-
$\epsilon_{rg}$	Relative permittivity of ground	-
$\Delta T$	Time step/Sampling time	s
$C$	Capacitance per-unit length	F/m
$C_{air}$	Air gap capacitance between surface of tree and conductor-cover	F
$C_d$	Distributed capacitance of Rogowski coil	F/m
$C_{ins}$	Covered-conductor insulation capacitance	F
$C_l$	Lumped capacitance of Rogowski coil	F
$D$	Height of CC above ground level	m
$d_1$	Internal diameter of Rogowski coil	m
$d_2$	External diameter of Rogowski coil	m
$D_e$	Electric flux density in conductor	C/m <sup>2</sup>
$d_{rc}$	Net diameter of Rogowski coil	m
$E_a$	Electric field inside conductor insulation	V/m
$E_c$	Electric field inside cavity	V/m
$f$	Frequency of propagated signal	Hz
$G$	Shunt conductance per-unit length	1/ $\Omega$ m
$H$	Sensitivity of Rogowski coil	V/A
$H(f)$	Transfer function, frequency domain	-
$h(t)$	Impulse response, time domain	-

<b>Symbol</b>	<b>Description</b>	<b>Units</b>
$h_C$	Penetration depth in conductor-core	m
$i(t)$	Current flowing in conductor-core	A
$l$	Length of CC line	m
$L$	Inductance per-unit length	H/m
$L_d$	Distributed inductance of Rogowski coil	H/m
$L_l$	Lumped inductance of Rogowski coil	H
$M$	Mutual inductance of Rogowski coil	H
$N$	Record depth/Number of acquired measurement points	-
$N_{rc}$	Number of turns of Rogowski coil	-
$q$	Magnitude of charge in leads of sample (apparent charge)	C
$q_1$	Magnitude of charge transferred in cavity	C
$R$	Series resistance per-unit length	$\Omega/m$
$R_C$	Radius of aluminum conductor-core	m
$R_{CC}$	Radius of CC line with insulated cover	m
$R_d$	Distributed resistance of Rogowski coil	$\Omega/m$
$R_l$	Lumped resistance of Rogowski coil	$\Omega$
$s$	Laplace variable	-
$S$	Cross-sectional area of conductor-core	$m^2$
$T$	Transmission coefficient	-
$\tan\Delta$	The loss tangent	-
$v$	Propagation velocity of signal	m/s
$v_1(t)$	Rogowski coil measured voltage at $P_1$	V
$v_2(t)$	Rogowski coil measured voltage at $P_2$	V
$v_{out}(t)$	Output voltage of Rogowski coil	V
$v_{rc}(t)$	Voltage induced in Rogowski coil	V
$Y$	Shunt conductance per-unit length	S/m
$Z$	Series impedance per-unit length	$\Omega/m$
$Z_0$	Characteristic impedance of CC line	$\Omega$
$Z_e$	External impedance of CC line	$\Omega$
$Z_g$	Ground-return path impedance	$\Omega$
$Z_i$	Internal impedance of covered-conductor	$\Omega$
$Z_L$	Load impedance	$\Omega$
$Z_{out}$	Terminating impedance of Rogowski coil	$\Omega$

## List of Acronyms

A/D	Analogue-to-digital
ABB	Asea Brown Boveri
AC	Alternating current
AM	Amplitude modulation
APD	Arc protection device
ATP	Alternative transient program
BLX	Belagt Linesystem (abbreviation used in Sweden and Norway for covered-conductor line insulated with XLPE)
CC	Covered-conductor
CT	Current transformer
CWT	Continuous wavelet transform
$D_1$ - $D_8$	DWT reconstructed detail levels 1, 2, ..., 8, respectively
DC	Direct current
DFT	Discrete Fourier transform
DSI	Discrete spectral interference
DSP	Digital signal processing
DUT	Device under test
DWT	Discrete wavelet transform
EMD	Electromagnetic disturbances
EMI	Electromagnetic interference
EMTP	Electromagnetic transient program
FFT	Fast Fourier transform
FIR	Finite impulse response
FM	Frequency modulation
GIS	Gas-insulated switchgear
HDPE	High density polyethylene
HV	High voltage
IDWT	Inverse discrete wavelet transform
IEC	International Electrotechnical Commission
IIR	Infinite impulse response
MSD	Multi-resolution signal decomposition
MV	Medium voltage
PAD	Power arc device
PAS	Päällystetty avojohto suurjännitteelle (abbreviation for a covered-conductor line in Finland)
PD	Partial discharge
PLC	Power line communications
PVC	Polyvinyl chloride
SAX	Trademark of Prysmian cables and systems for covered-conductor
SF <sub>6</sub>	Sulfur hexafluoride
SNR	Signal to noise ratio
SWR	Standing wave ratio

TDR	Time domain reflectometry
TKK	Helsinki University of Technology
TL	Transmission line
UK	United Kingdom
WT	Wavelet transform
XLPE	Cross-linked polyethylene

# Table of Contents

<b>1 Introduction.....</b>	<b>1</b>
1.1 Background.....	1
1.2 Problem statement.....	2
1.3 Major contributions.....	4
1.4 Organization of thesis.....	5
<b>2 Using CC Overhead Lines in Distribution Networks.....</b>	<b>7</b>
2.1 History of CC lines – a Scandinavian experience.....	7
2.2 Geometry of overhead covered-conductor.....	8
2.3 Covered-conductor overhead system representation.....	8
2.4 Tree leaning experiments and tests.....	11
2.4.1 Mechanical tests performance.....	11
2.4.2 Electrical tests performance.....	13
2.5 Equivalent circuit of a leaning tree on CC line.....	13
2.6 Objectives and challenges posed by CC system.....	15
2.7 Discussion.....	16
<b>3 On-line PD Detection in CC Overhead Distribution Networks.....</b>	<b>17</b>
3.1 Basic concepts.....	17
3.1.1 What is partial discharge (PD)?.....	17
3.1.2 Understanding initiation of PD signals.....	19
3.1.3 Quantities related to PD magnitude.....	21
3.1.4 PD signal characteristics.....	22
3.2 Conventional PD detectors and their limitations.....	23
3.3 Rogowski coil as a PD sensor.....	24
3.3.1 Construction of Rogowski coil.....	24
3.3.2 Working principle of Rogowski coil.....	26
3.3.3 Advantages of using Rogowski coil.....	28
3.4 Significance of on-line PD detection in CC lines.....	28
3.5 Experimental set-up.....	29
3.6 PD measurement methodology.....	32
3.7 PD Measurements and results.....	34
3.7.1 Calibration of on-line PD measuring system.....	34
3.7.2 HV measurements.....	41
3.8 Discussion.....	44
<b>4 Determining Wave Propagation Characteristics of CC Line.....</b>	<b>45</b>
4.1 Significance of wave propagation characteristics.....	45
4.2 Theoretical background of TDR.....	46
4.2.1 Operating principle of TDR instruments.....	47
4.3 Some considerations for TDR measurements.....	49
4.3.1 Digital TDR recording.....	49
4.3.2 Fourier transform analysis.....	50

4.4	Transmission line analysis .....	51
4.5	TDR measuring set-up .....	54
4.6	TDR parameters extraction method .....	55
4.7	Calibration of TDR measuring system .....	56
4.8	TDR measurements and results .....	57
4.9	Comparing wave propagation characteristics of XLPE cable and CC line .....	63
4.10	Discussion .....	65
<b>5</b>	<b>Theoretical Modeling and Experimental Verification of CC Line.....</b>	<b>67</b>
5.1	Motivation for developing CC line model .....	67
5.2	Developing theoretical model of CC line .....	68
5.3	Theoretical model verification.....	71
5.3.1	<i>Model parameters verification.....</i>	<i>72</i>
5.3.2	<i>Time domain verification using EMTP-ATP.....</i>	<i>74</i>
5.4	Theoretical model results.....	77
5.5	Discussion .....	82
<b>6</b>	<b>On-line PD Measuring System Modeling and Experimental Verification .....</b>	<b>85</b>
6.1	High frequency distributed parameters model of Rogowski coil .....	85
6.2	ATP simulation parameters calculation .....	87
6.2.1	<i>Rogowski coil parameters.....</i>	<i>87</i>
6.2.2	<i>Covered-conductor line parameters .....</i>	<i>89</i>
6.3	ATP simulation results for PD measuring system .....	90
6.3.1	<i>Modeling of on-line PD measuring system.....</i>	<i>90</i>
6.3.2	<i>Effect of Rogowski coil terminating impedance.....</i>	<i>95</i>
6.3.3	<i>Simulation results for practical CC lines.....</i>	<i>96</i>
6.4	Wireless sensors concept for on-line PD measurements .....	98
6.4.1	<i>Motivation for wireless sensors .....</i>	<i>98</i>
6.4.2	<i>Challenges in on-line condition monitoring using wireless sensors .....</i>	<i>99</i>
6.5	Discussion .....	100
<b>7</b>	<b>De-noising of On-line PD Signals using Wavelet Transform.....</b>	<b>101</b>
7.1	Significance of de-noising on-line PD signals.....	101
7.2	EMD sources corrupting on-line PD measurements.....	103
7.3	Wavelet transform analysis.....	103
7.3.1	<i>Brief introduction to the wavelet.....</i>	<i>103</i>
7.3.2	<i>Continuous wavelet transform (CWT) .....</i>	<i>104</i>
7.3.3	<i>Discrete wavelet transform (DWT) .....</i>	<i>104</i>
7.3.4	<i>Wavelet-based de-noising procedure based on MSD .....</i>	<i>105</i>
7.4	On-Line PD de-noising results.....	106
7.4.1	<i>Processing of laboratory measurements.....</i>	<i>106</i>
7.4.2	<i>Processing of on-site measurements .....</i>	<i>111</i>
7.5	Discussion .....	118

<b>8 Conclusions and Future Developments.....</b>	<b>119</b>
8.1 Conclusions.....	119
8.2 Future developments.....	122
<b>References.....</b>	<b>125</b>



# Chapter 1

## Introduction

*This chapter gives the background and the motivation of the project. The major contributions made by the author are listed here. The thesis outline is also drawn to give the reader an overview of the work.*

### 1.1 Background

The medium voltage (MV) distribution system in Finland has been constructed using mainly bare overhead lines. The most common voltage level is 20 kV. In normal circumstances such lines behave reliably, although they demand a lot of space. The space required for double and multiple line structures is especially broad. Exceptional situations produce difficulties for bare overhead lines, e.g. the clashes due to the fall of accumulated snow cause short-circuits and damage to the conductors. Trees falling on the lines cause damage to the structures and short-circuits between phases as well as earth faults [1].

In the Nordic countries, fault categories in MV overhead distribution networks are classified into snow burden 35%, falling trees 27%, branch on pole transformers 9%, diggers 6%, lightning impulses 6%; the rest are probably caused by animals [2]. Due to large forest area in these countries, the electrical network is exposed to faults due to leaning trees. The contact with the line is usually caused by a tree falling on a line in a storm or a tree pressing the conductor more lightly, for example due to snow load or tree growth. This is the weakness of traditional bare overhead lines. In Finland, such damage caused by trees is 2.3 per year per 100 km [1].

The use of covered-conductor (CC) or insulated lines has been expanding in MV networks throughout the world over the last 30 years [3]-[13]. The covering of the conductor provides the main benefit of a covered overhead line, i.e., the ability to allow grounded objects to touch the line and phases to touch each other without any tripping or outage [7]. CC systems are developed to reduce failure rates compared to bare wire MV networks and hence, to improve the security of the supplies [14]. The additional

investment cost is often fully compensated by savings in line spacing, reduced maintenance, and a better quality of network. CCs have replaced bare conductors due to better technical solutions, the reduction of operating costs, and simply because this technology is more compact and friendlier to people, and the environment as a whole [4], [9]. In spite of slightly higher capital costs, the overall costs are lower due to a significantly reduced number of failures [12], [15]. The operational reliability of these conductors is better since they have much more favorable electrical and mechanical properties than uncovered ones.

In Europe, the first CC lines went up in Finland in the 1970s (known as SAX-system and later also as PAS-system), followed by Sweden and Norway (known as BLX-system) in the late 1980s, and in the UK in the mid 1990s [13]. At the present time, there is more than 8500 km circuit length of PAS conductors in Finland, their share of new MV network construction totaling around 80%. Sweden has more than 9500 km circuit length of BLX conductors, their share of new MV network construction being as high as 80% [13]. Norway has more than 4000 km of CC line, while, in the UK, over 2000 km of line have now been erected. Several other European and South American countries are also showing great interest in CC overhead lines.

## 1.2 Problem statement

Partial discharges (PDs) are small discharges caused by strong and inhomogeneous electrical fields. The reason for such fields could be voids, bubbles, or defects in an insulating material. Detection of PD is performed in order to ascertain the condition of the insulating material in HV elements, e.g., cables and CCs. Since PD usually occurs before complete breakdown, PD monitoring provides a warning to remove the power system component from service before catastrophic failure occurs [16]. Therefore, the area of PD measurement and diagnosis is accepted as one of the most valuable non-destructive means for assessing the quality and technical integrity of HV power apparatus and cables.

CC lines have been frequently used in MV networks in Finland since 1970 [17]. The use of CC in the distribution networks started with the need for decreasing the number of faults caused by falling/leaning trees as well as reducing the expenses from tree clearance and maintenance. However, falling trees produce PDs, which may cause the insulation of the conductors to deteriorate through chemical, thermal, and electrical mechanisms, with the passage of time [18]. The falling trees may also produce knife traces on the conductor surface due to difference in wind pressures, which can aggravate the situation of initiating PDs, resulting in rupture of the conductor insulation. In short, PDs have a distinct effect in the ageing processes and lifetimes of HV insulation.

Experiences have proved that PD has been an efficient method for condition monitoring of electrical insulations. Traditionally, PD measurements have been carried out off-line during an interruption in the normal operation and with special equipment. In addition, an experienced specialist has usually been needed to interpret the results. The conventional PD measurement techniques have been in practice for several decades. Most conventional

PD detectors use a single input detection method to measure a voltage or a current signal at a terminal of the test object. It is based on the processing of analogue signals derived from the coupling impedance in the PD current path. These conventional techniques experience severe limitations when it comes to on-line monitoring due to the influence of background noise, absence of non-intrusive sensors, and processing facilities. Also, they have a limit in the detection frequency range, especially for CC overhead lines, due to the attenuation of high frequency PD signals. Low detection frequency for the detector imposes a fundamental limitation on locating the PD position, which is one of the major concerns in insulation monitoring.

On-line PD measurements have been carried out in many condition monitoring applications, such as transformers, cables, rotating machines, and gas-insulated switchgear (GIS) systems [19]-[23]. On-line PD monitoring has a number of important advantages. Firstly, the data is continuously registered so temporal PD activity, or PDs occurring shortly before failure are also captured, in contrast to occasional off-line tests. Secondly, installing the measuring system can, in principle, be done on-line without having to disrupt the power delivery. This, together with the fact that after installation on-line monitoring hardly requires any personnel effort, makes it relatively cheap to operate for utilities. Thirdly, the apparatus is tested under exact operating conditions that include over voltages and load variations, which may be more convincing as being indicative for the actual condition [24].

The design of an on-line system has a number of challenges to deal with. Since the cable or conductor is connected to the power grid, the amount of noise and interference is much larger than is the case for off-line measurements, so the requirements for signal processing are much higher. If measuring set-ups are required at both ends of the conductor to include localization of defects, extra requirements arise for communication and accurate synchronization [25]. Another challenge involves the coupling to the conductor to extract the PD signals that includes technical demands such as sensitivity, bandwidth, etc. The PD sensor must be installed in existing networks, preferably during operation, and it may not result in a safety risk or an additional risk of failure for the power grid.

On-line PD measurements have been taken using instrument transformers [26]; however, the responses of conventional current transformers (CTs) at high frequencies are not flat. On-line PD measurements have already been conducted on CC lines with a PD monitoring system installed using a capacitive voltage divider including CT on 20 and 110 kV test lines [27], [28]. Recently, the PD detection frequency range has been extended up to the radio frequency band with the development of new sensors e.g., Rogowski coils. The Rogowski coils have already been used for the on-site condition monitoring of MV cables [29]; however, using Rogowski coils for on-line PD detection due to falling trees on CC overhead distribution lines is a novel and interesting area for researchers.

In this research work, the Rogowski coil is used as a PD sensor because it is superior to the conventional PD detectors. It is non-intrusive and provides the needed bandwidth for

detecting PDs produced due to falling trees on CC overhead distribution lines. Since Rogowski coils are very accurate and are not prone to saturation, protection levels can be set to lower thresholds increasing the sensitivity of the scheme without affecting the reliability of operation. The system is immune to external magnetic fields, is simple, user friendly, requires less wiring and space, and can provide metering accuracy [30]. Flexible Rogowski coils are generally more convenient to use than rigid coils, but are less accurate. A typical mutual inductance of a standard flexible Rogowski coil is in the range of 200-300 nH and its resonant frequency lies in a high frequency spectrum [31]. The goal with this research is to assess the properties of PDs in this particular application so that a PD sensor can be designed. In that design, a trade-off must be found between the limitations of the sensor and the reliability of the measurements it can make.

In CC overhead distribution networks, a wide application of on-line PD measurement as a condition monitoring technique has not practically or economically been possible. This is partly because of the high costs of the equipment and resources needed, compared to the cost of the components to be monitored. One way of reducing the costs of implementing an on-line PD measuring system is to use as simple sensors as possible (e.g., Rogowski coils) and to integrate the PD monitoring functions for example to advanced network automation [29]. The challenge for on-line PD measurements is to find the optimal locations for these sensors with respect to their sensitivity, interference level, signal distinction, and universal applicability. The advantage of on-line PD monitoring allows for CC insulation diagnostics during normal operation as well as when the trees are leaning on the conductors. The falling trees cannot be detected with conventional earth fault detection methods or normal protection relays due to the high impedance of conductor covering, as well as the high resistance of the tree [27]. The big challenge faced by electric utilities using CC systems in overhead distribution networks in Finland is to develop an on-line automatic system that should be capable of detecting falling trees on the lines.

### 1.3 Major contributions

- A new methodology for detecting non-stationary, irregular, and high frequency PDs, produced due to falling trees on CC overhead distribution lines has been presented. The measurements have been taken using a wired Rogowski coil.
- The time domain reflectometry (TDR) measurement technique is presented to extract the frequency-dependent wave propagation characteristics (attenuation, phase constant, and propagation velocity) of CC overhead distribution lines. These measurements can be applied for the design and deployment of PD sensors over the entire length of the CC line for detecting PDs produced by falling/leaning trees.
- The theoretical modeling of the CC line based on its geometry is presented using two-wire transmission line (TL) theory and its frequency-dependent line characteristics have successfully been derived. The theoretical model is verified

experimentally using TDR measurements on the basis of the wave propagation characteristics determination. The TDR measuring system is also simulated in the electromagnetic transient program-alternative transient program (EMTP-ATP) for real time verification of the measurements. It is revealed that the model does not only give correct values of the wave propagation characteristics at lower frequencies, but it also works well at higher frequencies, where TDR measurements fail to extract these characteristics due to measuring limitations. The frequency-dependent TL characteristics are extracted from the presented theoretical model for the practical CC lines in MV networks located at different heights above the ground level. The effect of the CC height on the line characteristics is also presented. These characteristics can be used for the accurate modeling of the CC line in EMTP-ATP as well as for designing of Rogowski sensors to detect falling trees on the CC lines.

- The entire on-line single-phase PD monitoring system including CC line and Rogowski coil for detecting falling trees on CC overhead distribution lines is modeled in the EMTP-ATP simulation environment. The model is confirmed by the measurement results taken in the laboratory. The model can be used to estimate the length of the CC line at which the PDs due to falling trees can be detected; thus deciding the number and positioning of the sensors over a particular length of the CC line. Moreover, the challenges in on-line condition monitoring of falling trees on the CC lines using wireless sensors are also described.
- The wavelet transform (WT) technique is applied as a powerful tool to de-noise on-line PD signals produced due to falling trees on CC overhead distribution lines, which are completely buried by electromagnetic interference (EMI). The PD signals are captured in the laboratory environment and on-site measurements are simulated in MATLAB. The principle of de-noising based on multi-resolution signal decomposition (MSD) is implemented.

## 1.4 Organization of thesis

The thesis is organized into the following chapters:

**Chapter 2** gives an overview of the Scandinavian experiences in using CC overhead distribution networks. A system of overhead CCs (SAX or PAS) used in Finland is presented. The mechanical and electrical effects of leaning trees on the CC lines have been discussed. It is explained that falling trees produce PDs, which may cause the insulation of the conductors to deteriorate with the passage of time. The advantages and the challenges posed by CC systems are also described.

**Chapter 3** investigates a methodology for detecting on-line PDs produced due to falling trees on the CC overhead distribution lines. For this purpose, the Rogowski coil is used as a PD sensor. This sensor is non-intrusive and superior to the conventional PD detecting methods. The experimental set-up was arranged in the HV laboratory at TKK for real-

time analysis. A pulse calibrator was used for the calibration of the on-line PD measuring system. . The measurement results show that it is possible to detect the falling trees on the CC overhead lines using a Rogowski coil PD sensor.

**Chapter 4** gives a general background of the TDR measurements, explaining the response of electrical networks in the time domain. The work concentrates on determining the wave propagation characteristics (propagation constants, i.e., attenuation and phase constants, and propagation velocity) of CC lines using high frequency TDR measurements.

**Chapter 5** describes a step-by-step procedure to develop a theoretical model of the CC overhead distribution line and the frequency-dependent distributed TL parameters, wave propagation characteristics, and characteristic impedance are calculated. The derived wave propagation characteristics are compared with those obtained from the TDR measurements to validate the theoretical model of the CC line. The TDR measuring system is also simulated in EMTP-ATP as a real time verification.

**Chapter 6** presents EMTP-ATP simulations to model an on-line single-phase PD measuring system including CC line and Rogowski coil for the monitoring of falling trees on CC overhead distribution lines. The CC is modeled as a distributed parameters line and the Rogowski coil is represented based on its equivalent circuit as a saturable current transformer having linear magnetizing characteristics. The simulation results are compared with those obtained from the laboratory measurements. The challenges in on-line condition monitoring of falling trees on the CC lines using wireless sensors are also discussed.

**Chapter 7** presents the wavelet transform (WT) technique as a powerful tool to de-noise on-line PD signals in CC overhead distribution lines, which are completely buried by EMI. The PD signals are captured in the laboratory environment and on-site measurements are simulated in MATLAB. The principle of de-noising based on MSD is implemented.

**Chapter 8** contains the summary and conclusions of the research work. The future developments of the present research work are also discussed.

## Chapter 2

### Using CC Overhead Lines in Distribution Networks

*This chapter gives an overview of the Scandinavian experiences in using CC overhead distribution networks. A system of overhead CCs (SAX or PAS) used in Finland is presented. The mechanical and electrical effects of the leaning trees on the CC lines have been discussed. It is explained that falling trees produce partial discharges (PDs), which cause the insulation of the conductors to deteriorate with the passage of time. The advantages and the challenges posed by CCs system are also described.*

#### 2.1 History of CC lines – a Scandinavian experience

American utilities started to replace bare conductors with covered ones in MV distribution networks in the early 1960s. At the same time, Australian utilities also made similar changes in their networks [15]. The covering materials used were polyvinyl chloride (PVC), high density polyethylene (HDPE), and nylon. The life-span of CC lines was very limited and the general level of interest in them was quite low. In the area where a conductor was fixed to the insulator, it was necessary to remove insulation from the conductor, which caused very intensive corrosion. This was one of the major reasons that utilities were not consistent in their use.

In the early 1970s, the motivation for using CCs became high again due to the need for solutions to the corrosion problem as well as other problems. Some Nordic countries (Finland and Sweden) were earlier users and this technique offered increased reliability in adverse weather conditions, satisfied ecological considerations, and also proved to be cost-effective for the complete life cycle [12]. Utilities in Sweden and Norway soon adopted this system, which has since spread to utilities throughout Europe, the United States, Australia, and Japan. The use of CC lines with aluminum alloy conductor covered with a sheath of cross-linked polyethylene (XLPE) or HDPE has been expanding throughout the world ever since.

In the Nordic countries, the CC lines in distribution networks were originally introduced due to their good applicability for passing through forest areas and having better

operating safety. With so much forest throughout the Scandinavian countries, the problem could have been that of the forest fires caused by falling trees on the bare conductor resulting in the initiation of arc [6]. In the late 1980s, research was started in Finland into the suitability of CC line for forest areas; however, it was more likely to be the quality of the power supply that was the main reason for that research. Consumers in Scandinavia, especially industrial consumers, do not accept loss of supply that lightly. The Finnish research and more recent work carried out by Asea Brown Boveri (ABB), coupled with a developing history of general usage in the field have given very positive results during the last few years. Both the laboratory and practical experiences prove that CC lines are better option, as compared with conventional bare conductors installed in distribution networks in Scandinavian countries [6].

## 2.2 Geometry of overhead covered-conductor

The conductor material in CC overhead distribution lines is aluminum alloy and the insulation material is XLPE or HDPE, usually having a thickness of 2.3 mm. Carbon black is mixed with plastic to reduce the effect of ultra violet radiations. According to Finnish structure, the conductor is stranded and compacted. In Finland, corrosion in aluminum conductors is not a problem; therefore, CC structures are not greased [27]. The insulators used on CC lines are normally porcelain pin or post insulators. Epoxy resin insulators are also used. The phase-to-phase distances at poles are one-third as compared with bare conductor lines (40-50 cm on 20 kV lines) [4]. The CC line and its cross-sectional view are shown in Fig. 2.1 [32].

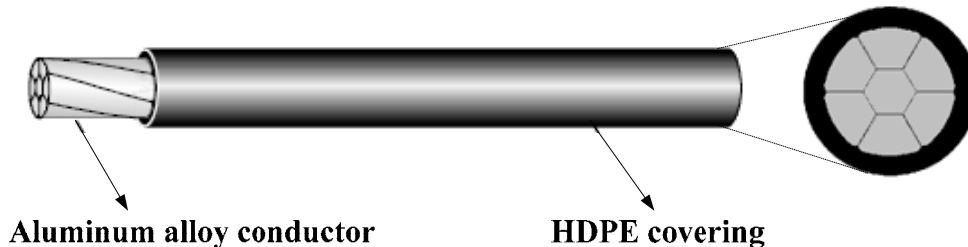


Fig. 2.1 Cross-sectional view of CC overhead in distribution networks

## 2.3 Covered-conductor overhead system representation

The idea of developing CC overhead lines (PAS or BLX type) was to reduce the deficiencies of traditional bare overhead lines. When the conductors are covered with a thin layer of insulation, clashes do not cause disruptions of use and the distance between the conductors can be reduced. The saving in space is considerable if the structures are constructed consisting of several lines in parallel.

One of the major drawbacks of CC lines is arc damage caused by lightning and susceptibility to damage from aeolian vibration. Unless special lightning protection steps are taken to overhead CC lines, lightning over voltage leads first to a flashover of a line

insulator and next to a breakdown of the solid conductor insulation. There is a high probability that such a lightning flashover will bring about a power frequency arc which keeps burning at the insulation breakdown point until the line is disconnected. The arc can easily burn the insulating covering and it may melt the conductor with high fault currents [33]. The main characteristics of aeolian vibration are high frequency and low amplitude, mainly in the vertical plane. It is observed that both lightning and vibration damage tend to be located at the insulators on the poles.

The technical considerations have been taken into account while designing the PAS (or SAX) system to prevent damages due to arcs and vibration. The attachment points of the conductors have been converted into suspension clamps which withstand vibrations well. An arc caused by over voltage or lightning on the CC line is not able to move along the conductor and it is burning on one point; the circuit breakers cannot respond quickly enough. The high induced energy and the duration of burning can destroy the conductor. However, this problem can be mitigated using arc protection device (APD), power arc device (PAD), surge arrester, or current limiting device. The protection is provided to the conductors, insulators, and transformers and it depends upon the network's short-circuit values as well as the economic attitude of the utility. No instance of damage has been reported in PAS system using APD to avoid arc damages [1].

The construction and layout of a typical PAS line is shown in Fig. 2.2 [13]. This type of line has been installed in Finland in various areas of electrical distribution using APDs, which are designed to direct the arc generated to a sufficient distance from the conductor and insulator. An APD implemented with an arcing horn is recommended for pin and line post insulators. While it is burning, the arc will not damage the conductor itself, but ignite over the insulator, after which it will move along the aluminum wire twisted onto the insulator's neck to the arcing horn. While burning at the end of the horn, the arc ionizes the air, making it conductive and creates a short circuit between the phases, at which point the circuit breakers are tripped. The distance between the horns must be no greater than the CC phase spacing. In radial network, an arc protection device should be installed on the side of the load, and in a ring network on both sides of the insulator. When installing the arc protection connectors, there is no need to remove the conductor covering. For phase spacing over 60 cm and with low short-circuit currents, APDs do not adequately protect the conductor and another method of protection, e.g., a PAD, must be chosen (see Fig. 2.3). With small short-circuit currents, an arc will move slowly and stress the insulator for a prolonged period. To avoid damage to the insulator, the arc must be ignited directly in the spark gap, so that the short-circuit occurs through the cross-arm and trips the circuit breakers. PADs are not dependent on the direction of power feed, and therefore can be installed on either side of the insulator. PADs can be used with tension and suspension insulators. An advantage of surge arresters and current limiting devices is uninterrupted distribution of electricity to consumers. However, these devices may be damaged due to high lightning currents as well as the fact that their costs are higher. Therefore, APDs and PADs are economical solutions for arc protection schemes implemented for CC systems in distribution networks [13].



Fig. 2.2 Construction of a typical PAS line – Suspension pole with pin insulators and lightning protection using APDs implemented with arcing horns [13]

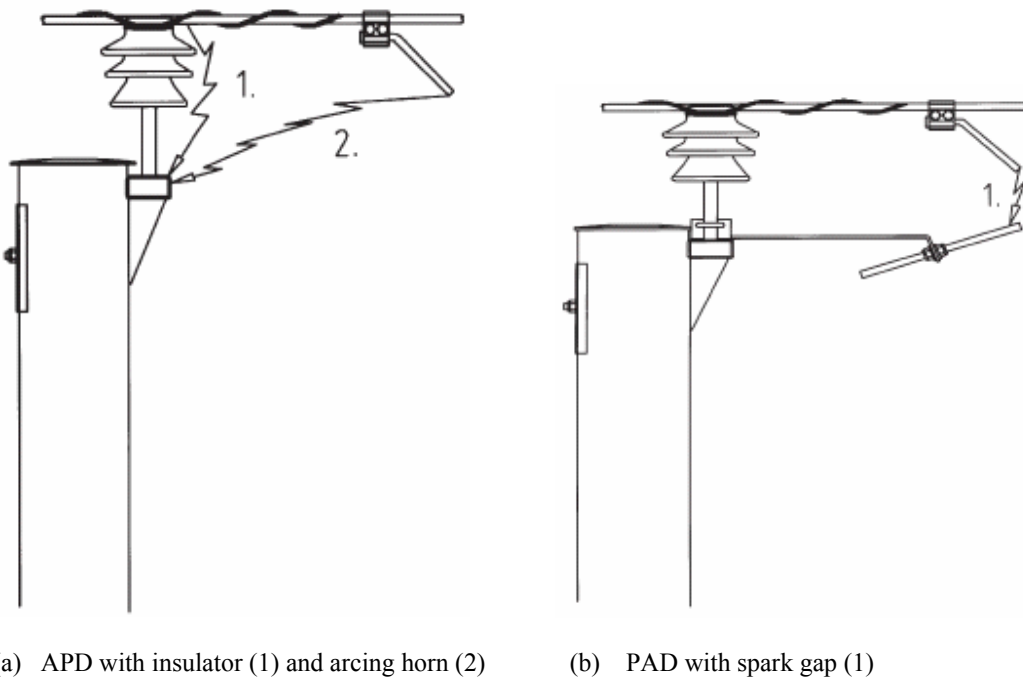


Fig. 2.3 Different arc protection schemes implemented for PAS line [13]

The CC line covers approximately 40% less space than that of a standard bare line [13]. This has enabled the use of overhead line installations in built-up areas, while in forests the required line corridor has narrowed to a larger extent. CC structures offer considerable space savings, especially in substation outputs, a desirable outcome in terms of preserving natural scenery. It is possible to save considerable space by laying parallel

(e.g., double) CC line structures (see Fig. 2.4), so saving the extra money incurred for buying wider right of way in case of bare conductors .



Fig. 2.4 Double 20 kV PAS line – no wider than a normal single bare copper line

Laying CC lines is a cheaper solution than underground cables for distributing energy to the consumers. However, it is costlier than bare conductor technology, e.g., CC lines (PAS 3×70) can be constructed at 50% less cost than underground cables (AHXMKW 3×70). On the other hand, this system bears 30% extra cost as compared to bare lines (54/9 AlFe RAVEN) [13]. CC line construction costs are moderate, considering their advantages over traditional bare line structures. When parallel lines are constructed, bare and CC lines costs have no difference due to narrower right of ways in CC lines.

## 2.4 Tree leaning experiments and tests

The research has already been carried out for the suitability of CCs system in forest areas using a comprehensive electrical and mechanical test series [1]. The tests simulated the situations in which trees most often caused damage to 20 kV overhead lines.

### 2.4.1 Mechanical tests performance

The mechanical tests were conducted to calculate the forces acting on the structures and conductors of the SAX system. The prevailing conditions resembled the reality as closely as possible to find out which structural part would fail first when a tree fell on the line. The test lines having length 4 km were constructed and the conductors were tensioned to the values recommended by the manufacturer. The trees used on the lines were normal mature Finnish pine, spruce, and birch. Various types of trees were used in order to find out whether this factor had any effect from the point of view of mechanical stress. The

trees used in the force measuring tests were pine, spruce, and birch, having length 20.9 m (weighed 4.6 kN), 22.2 m (weighed 5.1 kN), and 20 m (weighed 3.9 kN), respectively [1]. The dynamometers were located to measure the forces acting on all three phases of the line span onto which the tree had fallen. The dynamometers were equipped with strain-gauge sensors and the measurement results were stored in the microcomputer which output the results graphically. The results of the force test in which a pine was made to fall onto 70 mm<sup>2</sup> conductors are shown in Fig. 2.5. The results for forces exerted by spruce and birch were slightly lower because of the absorbing effect of their branches (only 10% difference). During the SAX system test series, a tree was made to fall onto the conductors 16 times, and there were no cases of rupture of the covering.

Following the strength tests, the average length of the trees was 18 m, with a weight of 3.5 kN, were made to fall onto the same span of the test line equipped with 35, 70, and 120 mm<sup>2</sup> conductors. The aim was to find out the weakest point in the pole and suspension clamp structures. It was confirmed that the 35 mm<sup>2</sup> line stood the weight of a 5 kN mature tree falling on the span and the conductor was the first part to break. It was revealed that the 70 mm<sup>2</sup> line withstood 5 corresponding trees falling on the span and the conductor was the weakest point. It was also revealed that the 120 mm<sup>2</sup> line withstood at least 10 trees falling on the span and the poles constituted the weakest structural component if all the trees fell on the same span [1]. It was further proved that using horizontal cross-arms, the ability of SAX lines to withstand fallen trees could be increased because the increase in total tension was distributed more evenly between different phase conductors than in the triangular construction. Moreover, the 2.3 mm plastics covering could withstand well the mechanical stress exerted by the fallen trees.

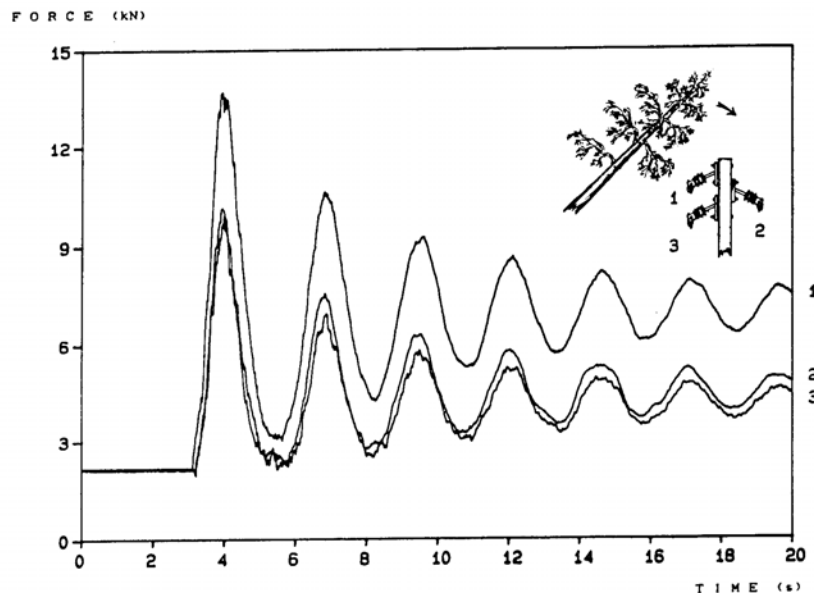


Fig. 2.5 Conductor forces vibrations when a mature pine is leaned against a 70 mm<sup>2</sup> SAX line in a sunny environment (10 °C) [1]

### 2.4.2 Electrical tests performance

For conducting electrical stress tests, a test voltage of 21 kV was applied to a 120 mm<sup>2</sup> line having 2.3 mm insulation thickness. When the voltage had been on for 123 days, a puncture occurred in the leaning tree test at the point where a birch tree was leaning on the conductor, this situation resulting in an earth fault [1]. The trunk was removed and the test continued with the other 9 tree trunks for 140 days. Apart from the puncture mentioned above, there had been no others during the test. For one of the spruce trunks, it was revealed that PDs at the contact point of the tree and conductor produced clearly perceptible sound phenomena, the intensity of which varied with variations in the humidity of the air. With the passage of time, these discharges also led to the conductor being pressed into the tree trunk (see Fig 2.6). In addition, the marks of PDs were visible on the surface of the conductor. The phenomenon of initiation of PDs due to leaning trees on the CC line has been explained in the next section.

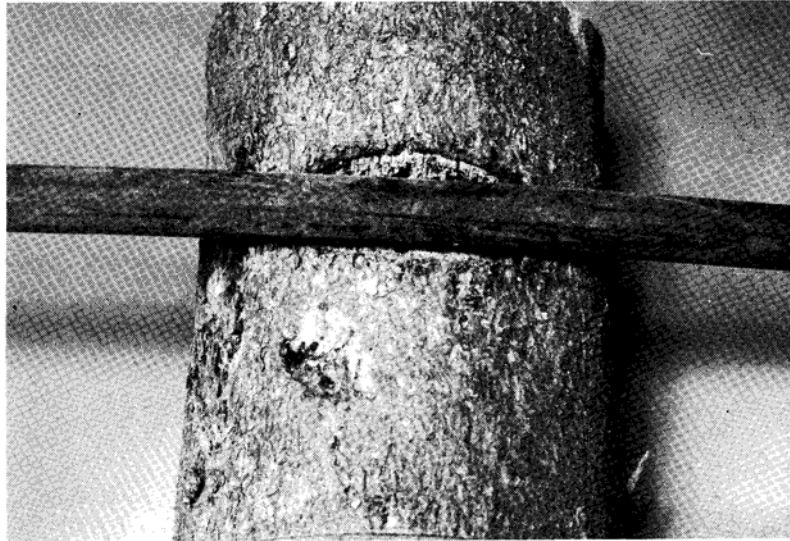


Fig. 2.6 Mark left on a spruce trunk by PDs when the trunk had been leaning on the tensioned conductor for 94 days [1]

## 2.5 Equivalent circuit of a leaning tree on CC line

A leaning tree on the CC line can be represented by a simplified electrical equivalent circuit, drawn in Fig. 2.7, which depicts a scenario when the trunk of the tree is in contact with conductor insulation [27]. The stranded conductor is made of aluminum. A capacitance  $C_{\text{ins}}$  represents the HDPE insulation cover on the conductor, while a capacitance  $C_{\text{air}}$  represents an air gap between the surface of the tree and conductor cover. The tree is modeled as a combination of parallel capacitances and resistances. The impedance of the tree depends upon several parameters, e.g., cellular structure of the tree, air humidity, tree humidity, temperature, and the state of the tree surface [27]. The earth is modeled as a resistance which thermal resistivity depends upon its density,

composition, and humidity (moisture contents) [34]. A more complex circuit may be drawn for a tree top (with leaves or needles) laying on the conductor. It is worth mentioning that equivalent circuit does not take into account the internal structure of the tree such as the different electrical characteristics of the bark of the tree, the tree itself, and the interface between the tree and the bark [27].

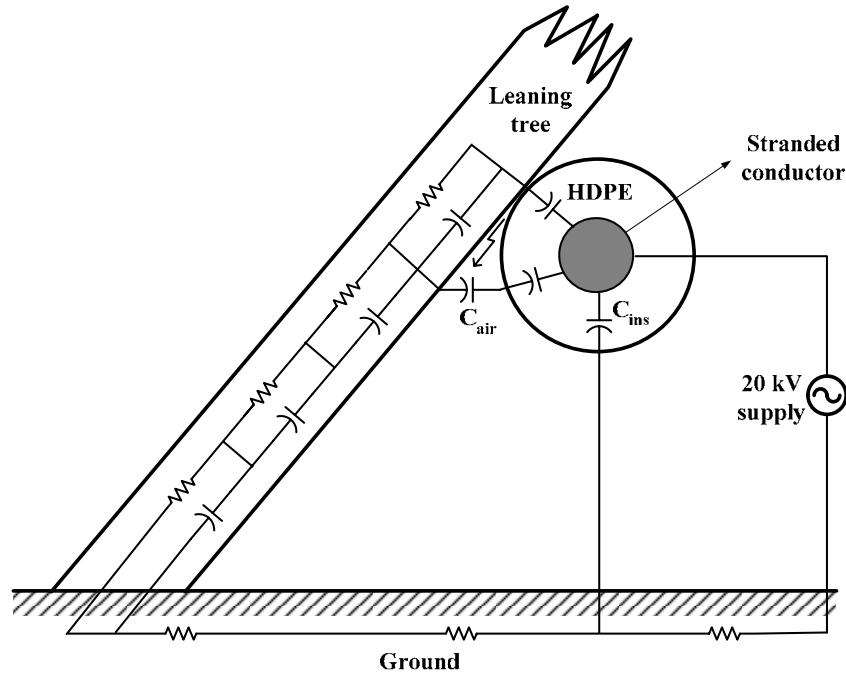


Fig. 2.7 An electrical equivalent circuit of the leaning tree on CC line [27]

PDs are produced due to the falling trees on the CC lines which can be treated as a gliding discharge. The relative permittivities of CC insulation (HDPE) and air are 2.26 and 1, respectively. The higher relative permittivity of HDPE compared to air causes the electric field strength to be higher in the air gap than in HDPE. The electric field around the conductor is heavily distorted due to the leaning tree and PDs are produced in the air gap between the surface of the tree and conductor insulation.

The contact resistance between the CC insulation and the tree is assumed to be time dependent during the fault, occurring due to the leaning tree. When the tree first leans on the line, the fault impedance is in the order of tens or a hundred  $M\Omega$  (including insulation and tree resistances), so the tree cannot be detected with conventional earth fault detection methods. Due to continuous PD activity, the carbonization starts occurring in the conductor covering and the tree, eventually leading to punch through in the CC insulation. The fault impedance mainly consists of the tree impedance itself and resistance between the tree and earth after the conductor cover has burned off from the contact point. The fault impedance varies depending upon the soil composition, soil density, moisture contents in the soil, and the size and type of the leaning tree. The fault impedance measurements on an experimental 20/12 kV bare conductor line having

earthed neutral are reported in [3]; the fault impedance is 10-58 k $\Omega$  in spring and summer conditions and is up to 2.1-3.2 M $\Omega$  in winter season.

In Finland, the rain often falls during the whole year. The rain water droplets may come between the surfaces of the tree and CC. The permittivity of water is quite frequency-dependent. Moreover, the resistivity of water is dependent upon the chemical materials at the surface of the tree and the ground. Therefore, a complex electrical circuit of the tree (consisting of a parallel circuit of capacitance and conductance due to the water droplets in series with the capacitance and conductance of the tree) can also be developed for deep analysis under such circumstances.

## 2.6 Objectives and challenges posed by CC system

The use of CC overhead lines in the distribution system started with the need to decrease the number of faults caused by the falling trees as well as reducing the expenses with tree clearances and the maintenance and system life span [8]. The statistics confirm that the number of faults dropped to 0.9 per year per 100 km compared to 4.5 per year per 100 km for lines with bare conductors [13]. The general objectives of the CC technology can be described as follows [11]:

- i) It has been revealed that power lines have a harmful impact on biodiversity because they divide artificially the surrounding nature. Using CC lines, the wayleaves (corridors) of the power lines can be constructed significantly narrower.
- ii) The safety of power lines improves with CC lines. Statistics show that a number of people die in HV accidents because of direct contact with HV conductors. Using CC lines, a greater part of these accidents can be avoided. In addition, many birds die every year by colliding with power lines. A number of these fatal collisions can also be avoided using this technique.
- iii) Using CC lines, the old lines can be upgraded without constructing a new transmission line. For instance, when there is a need to increase the voltage, it can be done only by changing the old conductors to covered ones without major changes in tower structures etc. This can benefit the environment considerably.
- iv) Power lines are surrounded by electric and magnetic fields. These fields possibly impact on people with health concerns. Low magnetic fields are present in the vicinity of the CC lines.

In addition to the above mentioned objectives, CC lines have several advantages, e.g., there are no faults or problems with snow or hoar frost, there are no interruptions from falling branches, no faults are caused when conductors are touching due to ice-shedding, and CC lines are a cheaper alternative to underground cable when laying in difficult terrain [10], [35]. However, these kinds of conductors pose some problems, such as:

- i) PDs are produced due to falling/leaning trees on the surface of CC lines. The falling trees may produce knife traces on the conductor surface due to difference in wind pressures, which may aggravate the situation of initiating PDs, resulting in rupture of the conductor insulation. The falling trees cannot be detected with normal protection relays.
- ii) The different dielectric constants of the material employed, generating electric field concentration and consequently the possibility of the corona effects.
- iii) CC lines are sensible to ultra-violet radiations.
- iv) CC lines are susceptible to thermo mechanical effects, which eventually cause cracks.

## 2.7 Discussion

The CC lines have been frequently used in MV networks in Finland for a long time. CC overhead lines (PAS and BLX) were developed in order to improve the reliability of the distribution system for transfer of electricity. The CC system has diminished the number of interruptions caused by faults. The plastic covering for CC lines prevents interruptions, or outages due to collisions or momentary contact with a foreign object. Due to its coating, faults caused by snow and ice falling from trees have been almost completely eliminated. According to statistics, the failure rate has been diminished to a larger extent for CC lines as compared to bare conductors. It has also helped to make line corridors narrow, a particular advantage in built-up areas. Using overhead line structures, it is possible to fit substation outputs into a small space; an excellent solution in aesthetic terms. Several years in use have proven the CC system to be an extremely functional, reliable, cost-effective, and a safe solution for overhead lines.

Over voltage is induced on the line when lightning strikes an overhead line or its vicinity. The magnitude of the over voltage is approximately the same in all phases and may rise to several hundred kV between the phase and earth. The power arc can move freely along an ordinary bare conductor line towards the load; however, the covering forms an obstacle in case of CC lines. In order to prevent damage, a CC line must be protected by installing APDs or PADs at the appropriate locations. The mechanical and electrical tests have already been conducted for falling trees on the CCs system and the SAX line structures succeeded well in these tests. The insulating layer of a CC line can withstand a tree for a certain time. However, the big challenge faced by the utilities is that falling trees on the CC lines produce PDs, which should be detected and removed for the better reliability of the supply to the consumers.

Several network companies have secured an interruption-free electricity supply for their key customers by choosing the CC structure for their MV networks. The good experiences in Northern Europe and the endeavor to prepare a European standard give a good background for CC system in future.

## Chapter 3

### On-line PD Detection in CC Overhead Distribution Networks

*This chapter describes basic concepts and the methodology for detecting PDs produced due to falling trees on the CC overhead distribution lines. For this purpose, the Rogowski coil is used as a PD sensor. This sensor is non-intrusive and superior to the conventional PD detecting methods. The advantage of on-line PD monitoring allows for conductor insulation diagnostics during normal operation as well as when the trees are leaning on the conductors. The experimental set-up was arranged in the HV laboratory for real-time analysis. A pulse calibrator was used for the calibration of the measuring system. The measurement results show that it is possible to detect falling trees on the CC overhead lines using a Rogowski coil PD sensor.*

#### 3.1 Basic concepts

##### 3.1.1 What is partial discharge (PD)?

The term “PD” is defined by International Electrotechnical Commission (IEC) 60270 High-Voltage Test Techniques – Partial Discharge Measurements, as a localized electrical discharge that only partially bridges the insulation between conductors and which may or may not occur adjacent to a conductor. A PD is confined in some way that does not permit complete failure of the system, i.e., collapse of the voltage between the energized electrodes such as the cable conductor and neutral wires. PD can result from breakdown of gas in a cavity, breakdown of gas in an electrical tree channel, breakdown along an interface, or breakdown between an energized electrode and a floating conductor, etc. [36].

PDs occur due to displacement of charge. This produces a rapid rate of change of current that occurs as the dielectric begins to breakdown. This rate of change is predominantly determined by both the nature of the dielectric and applied electric field.

As PD is a small electrical avalanche caused by locally disrupted electric fields in dielectric materials, it is a symptom of insulation weakness and at the same time can lead to severe deterioration of the insulating material. Therefore, it is known as one of the major factors to accelerate degradation of electrical insulation. The types of discharges are often divided into three groups due to their different origins as [37]-[40]:

### **A. Internal discharges**

- i) Cavity discharges, i.e., discharges from gas-filled voids, delaminations, cracks, etc. within solid insulation. A refined classification could be made to distinguish between the cavities that are on one side bounded by the metallic electrode, and the cavities that are completely surrounded by the insulating material. Voids may have their origin from cast insulation like epoxy spacers in sulfur hexafluoride ( $\text{SF}_6$ ) bus bars, from dried out origins in oil-impregnated paper cables, from gas bubbles in plastic insulation, etc. Delaminations occur in laminated insulation like the stator-bar insulation of large electrical machines that often is composed of mica based tapes with binding enamel like epoxy. Cracks could occur in mechanically stressed insulation, e.g., in loose stator bars that are vibrating.
- ii) Treeing discharges, i.e., current pulses within an electrical tree. The electrical tree may start from a protrusion on the electrode or from imperfections like contaminating particles embedded in the solid insulation.

Internal discharges are in many cases crucial for the life of the insulation. Voltage life depends on several variables, the most important ones being field strength, discharge magnitude, and material.

### **B. Surface discharges**

There are discharges on the surface of an electrical insulation where the tangential field is high, e.g., the porcelain or polymeric housing of HV devices. These discharges occur from the edges of the electrode parallel to the surface of the dielectric – the so called “gliding discharges” or “edge discharges” [18], [41]. The PDs produced due to falling trees on CC overhead distribution lines is an example of the surface discharges. Other common sources are terminations of cables or end-windings of stator windings. Another example could be corona discharges from an edge in a termination, which originates as a source for corona discharges, but that at a later stage start to propagate as surface discharges. Surface discharges are less dangerous than internal ones because they are less concentrated; considerably larger magnitudes, therefore, may be tolerated.

### **C. Corona discharges**

These discharges occur in gases (or liquids) caused by a locally enhanced field from sharp points on the electrodes. It is worth mentioning that in case of corona discharges, it

is not the possible damages to insulation which are of interest (as in case of ageing due to internal PDs) but the higher frequency disturbances arising out of these PDs, and quite often the energy dissipated (corona losses) together with its chemical after-effects [18], [41]. In short, Corona is often harmless, but by-products like ozone and nitric acids may chemically deteriorate nearby materials. The PDs occurring around electrodes of small radius of curvature, i.e., corona discharges, and those on the surface of solid insulating materials are known as “external discharges”

### 3.1.2 Understanding initiation of PD signals

The generation of PD signals could be analyzed by considering a cavity in the dielectric material of the CC line. The cavity is generally filled with air or some gas. The behavior of internal discharges at AC (alternating current) voltage can be described using the well-known *a-b-c* circuit (see Fig. 3.1). The capacity of the cavity is represented by a capacitance  $c$  which is shunted by a breakdown path. The capacity of a dielectric in series with the cavity is represented by a capacitance  $b$ . The sound part of the dielectric material is represented by capacitance  $a$ . In Fig. 3.1, the faulty part of the dielectric corresponds to I, the sound part to II [37].

The same representation can be given for surface discharges, which are produced due to falling trees on CC lines. The surface that is covered by the discharges has a capacity  $c$  to the electrode (a falling tree in this case) and a capacity  $b$  through the insulation. The rest of the dielectric is again represented by capacity  $a$  as may follow from Fig. 3.2.

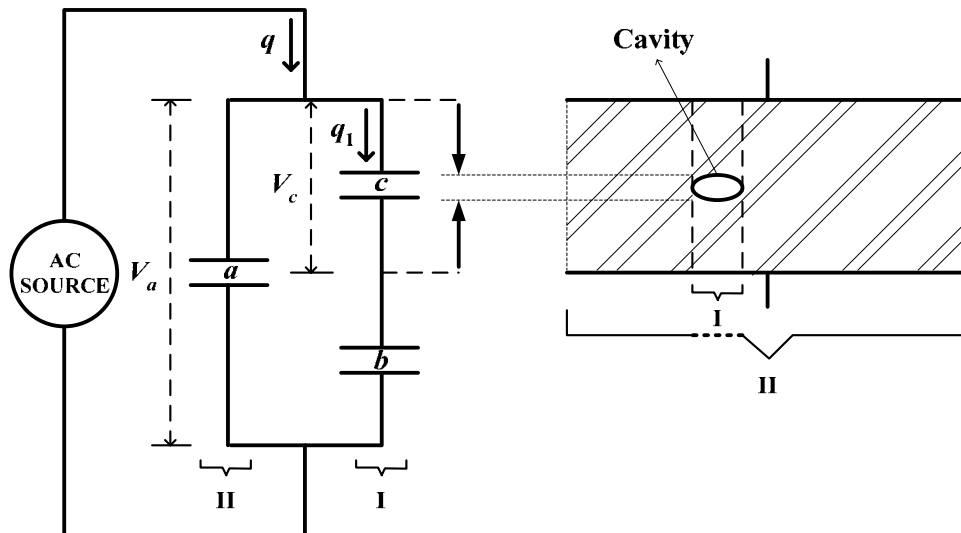


Fig. 3.1 Equivalent circuit of a dielectric with cavity [37]

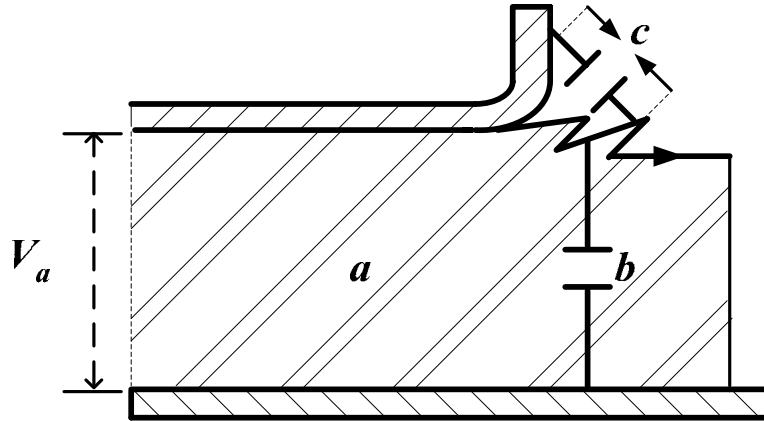


Fig. 3.2 A dielectric circuit for surface discharges due to falling trees on CC line [37]

The electric fields inside the conductor insulation ( $E_a$ ), and in cavity ( $E_c$ ) are given as:

$$E_a = \frac{D_e}{\epsilon_c} \quad (3.1)$$

$$E_c = \frac{D_e}{\epsilon_0} \quad (3.2)$$

where  $D_e$  is the electric flux density in the conductor and it is directly proportional to the applied voltage  $V_a$  to the conductor.  $\epsilon_c$  is the permittivity of the insulating material and  $\epsilon_c = \epsilon_0 \epsilon_{rc}$ , where  $\epsilon_{rc}$  is the dielectric constant (relative permittivity) of the conductor insulating material (always greater than unity), and  $\epsilon_0$  is the permittivity of the free space (or air). The electric field (or dielectric breakdown strength) is 3 kV/mm at 1 atmosphere air pressure. Its magnitude depends upon the shape, location, and pressure of air or gas inside the cavity.

As the applied voltage  $V_a$  is increased, the electric field in the cavity is greater than the field in the surrounding dielectric as a result of the lower permittivity of the air or gas in the cavity, i.e.,

as  $\epsilon_c > \epsilon_0$  then,  $E_c > E_a$

When the field becomes sufficiently higher in the cavity, the air can break down, in the process of which it goes from non-conducting to conducting, and the field in the cavity goes from very high to nearly zero immediately after the discharge. The measured PD signal is the result of the change in the image charge on the electrodes as a result of the transient change in the electric field distribution caused by the discharge. Such a discharge generates a voltage PD signal between the system conductors as a result of the change in the electric field configuration, which takes place when the discharge occurs.

This phenomenon could be well understood by considering the transient change in capacitance between the conductor and the ground shield of the conductor when the cavity goes from non-conducting to conducting. Obviously the capacitance increases when the cavity is conducting, which means that a current must flow down the conductor to charge the additional capacitance and to maintain constant voltage on the conductor. This current flows through the impedance of the cable and generates a voltage pulse, which propagates down the conductor [36].

### 3.1.3 Quantities related to PD magnitude

#### A. Charge transfer

The charge  $q_1$ , which is transferred in the cavity could be taken as a measure (see Fig. 3.1). If the sample is large as compared to the cavity, as will usually be the case, this charge transfer is equal to [37]:

$$q_1 \cong (b + c)\Delta V \quad (3.3)$$

Where  $\Delta V = V_i - V_e$ ,  $V_i$  is the breakdown voltage at which the discharge occurs in the cavity, and  $V_e$  is the voltage at which the discharge extinguishes. The equation (3.3) is not an exact relation, but an approximation by assuming that the sample is larger as compared to the cavity size. In that case, the capacitance of the specimen  $a$  is much larger than capacitances  $b$  and  $c$ .

As the deterioration of the dielectric certainly is related to the charge transfer in the defect,  $q_1$  would be an attractive choice. However,  $q_1$  cannot be measured with a discharge detector and it is therefore not a practical choice.

#### B. Apparent charge transfer in sample

The displacement of charge  $q$  in the leads of the sample can be taken (see Fig. 3.1). This quantity is equal to:

$$q = b\Delta V \quad (3.4)$$

It causes a voltage drop  $b\Delta V/(a+b)$  in the sample. Most discharge detectors respond to this voltage drop and, therefore, they are capable of determining  $q$ .

The charge  $q_1$  delivered at the cavity by the PD is not identical with that recouped from the power supply network, measurable at the terminals as "apparent" pulse charge  $q$ . Thus,

$$q = \left( \frac{b}{b+c} \right) q_1 \quad (3.5)$$

### C. Choice of $q$ as a measure of discharges

The characteristics of the transfer of charge  $q$  make it an attractive quantity for the measurement of discharges. These characteristics are [37]:

- i)  $q$  is directly related to the energy in the discharge
- ii)  $q$  is directly related to the size of the defect
- iii)  $q$  can readily be measured with an electrical discharge detector
- iv) It can be shown that the harmfulness of a discharge is related to the order of magnitude of  $q$  in powers of ten

It must be emphasized that the discharge magnitude is not equal to the charge transfer in a cavity. The charge transfer  $q_1$  is usually several tens of times larger than the apparent charge  $q$ . The only disadvantage in using  $q$  is that it is inversely proportional to the insulation thickness. Thicker insulations are thus measured with less sensitivity than thinner ones.

#### 3.1.4 PD signal characteristics

A PD pulse in a dielectric gives rise to an electromagnetic pulse (after the cavity collapses) with a rise time in the ns range and a pulse width in the range of 1.5 ns. The resulting voltage pulse propagates in both directions away from the PD source. The optimum bandwidth for detection of such a “fast” pulse is in the range of 300 MHz. Discharge from electrical trees in aged solid dielectrics often takes the form of a cascade of such fast pulses. In aged cavities, the PD pulse can broaden to have a rise time of up to several tens of ns and a pulse width up to some hundreds of ns. For such a broad pulse, a bandwidth in the range of 10 MHz is sufficient [42].

Empirical evidence suggests that the frequency spectrum is bounded for a specific dielectric. Results show that air discharges radiate the majority of their energy at frequencies below 200 MHz, whereas discharges in oil or SF<sub>6</sub> (stronger dielectrics) have a broader spectrum extending up to 1 GHz [43]. Generally the frequency components of a PD produced in extruded and impregnated laminar dielectric cables (or CCs) range from 200 kHz to the GHz region. However, all shielded power cables and CCs have substantial high frequency attenuation that increases the pulse width and decreases the pulse amplitude as a function of distance propagated, which also limits the optimum signal detection bandwidth [44], [45]. The PD propagation characteristics have been studied using a numerical electromagnetic analysis in reference [46]. Based on this work, Toshiba is said to have developed a sensing (fault location) system for a gas-insulated substation.

The PD data transferred need to be processed to obtain the PD characteristics such as peak value, apparent charge, phase position, repetition rate, and PD energy. The PD signal attenuates during its propagation and it gives rise to certain critical detection issues, such as sensor locations and sensitivity, measurement system response to attenuated signals, and noise detection and elimination.

## 3.2 Conventional PD detectors and their limitations

When a PD occurs, a current pulse is produced and this current pulse interacts with the insulation capacitance as well as the external elements in the test circuit. Consequently, a voltage pulse is superimposed on to the HV supply voltage. The conventional detection methods generally employ matching impedance consisting of resistors, inductors and capacitors in the PD current path. The measuring resonant circuit expands the discharge current pulses in the time domain for easier detection. In the event of PD taking place, a quantitative parameter is required to decide whether the apparatus needs to be repaired or replaced. This means that the detected signal needs to be accurately calibrated. In most cases, calibration is done by injecting a known amount of charge and measuring the voltage amplitude from the detector. There are following two different methods of conventional PD investigation [47].

- i) Straight detection including direct and indirect methods
- ii) Balance detection method (bridge circuit)

The conventional PD detection technique can identify discharges in short isolated cable lengths only. Unfortunately, it has insufficient sensitivity for a long circuit because of the large capacitance involved. It is also required to isolate the cable from the circuit. PD testing requires, besides the PD detector, additional HV components such as a test-voltage supply and a coupling capacitor, which are heavy and expensive and not suitable for on-site tests [48]. The capacitor is a very high impedance to the high ac voltage, while being a very low impedance to the high frequency PD pulse currents. The PDs are detected via a high-pass filter established by this capacitor and the resistive measuring impedance [24]. This method has two main disadvantages for on-line application:

- a) Since the HV capacitors have to be connected to the phase conductors, the cable has to be switched off, and power delivery is interrupted.
- b) The HV capacitor has to be connected for a long measuring time, or even permanently. HV capacitors are not always reliable in the long term and can, therefore, become a cause of faults themselves [24].

Instead of installing a lumped component, capacitive coupling can also be realized through a metal electrode, e.g., a plate can be installed at a certain distance from a phase conductor. The obtained capacitance, however, is now highly dependent on the geometry of the substation, cable termination, and positioning of this electrode. Furthermore, the capacitance is relatively low. In modern substations, a capacitor is sometimes integrated in the switchgear to detect the power frequency voltage on each phase conductor. The use of this capacitor for measuring small signals like PDs is in practice hard, due to its small value (usually <100pF). Moreover, this method would not be very universal, since it depends on the presence of this particular type of switchgear. In short, these conventional techniques experience severe limitations when it comes to on-line monitoring due to the influence of background noise, absence of non-intrusive sensors and processing facilities. They are, therefore, restricted to testing in a laboratory environment.

Recent studies have shown that radiation from PDs is impulsive in nature and consists of individual high-energy, wideband impulses of a few  $\mu\text{s}$  in length. The digital storage oscilloscopes and advanced digitizers enable study of the PD signals more closely using window processing, zooming and auto-advance features. Such techniques promise to be superior to the currently used conventional PD detector methods. Additional benefits may be gained if monitoring can be performed as a continuous on-line measurement with automatic PD data analysis [49]. Costs and need for personnel expertise are reduced and the reliability of condition assessment is improved [50]. Recently, the PD detection frequency range has been extended up to the radio frequency band with the development of new sensors e.g., Rogowski coils.

### 3.3 Rogowski coil as a PD sensor

In 1912, the Rogowski coil was introduced to measure magnetic fields. Since the coil output voltage and power were not sufficient enough to drive measuring equipments, it has been widely used for measuring fast, high-level pulsed currents in the range of a few mega-amperes rather than in power system [51]. With the improvement of today's microprocessor-based protection relays and measurement devices, the Rogowski coils are more suitable for such applications. They have generally been used where other methods are unsuitable [52]. They have become an increasingly popular method of measuring current within power electronics equipment due to their advantages of low insertion loss and reduced size as compared to an equivalent CT [53]. They are the preferred method of current measurements having more suitable features than CTs and other iron-cored devices.

The coils have also been used in conjunction with protection systems particularly high accuracy systems or where there are direct current (DC) offsets which would degrade the performance of CTs. This is useful when measuring the ripple current, e.g., on a DC line. The features of the Rogowski coils which make them particularly useful for transient measurements stem from their inherent linearity and wide dynamic range.

#### 3.3.1 Construction of Rogowski coil

A Rogowski coil is basically a low-noise, toroidal winding on a non-magnetic core (generally air-cored), placed around the conductor to be measured, a fact that makes them lighter and smaller than iron-core devices.

To prevent the influence of nearby conductors carrying high currents, the Rogowski coil is designed with two wire loops connected in electrically opposite directions [30]. This will cancel all electromagnetic fields coming from outside the coil loop. The first loop is made up of turns of the coil, and the other loop can be formed by returning the wire through the centre of the winding as shown in Fig. 3.3, where  $d_1$ ,  $d_2$ , and  $d_{rc}$  are the internal, external, and net diameters of the Rogowski coil, respectively. The coil is effectively a mutual inductor coupled to the conductor being measured and the output from the winding is an electromotive force proportional to the rate of change of current in

the conductor. This voltage is proportional to the current even when measuring complex waveforms, so these transducers are good for measuring transients and for applications where they can accurately measure asymmetrical current flows.

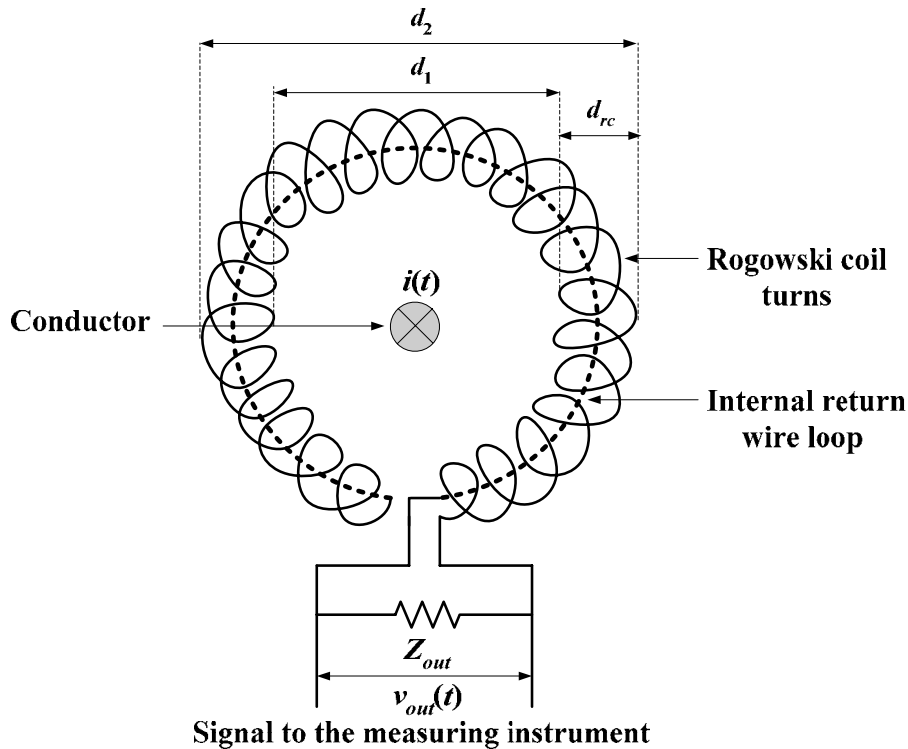


Fig. 3.3 Geometry and construction of the Rogowski coil

The self inductance of the coil is fixed, and its mutual inductance with the HV test circuit varies to some extent (or slightly) depending on the position of the coil in relation to the conductor. But once the coil is clamped and held stationary, the mutual inductance remains constant. Usually the coil is not loaded and the voltage appearing across it is used as PD measurement signal. Under this condition, the coil voltage is directly proportional to the derivative of the current in the conductor. Owing to the small value of the mutual inductance it acts as a high pass filter; the sensor, therefore, attenuates the power frequency component of the current in the conductor and minimizes EMI at lower frequencies. However, the PD signals are in the range of MHz generally and induce sufficiently large voltage in the range of mV.

The coils are designed to give a high degree of rejection to external magnetic fields, e.g., from nearby conductors. The coils are wound either on a flexible former, which can then be conveniently wrapped around the conductor to be measured or are wound on a rigid former, which is less convenient but more accurate. Both of these transducer types exhibit a wide dynamic range, so the same Rogowski coil can often be used to measure currents from mA to kA. They also exhibit wideband characteristics, working well at frequencies as low as 0.1 Hz, but are typically useful up to hundreds of kHz, too. All this with low

phase error and without the danger of open-circuited secondary (as could happen in case of CT). A typical mutual inductance of a standard flexible Rogowski coil (used in this research work) is up to 200-300 nH and its resonant frequency lies in the high frequency spectrum [31], [54].

### 3.3.2 Working principle of Rogowski coil

The Rogowski coil operates on the basic principle of Faraday's law. The air-cored coil is placed around the conductor, where current pulses produced by PDs are to be measured. This variable current produces a magnetic field and the rate of change in current induces a voltage in the coil given as:

$$v_{rc}(t) = -M \frac{di(t)}{dt} \quad (3.6)$$

where  $v_{rc}(t)$  is the voltage induced in the coil by the current  $i(t)$  flowing in the conductor due to the mutual inductance  $M$  between the main current and the coil, which is practically independent of the conductor location inside the coil loop.

For simplified analysis, the behavior of the Rogowski coil with terminating impedance  $Z_{out}$  can be represented by its equivalent circuit of the lumped parameters as shown in Fig. 3.4 [55], where  $R_l$ ,  $L_l$ , and  $C_l$  are the lumped resistance, inductance, and capacitance of the coil, respectively. The high frequency behavior of the coil, in particular its bandwidth and susceptibility to high frequency oscillations, is significantly influenced by the terminating impedance  $Z_{out}$ . There is a trade-off between the bandwidth and the sensitivity of the coil. The transfer function ( $V_{out}/V_{rc}$ ) of the Rogowski coil lumped parameters model (see Fig. 3.4) can be calculated as:

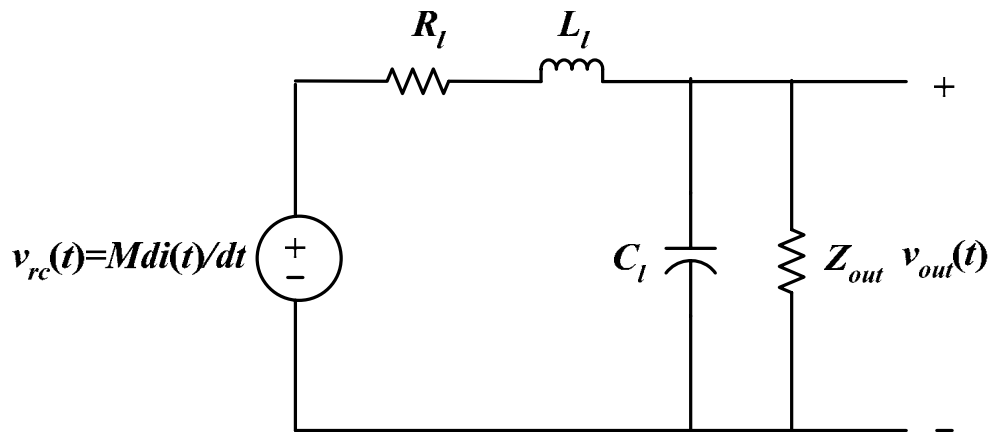


Fig. 3.4 The Rogowski coil equivalent circuit (lumped parameters model)

$$\frac{V_{out}}{V_{rc}} = \frac{Z_{out}}{s^2 L_l Z_{out} C_l + s(L_l + R_l Z_{out} C_l) + (R_l + Z_{out})} \quad (3.7)$$

Usually the air-cored coil is used in combination with large load impedance, i.e.,  $\omega L_l \ll Z_{out}$ .  $\omega$  is the angular velocity (rad/s), where  $\omega = 2\pi f$ , and  $f$  is the frequency (Hz) of the propagated signal. By assuming that the Rogowski coil has negligible resistance, the approximate measured voltage at terminals becomes:

$$v_{out}(t) \approx v_{rc}(t) \approx -M \frac{di(t)}{dt} \quad (3.8)$$

So the output voltage at the terminals of the winding wound around the toroidal coil is proportional to the time derivative of the current flowing in a conductor passing through the coil. An integrator is incorporated with the coil, which integrates the output voltage  $v_{out}(t)$  according to the following equation to convert it into the current following through the conductor,

$$i(t) = -\frac{1}{M} \int v_{out}(t) dt \quad (3.9)$$

The components of a flexible Rogowski coil i.e., the toroidal coil and integrator are shown in Fig. 3.5, which has been used in this research work. However, the Rogowski coil without integrator has been used to capture directly the voltage signals produced due to PDs.



Fig. 3.5 Components of a flexible Rogowski coil, make FLUKE i2000flex [56]

### ***3.3.3 Advantages of using Rogowski coil***

In the conventional PD sensor, the test circuit capacitance determines the frequency bandwidth and it is usually not very wide compared with this sensor. The frequency bandwidth of the Rogowski coil is not influenced by the capacitance of the test circuit. It is determined largely by the self inductance and the capacitance of the coil and signal cables. It has the following advantages:

- i) The frequency response of the Rogowski coil sensor is very wide.
- ii) There is no conductive coupling between the coil sensors and the HV test circuits. Furthermore, the coil installation does not necessitate disconnection of the grounding leads of the test objects and therefore becomes a non-intrusive sensor which is a very important aspect for on-site, on-line monitoring.
- iii) It has the advantage of possessing high signal to noise ratio (SNR) with wide frequency bandwidth.
- iv) There is no saturation due to air-cored coil; therefore, it is not damaged by over current.
- v) It has very good linearity due to the absence of magnetic materials.
- vi) The Rogowski coil based PD measurement system is a low cost solution and can be easily implemented on-site due to its light weight.

These advantages are essential for on-line PD measurements; therefore, the Rogowski coils are preferred over conventional PD sensors to take measurements for detecting falling trees on CC overhead distribution lines.

## **3.4 Significance of on-line PD detection in CC lines**

The CC lines have been used in MV networks throughout the world since long. One compelling reason to use CC lines is that they are more compact and environment-friendly than bare conductors. The CC line also withstands clashing and fallen trees for a considerable time without interruption to the power supply. In this way, the line can continue to function despite the tree contact and the removal of the trees can be scheduled appropriately. A drawback of CC lines in distribution networks is that falling trees on the line can neither be detected with normal protection relays nor be localized by advanced high impedance relays because the fault current is approximately nothing due to the CC insulation and tree resistances. However, these leaning trees produce PDs in the insulation of the CC lines as mentioned in the previous chapter, which may rupture after the passage of a certain time, resulting in different kind of faults being introduced into the network. By monitoring these PDs on-line, progressive deterioration of the insulation can be indicated. Early detection of developing faults leads to better power quality and increased customer satisfaction. PD monitoring involves an analysis of materials, electric fields, arcing characteristics, pulse wave propagation and attenuation, sensor spatial sensitivity, frequency response, calibration, noise, and data interpretation.

For electric power distribution industries, continuous monitoring of installed and operating HV apparatus is of particular importance from the point of view of safety and reliability. The relatively new and challenging application is conducting on-line high frequency PD measurements for the monitoring of falling trees on the CC overhead distribution lines [57]. The advantage of on-line PD monitoring allows for conductor insulation diagnostics during normal operation, and specifically, when the trees are leaning on the conductors. The falling trees produce PDs, whose magnitude increases when trees cause the surface of the conductors to deteriorate. Automatic detection of the falling trees will reduce visual inspection work after storms and it will improve reliability and safety of the distribution system. Recently, a great interest has been shown by electric utilities using CC system in distribution networks in Finland to develop an on-line automatic system that should be capable of detecting falling trees on the lines. The system can be planned to be integrated into the distribution automation system to reduce the overall costs of the CC lines [27].

For the development of the on-line PD measuring system using a Rogowski coil to detect falling trees on the CC lines, the following few experiments were conducted to investigate the PD wave propagation over the CC line as well as to analyze the behavior of the Rogowski coil for high frequency measurements.

### 3.5 Experimental set-up

An experimental set-up was arranged in the HV laboratory at TKK. A single-phase CC line was laid at a certain height ( $\approx 3$  m) above the ground level, and the return path was provided through the ground. The experimental system consisted of:

- i) CC having length of 29.2 m, 10 mm inner diameter of the aluminum conductor and 14.5 mm outer diameter along with HDPE insulation
- ii) Flexible Rogowski coil (without integrator) mounted around the CC
- iii) A pine tree leaning on the conductor to simulate a real world situation
- iv) Pulse calibrator, for calibrating the PD measuring system
- v) Digital oscilloscope, model Lecroy 9384TM
- vi) Computing system (laptop) for data acquisition
- vii) Grounding capacitor  $C_g$  of magnitude 500 pF, for connecting conductor-end to the ground, and
- viii) HV power supply, 20 kV (line-to-line) AC

Figs. 3.6, 3.7, and 3.8 depict an on-line single-phase PD measuring set-up. The Rogowski coil is looped around the CC line to capture the PD signals produced by the pulse calibrator and due to a leaning pine tree when the line is energized as shown in Fig. 3.6. The PD signals are displayed on the oscilloscope and the data is stored for further processing and features extraction. The 20 kV AC power is supplied by a step-down transformer as shown in Fig. 3.7. The close-up view of the leaning pine tree can be seen in Fig. 3.8. The height of the CC line is not fixed at all points because it is looped with the supporting ropes. Moreover, the CC line comes nearer to the ground at the point where the tree is leaning on it.

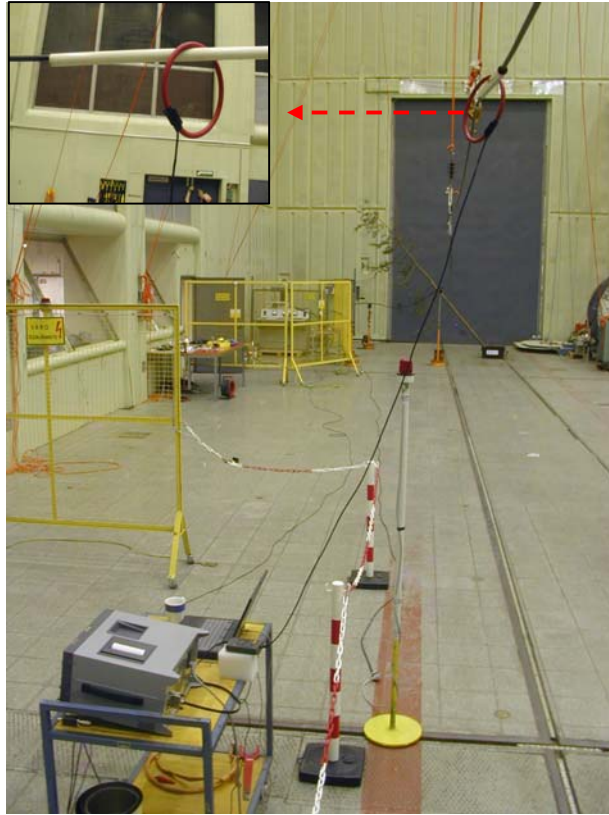


Fig. 3.6 On-line single-phase PD measuring set-up



Fig. 3.7 Application of 20 kV AC supply for energizing conductor



Fig. 3.8 A pine tree leaning on the CC line

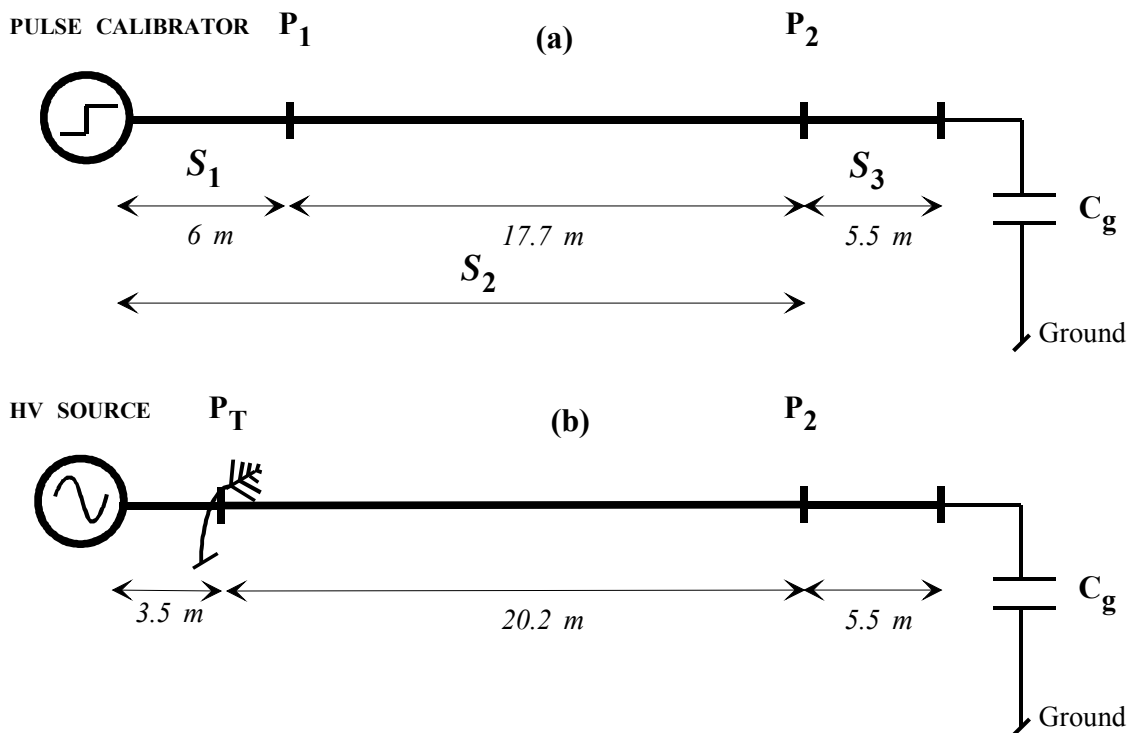


Fig. 3.9 Single-line diagram for on-line PD measuring system with:  
(a) pulse calibrator, (b) HV 20 KV supply

Two sets of PD measurements are performed on the CC line. First, for calibrating the PD measuring system, a pulse of known magnitude is injected into the conductor by a pulse calibrator, and the Rogowski coil measurements are taken at points  $P_1$  and  $P_2$ , as shown in Fig. 3.9 (a). Second, the conductor is energized with 20 kV distribution voltage, trees are leaned at point  $P_T$  on the conductor, and the Rogowski coil measurements are taken at point  $P_2$  as shown in Fig. 3.9 (b). The distances of the measuring point  $P_1$  and tree leaning point  $P_T$  from the sources have been taken randomly; these do not affect the performance of measurements in general.

### 3.6 PD measurement methodology

The PD data captured by the Rogowski coil is essentially an oscillatory voltage pulse, which needs to be processed to obtain PD characteristics such as peak value, apparent charge, phase position, repetition rate, and PD energy. The apparent charge  $q(t)$  entering into the system due to PDs is given as:

$$q(t) = \int i(t)dt = -\frac{1}{M} \int \int v_{out}(t) dt^2 \quad (3.10)$$

where  $v_{out}(t)$  is the oscillating voltage appearing at the output terminals of the sensor,  $M$  is the mutual inductance of the Rogowski coil (which is taken as 200 nH in this case), and  $i(t)$  is the current flowing in the conductor due to PDs.

The fast Fourier transforms (FFTs) of the acquired pulses show the spectrum of frequency contents present in the signals. An infinite impulse response (IIR) band-pass filter (Butterworth type) of order 16 having frequency band (1-6 MHz), depending on the frequency contents of the interferences and disturbances in the signal, is applied for noise elimination. Using the above steps and mathematical expression of equation (3.10), the following Simulink model can be used to measure the PD magnitude by the Rogowski coil (see Fig. 3.10).

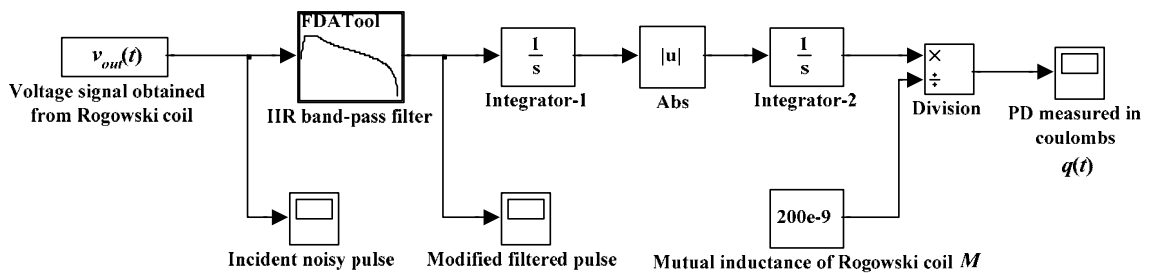


Fig. 3.10 Simulink model for PD measurements

If the Rogowski coil geometry is not symmetrically positioned around the CC line, the experimental results are logically influenced, however, no significant effect has practically been found in time or frequency domain behavior measurements (see Fig. 3.11). It proves that the mutual inductance of the coil is independent of its position around the CC line. Therefore, a constant value of  $M$  (200 nH) is used in the calculations. In Fig. 3.11, the symmetrical geometry is defined when the CC line is in the middle of the Rogowski coil, and asymmetrical geometry is defined when the Rogowski coil is touching the surface of the CC line insulation.

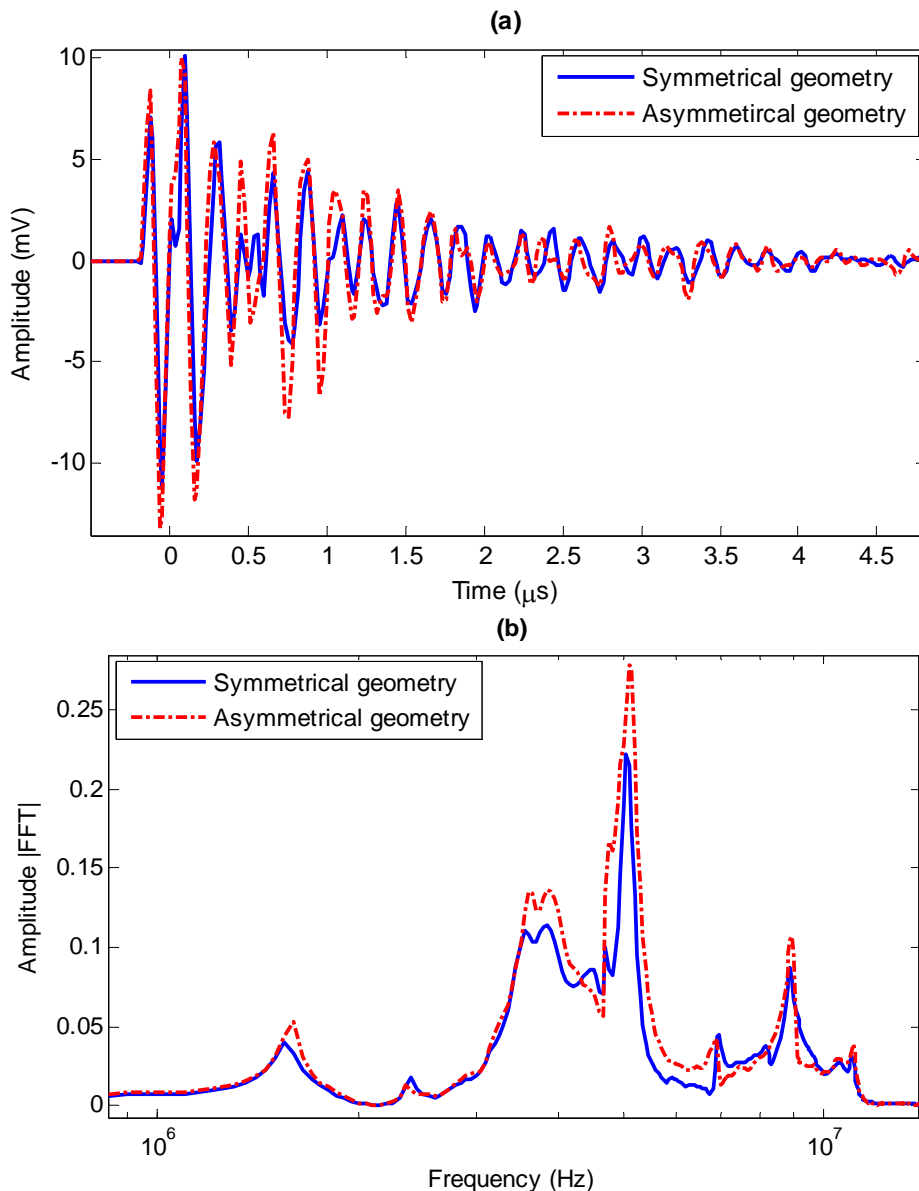


Fig. 3.11 Rogowski coil responses for 5 nC calibrator pulse at point  $P_2$  for its different geometries around the CC line; (a) time domain, (b) frequency domain

### 3.7 PD Measurements and results

In order to establish the relationship between the magnitude of a discharge in the sample and the signal received, calibration is always required. Conventionally, this can be done by connecting a standard discharge calibrator across the sample, usually before testing [47]. A rectangular step voltage of amplitude  $V_0$ , in series with a small known capacitance  $C_0$ , is connected to one end of the sample. The charge injected into the sample is equivalent to a discharge of magnitude  $Q_0$  given as:

$$Q_0 = C_0 V_0 \quad (3.11)$$

As the injected charge between the conductor and shield is known, the calibration factor  $k$  which is the ratio of PD measurement voltage output,  $V$ , and the injected charge,  $Q_0$ , can be calculated as:

$$k = \frac{V}{Q_0} = \frac{V}{C_0 V_0} \quad (3.12)$$

A linear relationship between the discharge magnitude and the signal received from the sensor is obtained, indicating a constant  $k$ . This method is suitable for laboratory tests where a short piece of sample is often encountered. However, detecting PDs on the CC lines is a different scenario where very long lines are investigated in real systems. The effect of on-line/on-site interferences and disturbances are also taken into account and the actual measurements must be de-noised to get the reliable PD detection results. Therefore, the applicability of conventional calibrating systems is limited and the calibration of the on-line PD measuring system is carried out on the basis of actual measuring system (depicted in Fig. 3.10).

#### 3.7.1 Calibration of on-line PD measuring system

A 50 nC calibrator pulse is sent from one end of the conductor and the Rogowski coil measurements are taken at points  $P_1$  and  $P_2$ , at the distance of 6 and 23.6 m from the point of the insertion of the calibrator pulse, respectively. These measurements are taken to calibrate the measuring system. The voltage pulse captured by the Rogowski coil sensor at point  $P_1$  for the 50 nC calibrator pulse is shown in Fig. 3.12. This pulse is taken and is padded with zeros up to the length  $N=2^n$  for  $n=16$  ( $N=65536$  points) and its FFT is drawn in Fig. 3.13. A time step of  $\Delta T=20$  ns is used in the Fourier analysis. From the FFT, it is clear that the dominant contents of the signal lie in the frequency range from 1-4 MHz and noise can also be seen in higher frequency ranges. The noise is removed by implying an infinite impulse response (IIR) band-pass filter (1-4 MHz). The pulse becomes smoother after noise suppression as shown in Fig. 3.14. The de-noised pulse is processed in the Simulink model to determine the quantity of the PDs.

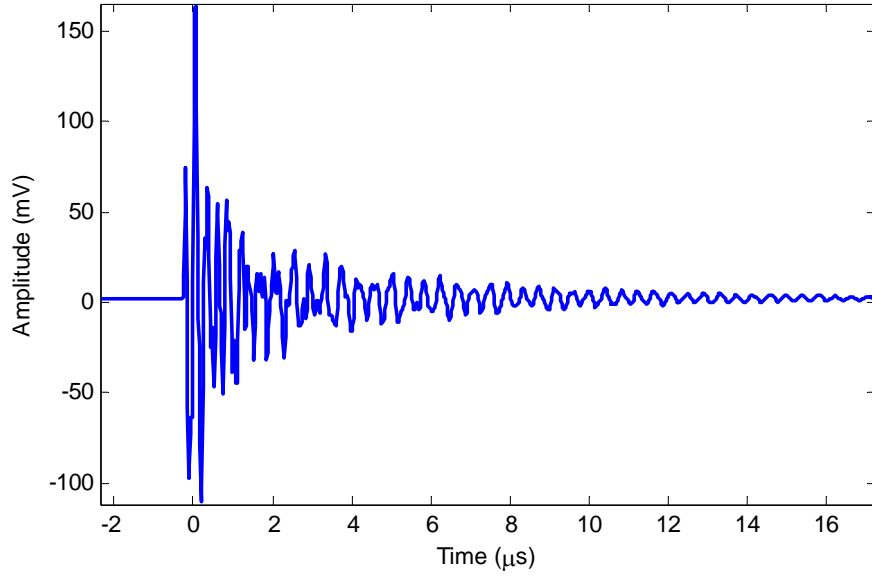


Fig. 3.12 The Rogowski coil voltage response for 50nC calibrator pulse at  $P_1$

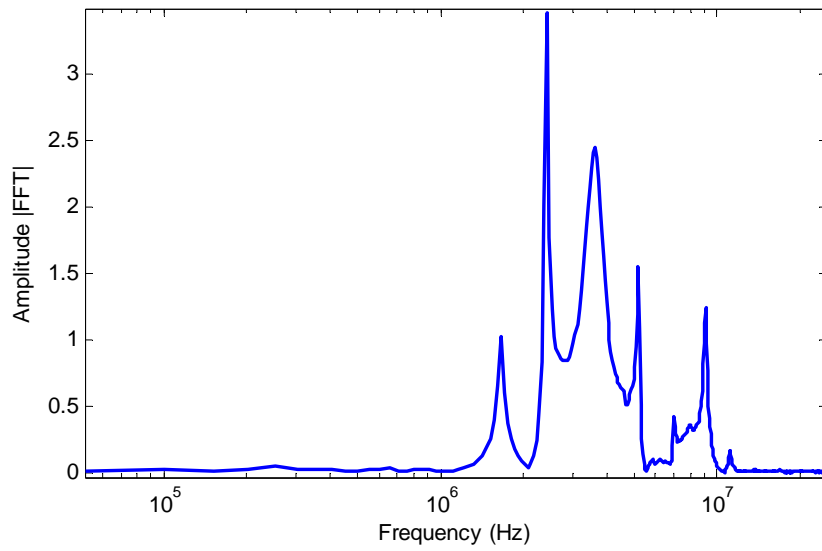


Fig. 3.13 FFT of the Rogowski coil voltage for 50nC calibrator pulse at  $P_1$

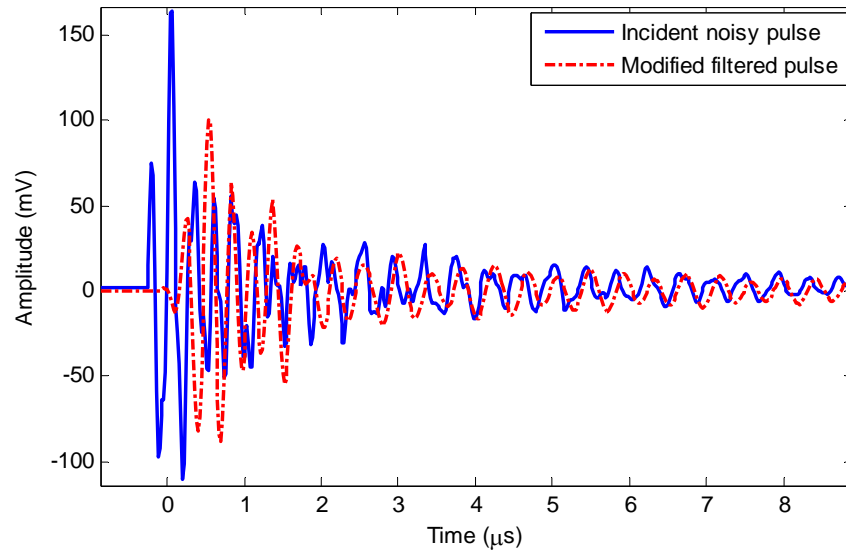


Fig. 3.14 The Rogowski coil voltage responses before and after filtering for 50nC pulse at  $P_1$

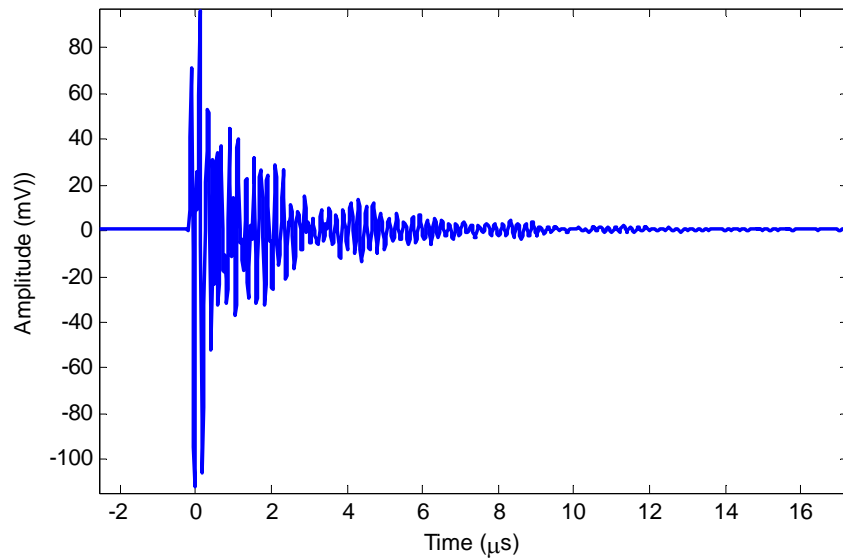


Fig. 3.15 The Rogowski coil voltage response for 50nC calibrator pulse at  $P_2$

The 50 nC calibrator pulses captured by a Rogowski coil at point  $P_2$  in the time and frequency domain are shown in Figs. 3.15 and 3.16, respectively. The PD measured for 50 nC pulse calibrator charge at  $P_1$  (37 nC) and  $P_2$  (10 nC) using Simulink model of Fig. 3.10 are shown in Fig. 3.17.

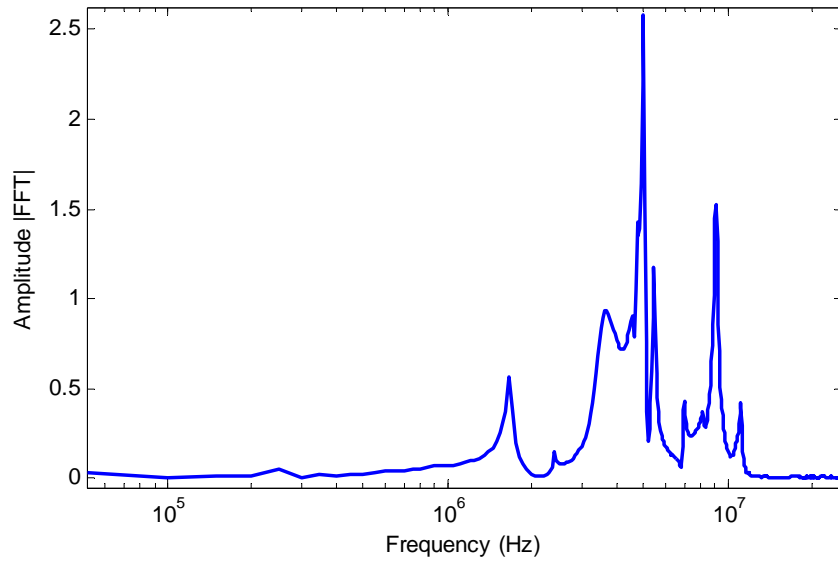


Fig. 3.16 FFT of the Rogowski coil voltage for 50nC calibrator pulse at  $P_2$

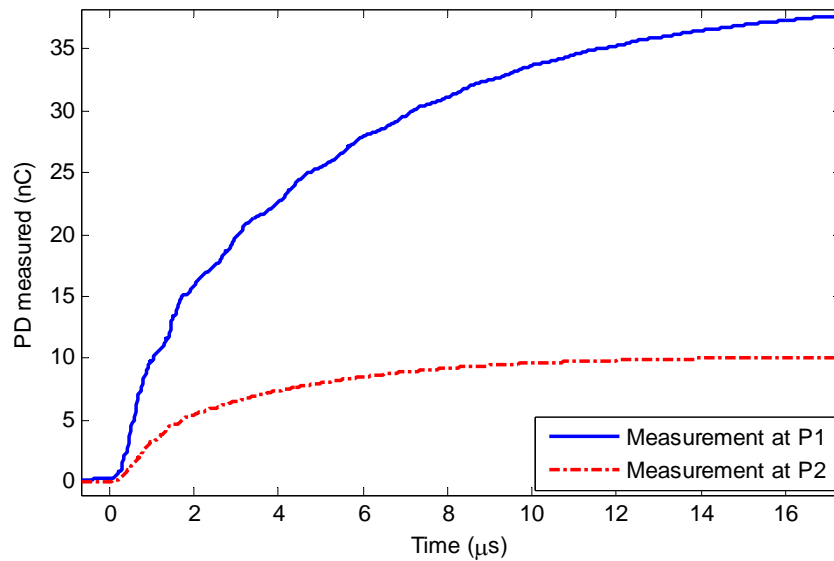


Fig. 3.17 PD measurements for 50nC calibrator pulse at  $P_1$  and  $P_2$

The different values of PDs measured at different locations can be explained by the phenomenon of attenuation of PD signals when traveling along the conductor. The voltage pulses at different points on the conductor, i.e.,  $v_1(t)$  and  $v_2(t)$  at  $P_1$  and  $P_2$  respectively, have different amplitudes (see Fig. 3.18) decreasing towards the downstream. This clearly indicates the attenuation of the PD signals while transmitting through the conductor.

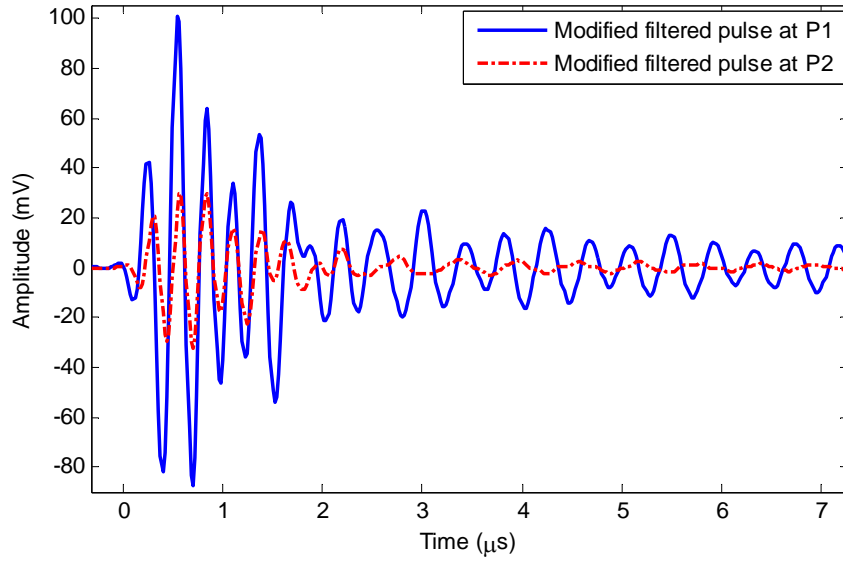


Fig. 3.18 Effect of signal attenuation for the Rogowski coil voltage responses

The conservation of charge implies that the measured charge is only reduced by the amount of the attenuation  $\alpha(\omega)$ , the same value for voltage attenuation because voltage=charge/capacitance, provided the capacitance of the line is assumed to be constant. By taking the FFTs of the voltage waveforms shown in Fig. 3.18,  $\alpha(\omega)$  can be calculated using the following expressions:

$$\left| \frac{V_2(\omega)}{V_1(\omega)} \right| = e^{-\alpha(\omega)17.7} \quad (3.13)$$

$$\alpha(\omega) = -\frac{1}{17.7} \cdot \ln \left| \frac{V_2(\omega)}{V_1(\omega)} \right| \quad (3.14)$$

where  $V_1(\omega)$  and  $V_2(\omega)$  are the FFTs of the Rogowski coil measured filtered voltage waveforms (see in Fig. 3.18) at points P<sub>1</sub> and P<sub>2</sub>, respectively, which are separated at a distance of 17.7 m from each other.  $\alpha(\omega)$  is given in Np/m.

The attenuation of the PD signals (in dB/m) traveling along the conductor is calculated using above expressions and its frequency-dependent behavior is drawn in Fig. 3.19. At lower frequencies, attenuation is constant (0.21 dB/m). However, it increases by increasing the frequency of the propagated signals in high frequency range. Oscillations are observed at higher frequencies because the voltage waveforms  $v_1(t)$  and  $v_2(t)$  are oscillatory in nature due to the behavior of the Rogowski coil. Therefore, this method is not useful to calculate the attenuation of the signals in the frequency range of 1-6 MHz. This technique gives better results at higher frequencies if the voltage waveforms are impulsive in nature.

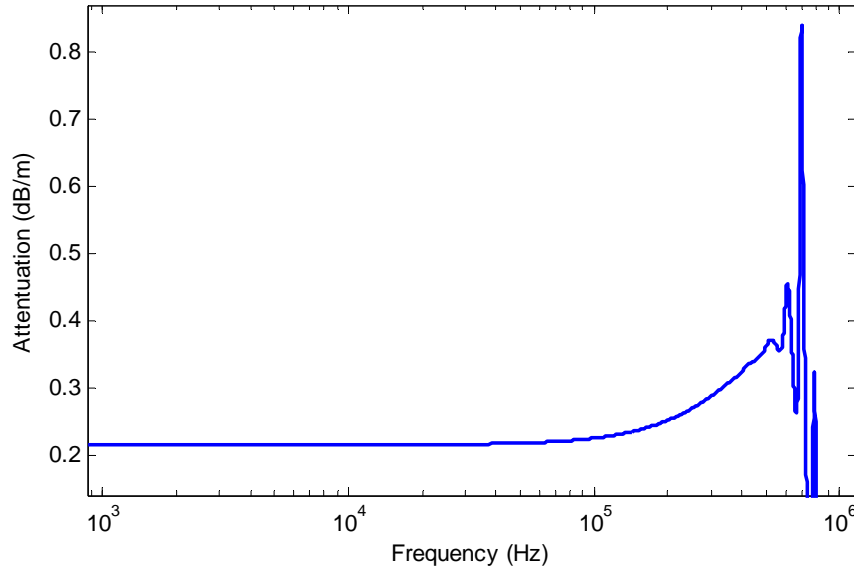


Fig. 3.19 Dependency of signal attenuation on frequency

Another approximation to calculate the average value of the attenuation in this bandwidth (1-6 MHz) is to use the PD magnitudes at points  $P_1$  and  $P_2$  (see Fig. 3.17) in the following expression:

$$\alpha(\Delta\omega) = -\frac{1}{17.7} \cdot 20 \cdot \log \left| \frac{q_2(t)}{q_1(t)} \right| \quad (3.15)$$

where  $|q_1(t)|$  and  $|q_2(t)|$  are the magnitudes of charges at  $P_1$  (37 nC) and  $P_2$  (10 nC), respectively, and  $\Delta\omega$  is the required frequency band. For 50 nC calibrator pulse, the value of the charge attenuation  $\alpha(\Delta\omega)$  is 0.64 dB/m. As the calibrator is kept at 6 m away from the point  $P_1$ , the actual magnitude of charge produced by the calibrator pulse,  $|q_c(t)|$ , can be calculated as:

$$|q_c(t)| = -|q_1(t)| \cdot \frac{1}{\log^{-1} \left[ \frac{\alpha(\Delta\omega)6}{20} \right]} \quad (3.16)$$

The above mentioned practice is revised for different magnitudes of calibrator pulses to calibrate the PD measuring system and the details are given in Table 3.1. It is revealed that calculations made on the basis of actual measurements taken by the Rogowski coil have a good agreement with the pulse calibrator charges; however, they do not exactly match. The reason for these small errors can be due to using approximate value of the attenuation (e.g., 0.64 dB/m for 50 nC calibrator pulse) for a frequency band of 1-6 MHz, while it is changing continuously by changing the frequency of the signal. This can also be possible due to the addition of unwanted signals (noise) from the laboratory

environment or EMI with the actual measuring signals. The other possible reason can be due to the fact that the measurements taken at point  $P_2$  may include the reflections from the load-end of the conductor due to the mismatch between the characteristic impedance of the conductor and capacitive reactance of the grounding capacitor. Fig. 3.20 depicts the variations of an on-line PD measuring system calibration from an ideal system calibration. Designing an EMTP-ATP model of the experimental set-up may give information about the actual source of this error. TDR measurements taken on the CC would also give an exact value of the attenuation of the signals over a wide range of frequency, thus eliminating errors in the PD measurements.

TABLE 3.1 CALIBRATION OF PD MEASURING SYSTEM

Calibrator pulse (nC)	PD magnitude at $P_1$ (nC)	PD magnitude at $P_2$ (nC)	Charge attenuation (dB/m)	Estimated calibrator charge (nC)	%age error
2	1.3	0.3	0.70	2.2	+10%
5	3.8	1.0	0.66	6.0	+20%
10	7.0	2.0	0.62	10.7	+7%
20	14	4.0	0.62	21.4	+7%
50	37	10	0.64	57.7	+15%

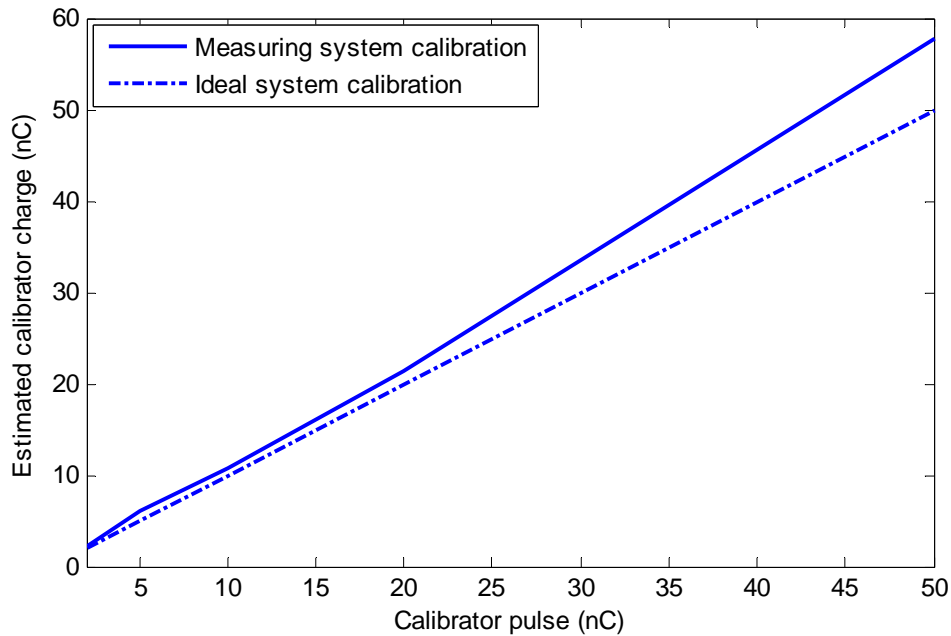


Fig. 3.20 Calibration of on-line PD measuring system

### 3.7.2 HV measurements

The HV measurements are made by applying 20 kV distribution voltage to the conductor. The leaning trees are placed at a distance of 3.5 m (at  $P_T$ ) from the point of input of the HV supply, and measurements are taken using a Rogowski coil at point  $P_2$ , as depicted in Fig. 3.9 (b). The knife traces, passed through the conductor jacket, are impressed artificially at point  $P_T$  to simulate the actual condition when the leaning trees may cause the conductor insulation to deteriorate with the passage of a certain amount of time. The HV measurements are taken by a Rogowski coil at point  $P_2$ , under the following specific arrangements:

- a) Knife traces are made on the conductor insulation
- b) A pine tree is leaning on the conductor
- c) Knife traces are made on the conductor insulation and a pine tree is leaning on the conductor (see Fig. 3.21)
- d) Knife traces are made and two pine trees are leaning on the conductor

The Rogowski coil voltage response for HV measurement (c) is shown in Fig. 3.22 and its FFT is drawn in Fig. 3.23. It is revealed that dominant frequency contents lie in the frequency range from 1-6 MHz.

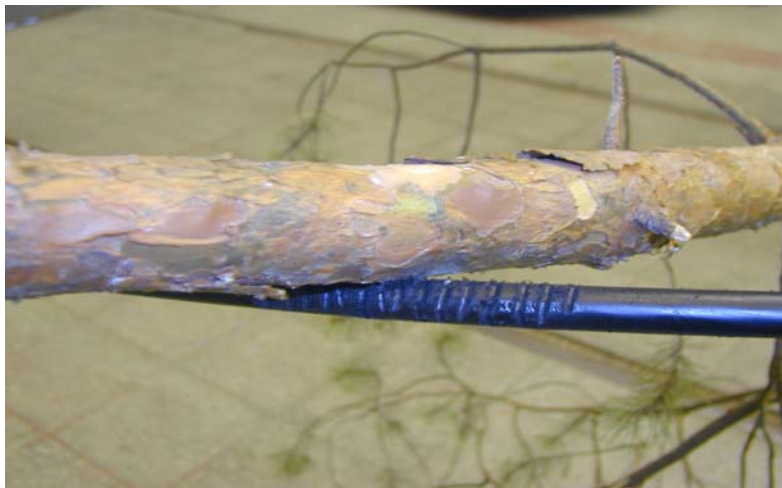


Fig. 3.21 A pine tree is leaning and knife traces are made on the conductor insulation

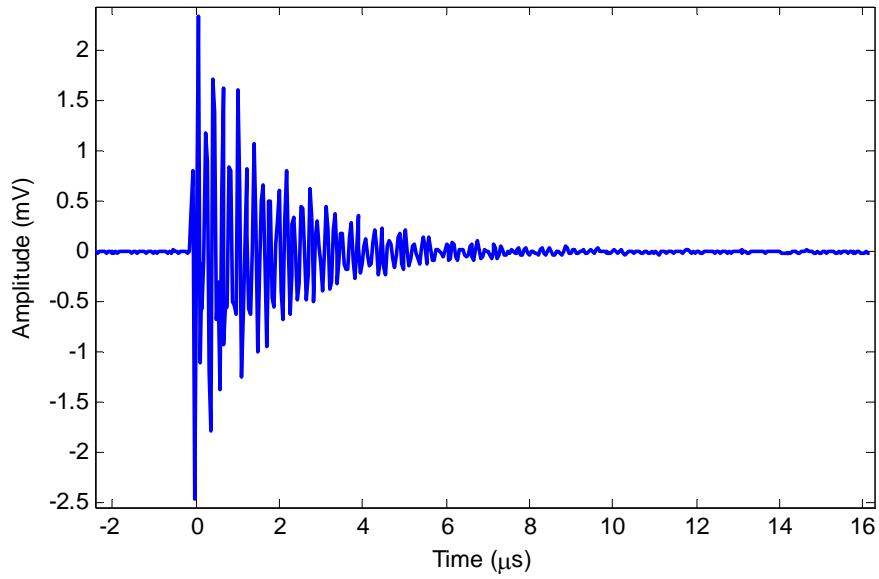


Fig. 3.22 The Rogowski coil voltage response for HV measurement (c)

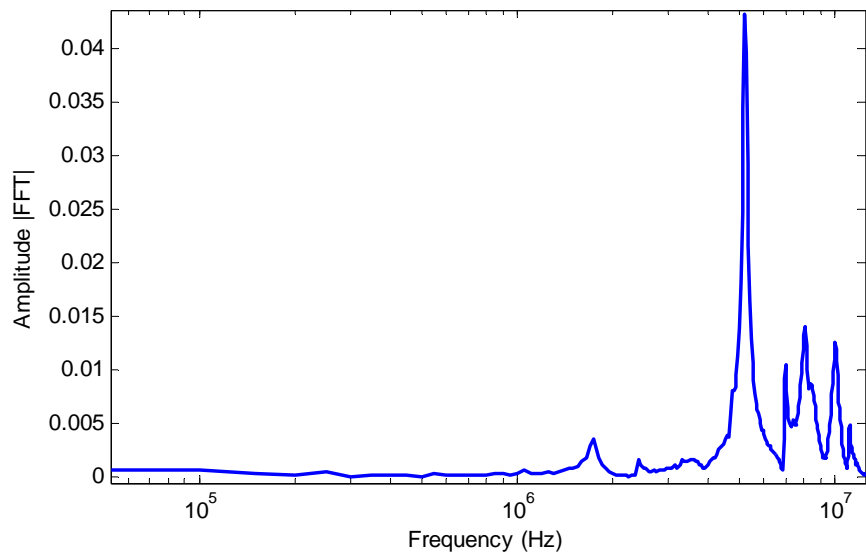


Fig. 3.23 FFT of the Rogowski coil voltage for HV measurement (c)

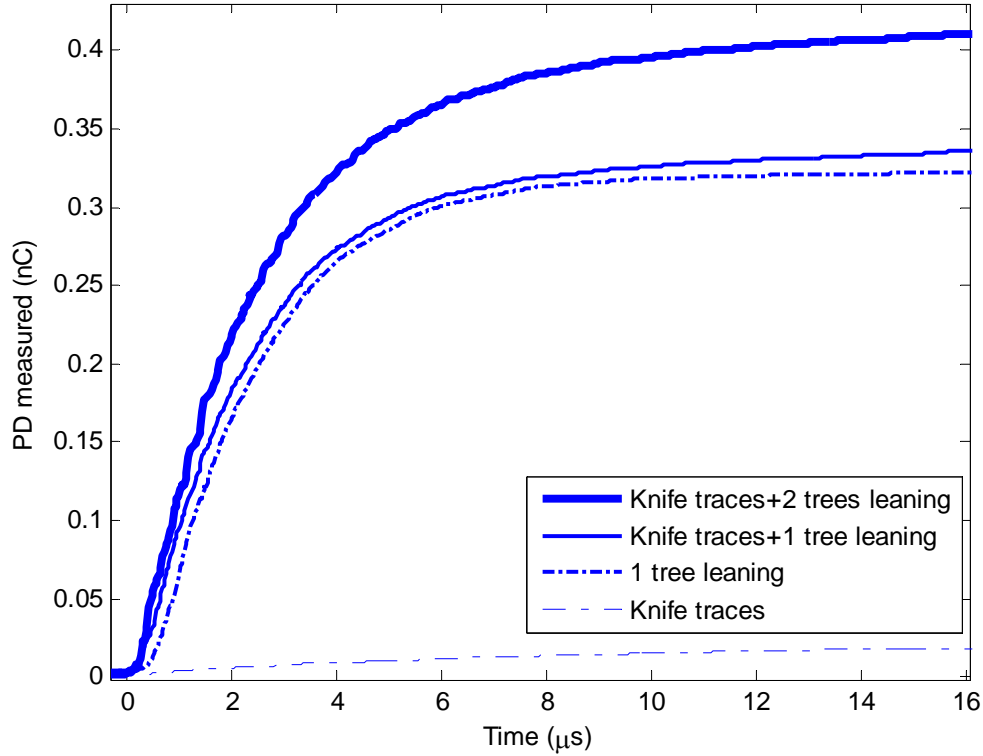


Fig. 3.24 The Rogowski coil HV measurements at point  $P_2$

The PD magnitudes for HV measurements using a Rogowski coil at point  $P_2$  are shown in Fig. 3.24. However, the given results are not the actual PD magnitudes due to falling trees on the CC line at point  $P_T$ . To convert the measured PD magnitudes into the actual PDs produced due to falling trees, the following equation can be used as:

$$|q_T(t)| = -2|q_2(t)| \cdot \frac{1}{\log^{-1}\left[\frac{\alpha(\Delta\omega)20.2}{20}\right]} \quad (3.17)$$

where  $|q_T(t)|$  is the magnitude of PDs at point  $P_T$  and  $\alpha(\Delta\omega)$  is taken as 0.65 dB/m (by considering the average charge attenuation from Table 3.1). The PD measured, e.g., by the Rogowski coil is 19 pC, when the knife traces are made on the surface of the conductor (see Fig. 3.24). The source of PD is at the distance of 20.2 m from the sensor, so the PD magnitude produced by the source is 86 pC. Since a PD results in both a forward and backward traveling pulse, this amount only corresponds to a fraction (factor 1/2 if the impedance to the left and right are equal) of the induced charge because only the forward traveling pulse has been considered [58]. So the actual amount of PD produced by knife traces is estimated to be 172 pC using (3.17). Similarly the PD magnitudes produced are 2.9, 3, and 3.7 nC when a pine tree without knife scratches, a pine tree with knife scratches, and two pine trees with knife scratches, respectively, are falling on the conductor at point  $P_T$ .

### 3.8 Discussion

A new on-line PD detection technique for the monitoring of falling trees on the CC overhead distribution lines has been presented. The Rogowski coil takes the measurements, when pulses of different magnitudes (charges) are sent by the pulse calibrator. The results show a good agreement between the actual and the measured quantities. The measurement results can be improved by impedance matching on the load-end of the conductor, as well as by improving the band-pass filter design so that it can identify and distinguish PD signals from noise and corona discharges. The HV test results show that by increasing the numbers of falling trees, the PD quantities also increase. In addition, knife traces produce PDs. The PD signals initiated by different sources have different frequency ranges ( $>1$  MHz) and this observation is important for the design of a wireless PD sensor to detect falling trees on the CC lines; especially for the development of the low-power signal processing algorithm inside it.

The measurements conducted in the laboratory environment show that PD magnitude due to leaning of a pine tree is around 3 nC; however, this magnitude may vary between 3-10 nC as reported in [49]. The variation of PD magnitude as a function of various environmental parameters should also be deeply investigated in order to detect the leaning trees on CC lines using the proposed technique.

The two important aspects which have been investigated during the measurements are: the high attenuation of PD signals while propagating along the CC line; and the PD measurements at different locations which have different frequency bands, i.e., 1-4 MHz (at point  $P_1$ ) and 1-6 MHz (at point  $P_2$ ). It reveals the fact that PD propagation in a power network is a very complicated phenomenon and may result in characteristic resonance frequencies with attenuation depending on the distance from origin to the measuring location [59]. The deep investigation on the PD wave propagation in the coming chapters will explain more about these issues.

In order to estimate the maximum length of the CC line that can be monitored with one Rogowski coil sensor for detecting PDs due to leaning trees, the wave propagation characteristics of the line should be determined. The reliable PD detection depends upon the PD magnitude caused by the fault, the attenuation of the line, and the magnitude of the interference signals on the line. The amplitude of the PD pulse decreases and the pulse is distorted while traveling on the line due to attenuation phenomenon. As the PD pulse has short duration (in ns) compared to the length of the line, the propagation must be considered as a traveling wave problem. TDR measurements can be performed on a CC line to determine its wave propagation characteristics [60]. Therefore, the propagation of PD signals over the CC line can be investigated using these measurements.

## Chapter 4

### Determining Wave Propagation Characteristics of CC Line

*This chapter gives a general background of the TDR measurements, explaining the response of electrical networks in the time domain. The work concentrates on determining the wave propagation characteristics (propagation constants, i.e., attenuation and phase constants, and propagation velocity) of a CC line using high frequency measurements. For this purpose, the TDR measurement technique is applied. The measurement results show that the attenuation and the propagation velocity are frequency- dependent and these values become higher as the frequency of a signal goes up. These results can be used for designing and positioning of PD sensors for on-line PD detection in CC overhead distribution lines.*

#### 4.1 Significance of wave propagation characteristics

Any signal will lose some of its energy or signal strength as it propagates down the conductor. This loss is attenuation, which is frequency-dependent. Propagation velocity is a specification of the conductor indicating the speed at which a signal travels down through it. Different conductors have different propagation velocities. Typically, propagation velocity of a communication cable under test is listed in the cable manufacturer's catalogue. However, this figure for MV power cables or CC lines is not specified. In this case, a required procedure is to make a TDR measurement on a known length of the conductor. An even more accurate way to estimate propagation velocity is to make measurements from both ends of the conductor. Propagation velocity depends upon the phase constant and the frequency of the impressed signal.

The challenge for on-line PD measurements due to leaning trees on CC lines is to find the optimal locations for PD sensors with respect to their sensitivity, interference level, signal distinction, and universal applicability [61]. PD pulses attenuate when traveling along the CC line. The measurement of the attenuation can give an idea about the length of the conductor at which the PD signal dies, so that the sensor location could be assured of getting the required signal. Therefore, attenuation of the PD pulses is an important

consideration while deciding the numbers of sensors and their positioning. To work with these design aspects of a sensor and in order to relate a measured signal to specific PD amplitude, the wave propagation characteristics (propagation constants, i.e., attenuation and phase constants, and propagation velocity) of the CC line should accurately be determined. For this purpose, TDR measurement technique is applied on a specific length of the CC line.

A short duration pulse is sent into the device under test (DUT). The incident and the reflected signals are analyzed. These signals are distorted or changed in one way or the other by the transmission medium and the extraction techniques are applied to get the desired parameters from the measurements. The attenuation and propagation velocity of the signal depend on the distance traveled, the radial geometry, and the electrical properties of the CC material [62]. These values can be helpful in selecting the optimal locations of the sensors over the entire length of CC line for reliable PD signals detection.

## 4.2 Theoretical background of TDR

The most common method for evaluating a TL and its load has traditionally been carried out by applying a sine wave to a system and measuring waves resulting from discontinuities on the line. From the measurements, the standing wave ratio (SWR) is calculated and used as a figure of merit for the transmission system. When the system includes several discontinuities, however, the SWR measurement fails to isolate them. In addition, when the broadband quality of a transmission system is to be determined,  $S$ -measurements must be made at many frequencies. This method soon becomes very time consuming and tedious.

When compared to other measurement techniques, TDR provides a more intuitive and direct look at the characteristics of the DUT. Additionally, TDR gives more meaningful information concerning the broadband response of a transmission system than any other measuring techniques. Using a high speed oscilloscope and a pulse/step generator, a fast edge is launched into the TL under investigation. The incident and the reflected voltage waves are monitored by the oscilloscope at a particular point on the line. The block diagram of a domain reflectometer is shown in Fig. 4.1 [63], [14].

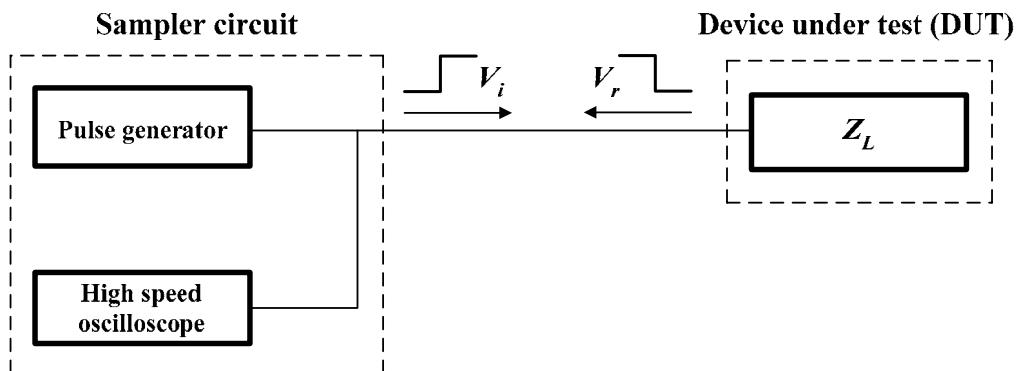


Fig. 4.1 Functional block diagram of time domain reflectometer

### 4.2.1 Operating principle of TDR instruments

TDR instruments work on the same principle as radar, but instead of air, they work through wires. A pulse of energy is transmitted down a line. When the launched propagating wave reaches the end of the line or any impedance change along the TL, part or all of the pulse energy is reflected back to the instrument. This reflected wave is energy that is not delivered to the load. The magnitude of the impedance change can be calculated using the reflection coefficient  $\Gamma$ , defined in the frequency domain as the ratio between the reflected voltage wave  $V_r$  and the incident voltage wave  $V_i$ .  $\Gamma$  is related to the load impedance  $Z_L$  and the characteristic impedance of the line  $Z_0$ , by the following expression [64]:

$$\Gamma = \frac{V_r}{V_i} = \frac{Z_L - Z_0}{Z_L + Z_0} \quad (4.1)$$

The transmission coefficient T is given as:

$$T = \frac{2Z_L}{Z_L + Z_0} \quad (4.2)$$

The amplitude of the transmitted pulse through the point of mismatch is calculated as:

$$V_t = V_i T \quad (4.3)$$

where  $V_t$  is the transmitted wave. The transmission and reflection coefficients are related by the following expression as:

$$1 + \Gamma = T \quad (4.4)$$

The distance to the impedance change can also be estimated knowing the speed of the propagated wave  $v$ . Let S be the distance and  $t$  is the time of arrival of the reflection from the impedance change, the following relation holds:

$$S = v \frac{t}{2} \quad (4.5)$$

The reflections produced by complex impedances are of great interest. Four basic examples of these reflections are shown in Fig. 4.2 which presents measurements obtained with the system shown in Fig. 4.1 [65]. At time  $t=0$ , the reflection from the far TL end is entering into the oscilloscope.  $E_i$  is the amplitude of the incident pulse,  $R_1$ - $R_4$  are the resistances,  $L_1$  and  $L_3$  are the inductances,  $C_2$  and  $C_4$  are the capacitances of the complex loads under consideration (see Fig. 4.2).

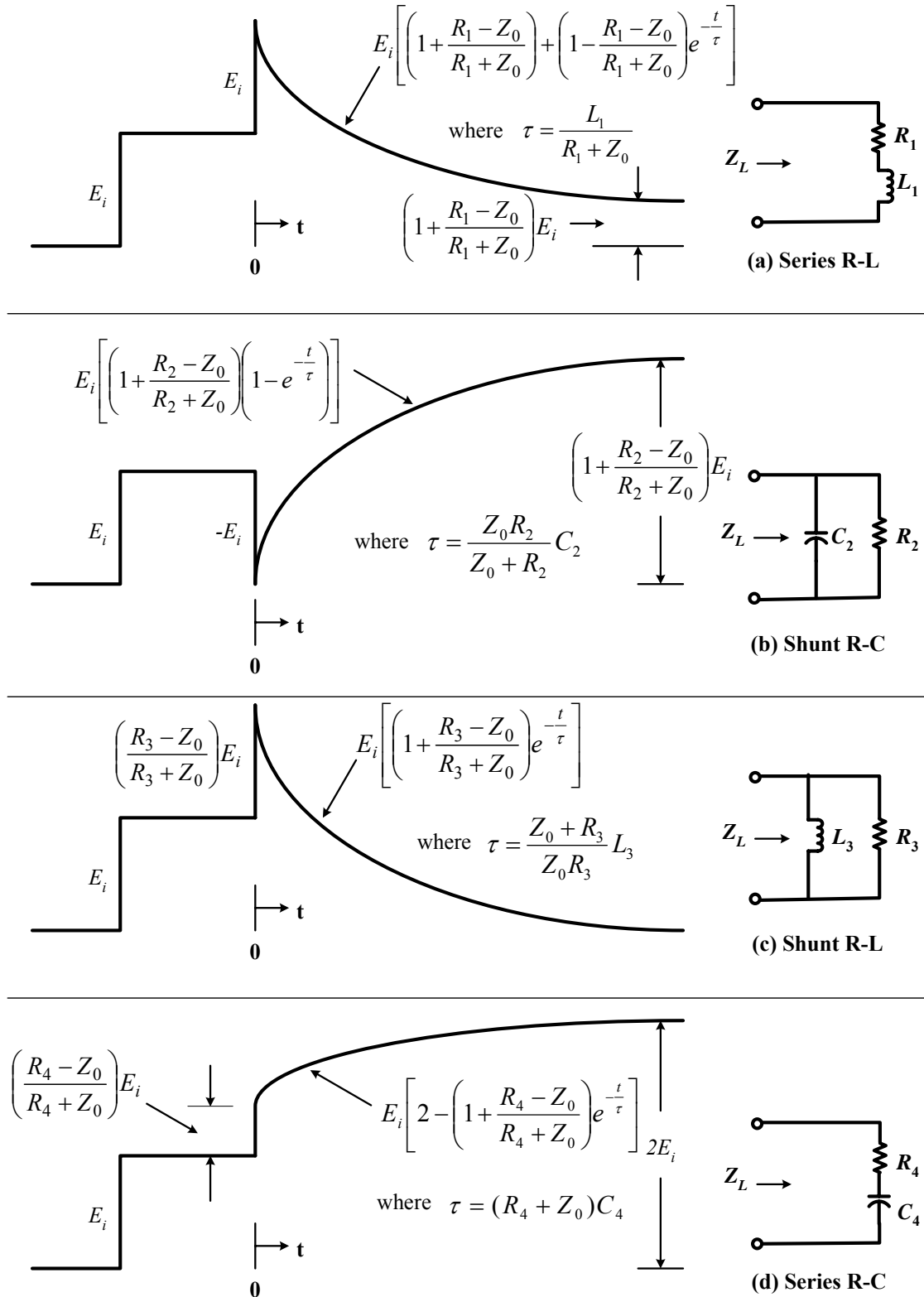


Fig. 4.2 TDR displays for four basic complex loads where the measurements are performed with the set-up shown in Fig. 4.1 [65]

## 4.3 Some considerations for TDR measurements

### 4.3.1 Digital TDR recording

Some of the parameters of digital signal recording that are relevant to this work are listed below. The understanding of both the theoretical and the practical limitations to a measurement is crucial when constructing a TDR measuring system for specific applications.

For an accurate and informative measurement, it is crucial to match the effects of bandwidth, sampling rate, and memory depth, and take advantage of features like averaging. Knowledge about these aspects of digital measurements will make it possible to reduce to a minimum the negative influence of electromagnetic noise, signal generator instabilities, etc [63].

#### A. Bandwidth

The bandwidth has traditionally been a principal figure of merit of the oscilloscope. A bandwidth of scope is typically defined as the frequency above which the signal amplitude is degraded by more than 3 dB (the amplitude is attenuated by approximately 30%). If the bandwidth of the scope is not sufficient to faithfully reproduce the applied signal to the input, it will introduce errors in the amplitude and/or time-interval measurements.

#### B. Sampling rate

For each occurrence of the trigger event, the scope will fill up its memory with samples taken at each sample interval. Inadequate sampling rate has the same effect as insufficient bandwidth; loss of high frequency information in the signal. However, there is an additional complication associated with sampling a signal. If the signal contains frequencies higher than half the sampling rate, there will be errors due to aliasing.

#### C. Memory depth

Memory depth and sampling rate are intimately related. The needed memory depth depends upon the required overall measured time span and the time resolution. The longer the time interval to be captured and the finer the resolution, the more memory will be required. Obviously, deeper memory allows the sampling circuitry of scope running faster at slow sweep speeds, providing higher frequency details of the waveforms and more critically reducing the chance of aliasing.

From the measurement perspective, the amount of memory required to display a given waveform can be expressed mathematically. The required record depth (N) is equal to the time span being measured divided by the needed resolution; both in same units, and is given as [65]:

$$N = \frac{\text{Time span}}{\text{Needed resolution}} \quad (4.6)$$

The highest measured frequency (Nyquist frequency –  $f_{\max}$ ) can be estimated from the record depth and the total recorded time in the measurement as:

$$f_{\max} = \frac{N}{2} \cdot \frac{1}{\text{Period of time record}} \quad (4.7)$$

## D. Averaging

In the real world, the desired signal is mostly measured in the presence of significant noise. At other times, the signals we are trying to measure are more like noise themselves. Because of these two common conditions, the techniques must be developed to measure signals in the presence of noise and to measure the noise itself.

The standard technique in statistics to improve the estimates of a value is to average. In other words, the averaging increases the resolution which is of considerable importance when measuring comparatively small signals. Signal averaging of  $N$  acquisitions increases bit resolution by  $\log_2(N)$  [65]. This approach increases the bit resolution up to 14 bits (32 averages) for the specific case. Of course, depending upon the sampling rate, record length, and repetition rate of the signal, averaging can substantially increase the time needed for a single curve acquisition (e.g., at 1 Hz repetition rate, a measurement with an averaging of 512 acquisitions take 8.5 min). Therefore, averaging must be used with a balance between resolution, bandwidth, SNR, time, and ease of measurement.

### 4.3.2 Fourier transform analysis

All signals measured in the time domain can alternatively be represented in the frequency domain and vice versa. This can be achieved for each linear and time invariant network where its impulse response  $h(t)$  can alternatively be represented as its transfer function  $H(f)$ . The relation between the two forms of representation is given by the Fourier transform as follows [65]:

$$H(f) = \int_{-\infty}^{+\infty} h(t)e^{-j2\pi ft} dt \quad (4.8)$$

Applying the Fourier transform, the impulse response is transformed to the spectral representation of the network in the frequency domain. Conversely, the data measured in the frequency domain by a network analyzer can be transformed into time domain using inverse Fourier transform as:

$$h(t) = \int_{-\infty}^{+\infty} H(f)e^{j2\pi ft} df \quad (4.9)$$

## A. Discrete Fourier transform (DFT)

To compute the Fourier transform digitally, a numerical integration must be performed. It will give an approximation to a true Fourier transform called DFT.

Three distinct difficulties are associated with computing Fourier transform. First, the desired result is a continuous function; however, it would only be possible to calculate its value at discrete points. Second, an integral must be evaluated which is equal to the computed area under a curve. It would be done by adding together the areas of narrow rectangles under the curve. Third, even with summation approximation to the integral, the samples must be summed up over all time from minus to plus infinity. Clearly, the transform must be limited to a finite time interval.

The Fourier transform after the above mentioned considerations becomes [65]:

$$H(m\Delta f) \approx \Delta t \sum_{n=0}^{n-1} h(n\Delta t) e^{-j2\pi m\Delta f n\Delta t} \quad (4.10)$$

where  $m=0, \pm 1, \pm 2$ ,  $\Delta f$  is the frequency spacing of samples, and  $\Delta t$  is the time interval between any two consecutive samples.

## B. Fast Fourier transform (FFT)

The FFT is an algorithm for computing DFT [65], [66]. Before the development of the FFT, the DFT required excessive amounts of computation time, particularly when high resolution is required.

The FFT forces one further assumption that the number of points acquired or the record depth  $N$  is a multiple of 2. This allows certain symmetries to occur reducing the number of calculation which have to be done. This assumption requires in certain cases data points to be added to the time domain signal to make  $N$  a multiple of 2.

## 4.4 Transmission line analysis

In the following analysis, the live CC line and the ground return path are used as a transmission channel and are approximated as a close form of the two-wire TL. According to [67], the two-wire TL must be a pair of parallel conducting wires separated by a uniform distance. Based on the above considerations, the single phase CC line with ground return is regarded as a distributed parameter network, where the voltages and the currents can vary in magnitude and phase over its length. Therefore, it can be described by circuit parameters that are distributed over its length.

A differential length  $\Delta z$  of a TL is described by its distributed parameters  $R$ ,  $L$ ,  $C$ , and  $G$  as shown in Fig. 4.3.  $R$  defines the resistance per-unit length for both conductors (in

$\Omega/\text{m}$ ),  $L$  defines the inductance per-unit length for both conductors (in H/m),  $G$  is the conductance per-unit length (in S/m), and  $C$  is the capacitance per-unit length (in F/m). The quantities  $v(z, t)$  and  $v(z+\Delta z, t)$  denote the instantaneous voltages at locations  $z$  and  $z+\Delta z$  respectively. Similarly,  $i(z, t)$  and  $i(z+\Delta z, t)$  denote the instantaneous currents at the respective locations.

In the circuit of Fig. 4.3 (b), applying Kirchhoff's voltage and current laws, respectively, the following two equations can be obtained as [68]:

$$v(z, t) - R\Delta z \cdot i(z, t) - L\Delta z \cdot \frac{\partial i(z, t)}{\partial t} - v(z + \Delta z, t) = 0 \quad (4.11)$$

$$i(z, t) - G\Delta z \cdot v(z + \Delta z, t) - C\Delta z \cdot \frac{\partial v(z + \Delta z, t)}{\partial t} - i(z + \Delta z, t) = 0 \quad (4.12)$$

If  $v$  and  $i$  are expressed in phasor form, i.e.,  $v(z, t) = \text{Re}[V(z) \cdot e^{j\omega t}]$  and  $i(z, t) = \text{Re}[I(z) \cdot e^{j\omega t}]$  and when  $\Delta z \rightarrow 0$ , the time harmonic line equations can be derived from (4.11) and (4.12) as:

$$-\frac{dV(z)}{dz} = (R + j\omega L) \cdot I(z) \quad (4.13)$$

$$-\frac{dI(z)}{dz} = (G + j\omega C) \cdot V(z) \quad (4.14)$$

The coupled time harmonic transmission line equations can be combined to solve for  $V(z)$  and  $I(z)$  as:

$$\frac{d^2 V(z)}{dz^2} = \gamma^2 V(z) \quad (4.15)$$

$$\frac{d^2 I(z)}{dz^2} = \gamma^2 I(z) \quad (4.16)$$

and

$$\gamma(\omega) = \alpha(\omega) + j\beta(\omega) = \sqrt{(R + j\omega L) \cdot (G + j\omega C)} \quad (4.17)$$

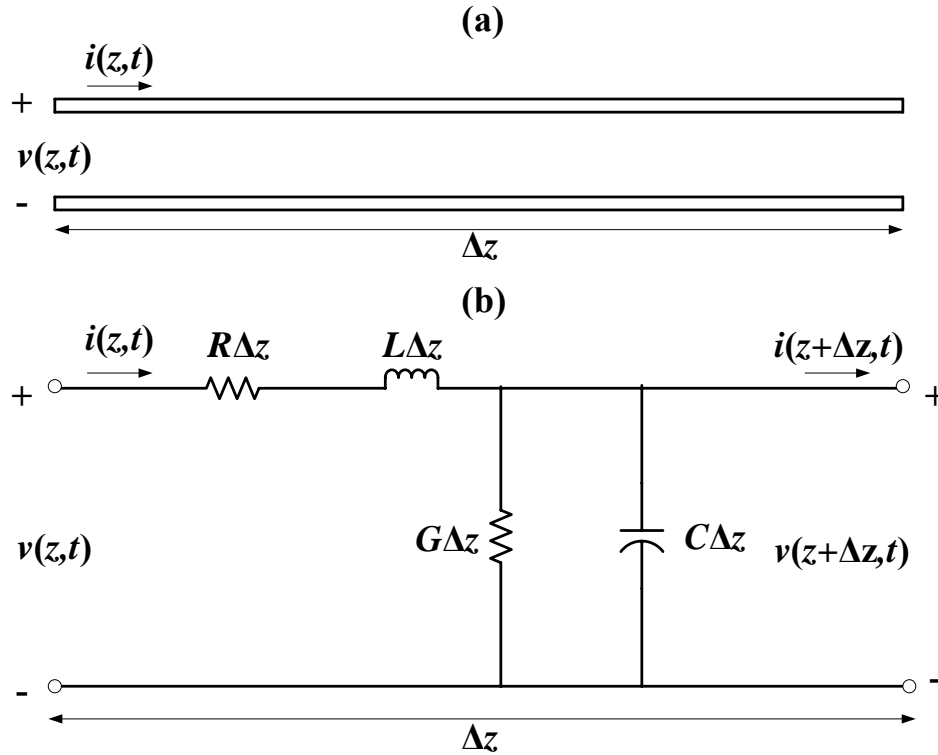


Fig. 4.3 (a) The voltage and current definitions of two-wire TL (b) The equivalent lumped-element circuit

where  $\gamma$  is the propagation constant whose real and imaginary parts,  $\alpha$  and  $\beta$ , are the attenuation constant (Np/m) and phase constant (rad/m) of the line respectively. The complex propagation constant is also given as:

$$\gamma(\omega) = \sqrt{Z \cdot Y} \quad (4.18)$$

where  $Z = R + j\omega L$  is the series impedance per-unit length and  $Y = G + j\omega C$  is the shunt admittance per-unit length of the line. The characteristic impedance of the line is given as:

$$Z_0 = \sqrt{\frac{R + j\omega L}{G + j\omega C}} = \sqrt{\frac{Z}{Y}} \quad (4.19)$$

It is clear from (4.17) and (4.19) that  $\gamma$  and  $Z_0$  are the characteristic properties of a line whether or not the line is infinitely long. They depend on  $R$ ,  $L$ ,  $G$ ,  $C$ , and  $\omega$  but not on the line length [68].

## 4.5 TDR measuring set-up

The TDR measuring set-up was arranged in the HV laboratory at TKK. The measuring set-up consisted of: (i) DUT; and (ii) measuring system (see Fig. 4.4). DUT was a polyethylene CC line of 20 m length, 10 mm inner diameter of the aluminum conductor and 14.5 mm outer diameter along with insulation. In practice, a narrow electric pulse was applied to the CC and the incident and reflected waves were measured by means of a digital oscilloscope at point M. The measured data was transferred to the computing system (laptop) connected to the oscilloscope through the general purpose interface bus (GPIB), where the analysis was done using MATLAB.

A pulse of 3 V amplitude, having 40 ns pulse-width, is fed into the DUT at point A. The incident (source) pulse is reflected from point B (open ended) with positive  $\Gamma$  ( $Z_L > Z_0$ ). This reflected pulse from point B travels towards point A and then reflects back from point A with negative  $\Gamma$  ( $Z_M < Z_0$ ), where  $Z_M$  is the equivalent impedance seen at point M when the signal propagates from conductor end B to A. Therefore, a negative amplitude of the reflected pulse from point A is seen in Fig. 4.5. These reflections continue from both ends of the CC, and finally the signal dies. To extract the wave propagation characteristics of CC line from the TDR measurements, the analysis of TL will be performed in the next section.

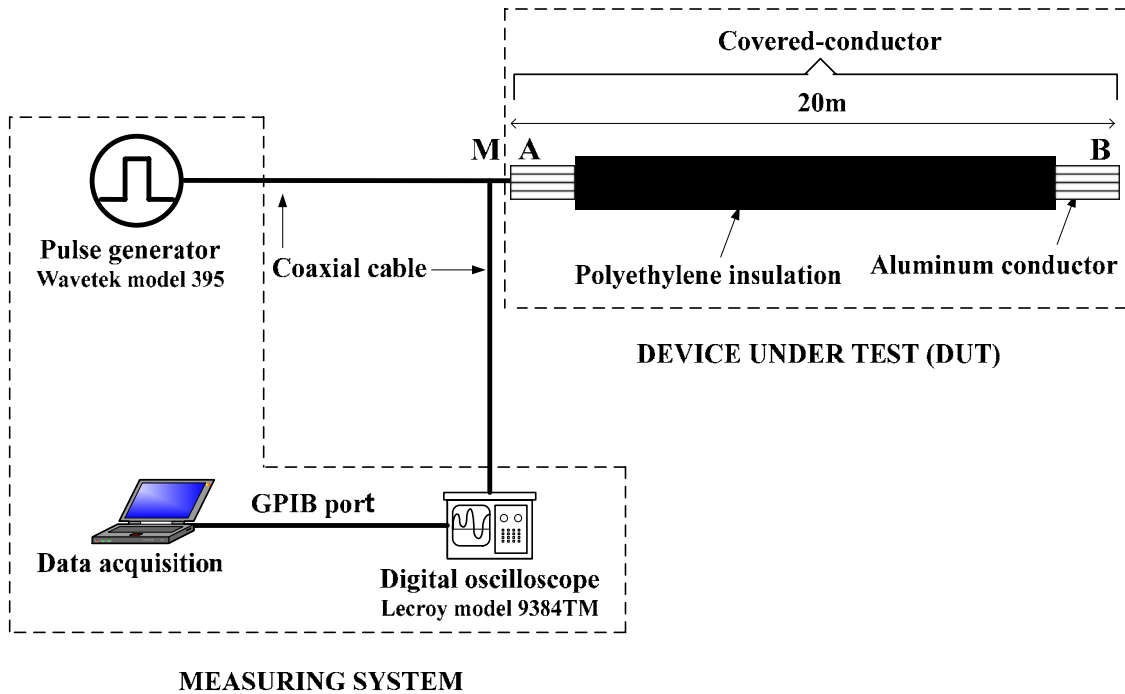


Fig. 4.4 Schematic drawing of the TDR measuring set-up

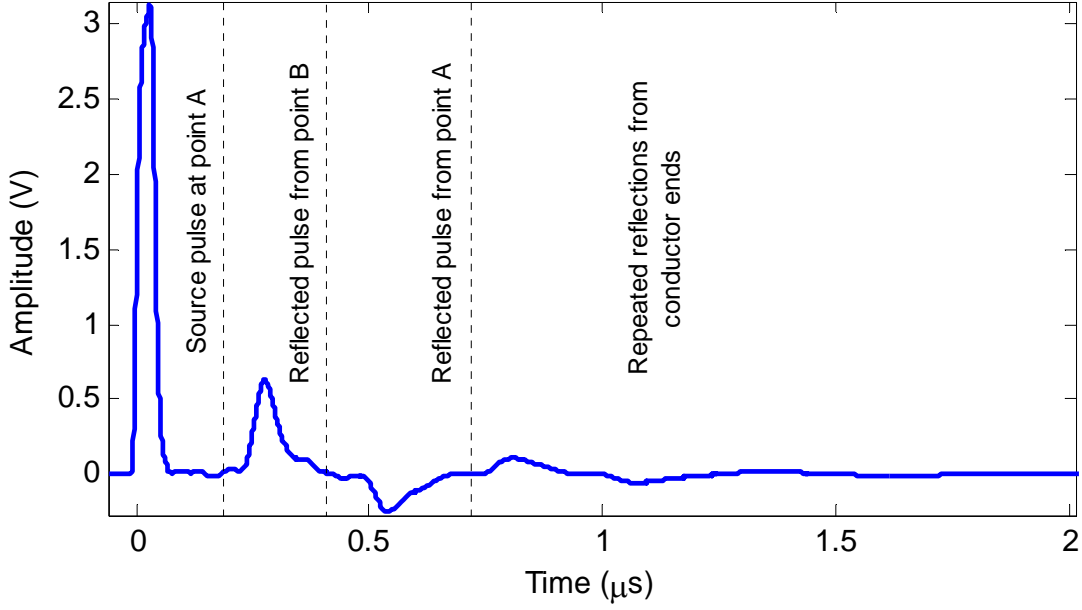


Fig. 4.5 TDR response of the CC line (DUT)

## 4.6 TDR parameters extraction method

The attenuation and phase shift of a wave traveling along a TL segment of a length  $l$  is the complex voltage ratio between the input (incident pulse) and the output (reflected pulse) of a line segment as:

$$\frac{V_{out}}{V_{in}} = e^{-\gamma(\omega)l} \quad (4.20)$$

It is revealed that this ratio depends on both the distance traveled  $l$  and the angular frequency  $\omega$ . If the distance is kept fixed, then in the frequency domain:

$$H(\omega) = \frac{V_{out}(\omega)}{V_{in}(\omega)} = e^{-\gamma(\omega)l} \quad (4.21)$$

If the CC line is considered as a linear system, then  $H(\omega)$  is the transfer function. In the measuring system, the incident and reflected pulses are measured in the time domain. Since the measurements are done at the input side (at point M in Fig. 4.4), the total traveling distance is twice the length of the DUT, i.e.,  $2l$ . These time domain measurements are then transformed into the frequency domain by the use of the FFTs in MATLAB. It can be deduced that:

$$\alpha(\omega) = -\frac{1}{2l} \cdot \ln|H(\omega)| \quad (4.22)$$

$$\beta(\omega) = -\frac{1}{2l} \angle H(\omega) \quad (4.23)$$

Thus, the attenuation and phase constant are determined using the time domain measurements obtained. The propagation velocity,  $v$  (m/s), can be determined using phase constant  $\beta$  as:

$$v = \frac{\omega}{\beta} = \frac{2\pi f}{\beta} \quad (4.24)$$

## 4.7 Calibration of TDR measuring system

The equivalent circuit of the TDR measuring set-up (of Fig. 4.4) is shown in Fig. 4.6. The pulse is fed from a pulse generator to the DUT through a coaxial cable ( $Z_1=50 \Omega$ ). The measurements are taken at point M by means of a digital oscilloscope, which is connected to the measuring point through another coaxial cable ( $Z_2=50 \Omega$ ).  $R_g$  and  $R_{os}$  are the internal resistances of the pulse generator and digital oscilloscope, respectively, and  $Z_0$  is the characteristic impedance of the DUT. The value of  $Z_0$  for the practical CC overhead distribution line is taken as  $480 \Omega$  [14]. However, in the experimental set-up, the CC line is placed at a distance of 7 cm from the ground. Therefore, the approximate value of  $Z_0$  is taken as  $120 \Omega$  in this work [64]. The CC line is placed at a very small distance from the ground due to its limited dimensions for laboratory measurements. Moreover, the noise level in TDR measurements was observed very low at this small elevation.

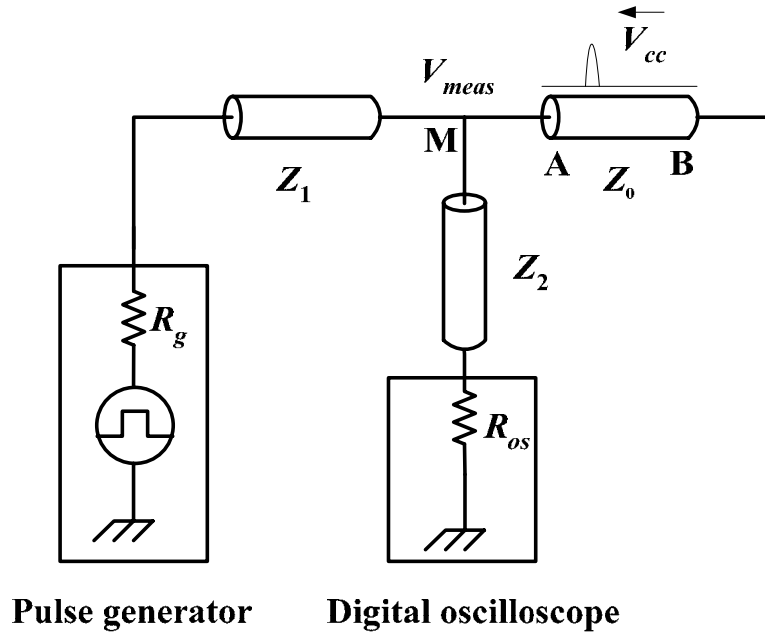


Fig. 4.6 Equivalent circuit of the TDR measuring set-up

For the incident pulse, the measured voltage ( $V_{meas}$ ) is equal to the amplitude of the pulse transmitted into the DUT ( $V_{cc}$ ) at point A (see Fig. 4.6) [69]. As the far end of the DUT is open circuited, this pulse is totally reflected and returns to the connection point A. Due to the mismatch of impedances at point A, this discontinuity point causes a reflection back into the DUT and a measured signal with reduced amplitude as a consequence. The relationship between the measured pulse and the pulse from the DUT (for relected pulse from point B) is given using (4.3) as:

$$V_{meas} = V_{cc} \cdot \frac{2 \cdot Z_1 \parallel Z_2}{Z_1 \parallel Z_2 + Z_0} \quad (4.25)$$

It can also be written as:

$$V_{cc} = V_{meas} \cdot \frac{Z_1 \parallel Z_2 + Z_0}{2 \cdot Z_1 \parallel Z_2} \quad (4.26)$$

By putting the values of  $Z_0=120 \Omega$ ,  $Z_1=50 \Omega$ , and  $Z_2=50 \Omega$  in equation (4.26), the following relation can be obtained.

$$V_{cc} = 2.9V_{meas} \quad (4.27)$$

Therefore, the amplitude of the reflected pulse is corrected according to (4.27) before using it in MATLAB for the wave propagation parameters extraction.

## 4.8 TDR measurements and results

The incident pulse at point A is taken from Fig. 4.5 and is padded with zeroes up to length  $N = 2^n$ , for  $n = 16$  ( $N=65536$ ), as shown in Fig. 4.7. Similarly, the reflected pulse from point B is taken and is padded with zeros to the same length as that of the incident pulse as shown in Fig. 4.8. A time step of  $T = 0.5$  ns is used in the Fourier analysis.

As the two pulses travel unequal lengths of line, the shapes of the incident and the reflected waves will differ as a result of the frequency-dependent attenuation [42], [70]. To determine the accurate values of the propagation constant, (4.21) is corrected using a correction factor of 2.9 as:

$$H(\omega) = \frac{V_{out}(\omega)}{V_{in}(\omega)} = (2.9) \times e^{-\gamma(\omega)l} \quad (4.28)$$

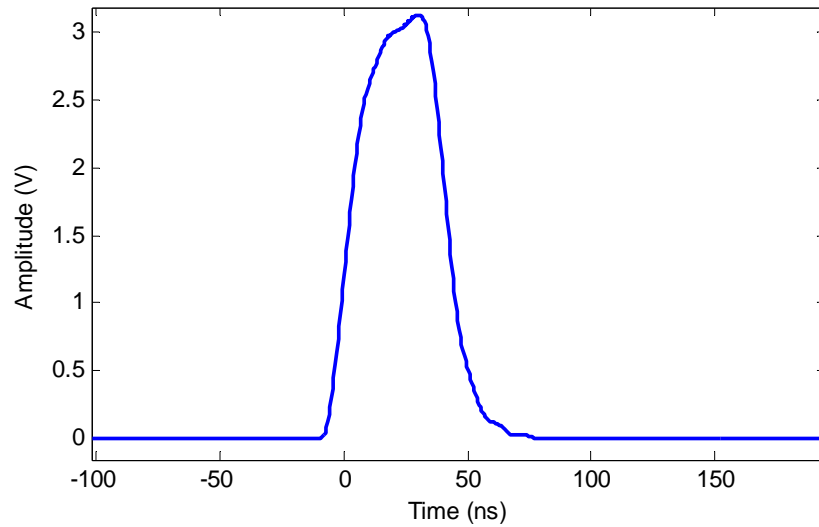


Fig. 4.7 Incident pulse after padding with zeros

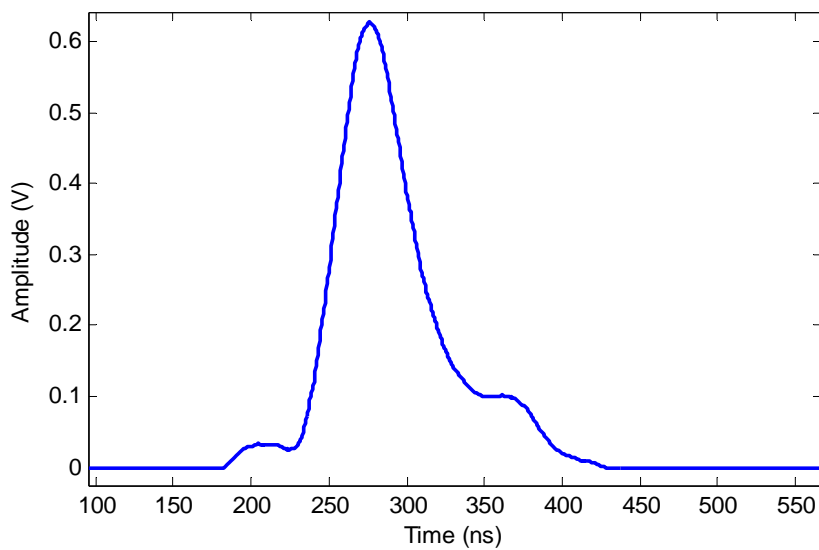


Fig. 4.8 Reflected pulse after padding with zeros

The information related to the attenuation is determined by the magnitude of the above transfer function  $H(\omega)$  using (4.22). The argument of this transfer function gives the phase constant. The information related to phase constant is determined by the time interval between the incident and reflected pulses. Using the measured data, the phase constant versus signal frequency characteristics is obtained using (4.23) and is drawn in Fig. 4.9. It is revealed from Fig. 4.9 that the phase constant is changing between  $-\pi$  and  $+\pi$ . Using the function “unwrap” in MATLAB, these jumps can be removed to give the continuous characteristics as shown in Fig. 4.10.

The curves for the attenuation constant and wave propagation velocity using unwrapped phase constant are obtained and the dependency of these parameters on the frequency is shown in Fig. 4.11 [71]. It is clear that the attenuation and propagation velocity are fairly constant at lower frequencies (0.001 dB/m and 150 m/ $\mu$ s). At higher frequencies, these parameters begin to increase (after 0.2 MHz) with an increase in frequency. The resolution of both characteristics is good up to about 25 MHz, beyond which it is lost in the certain repetitive disturbances or noise level [71].

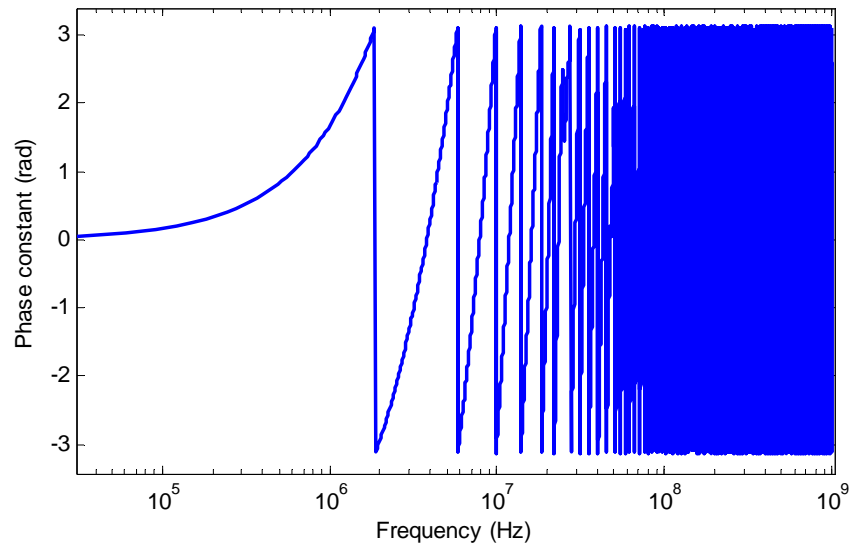


Fig. 4.9 Phase constant versus signal frequency

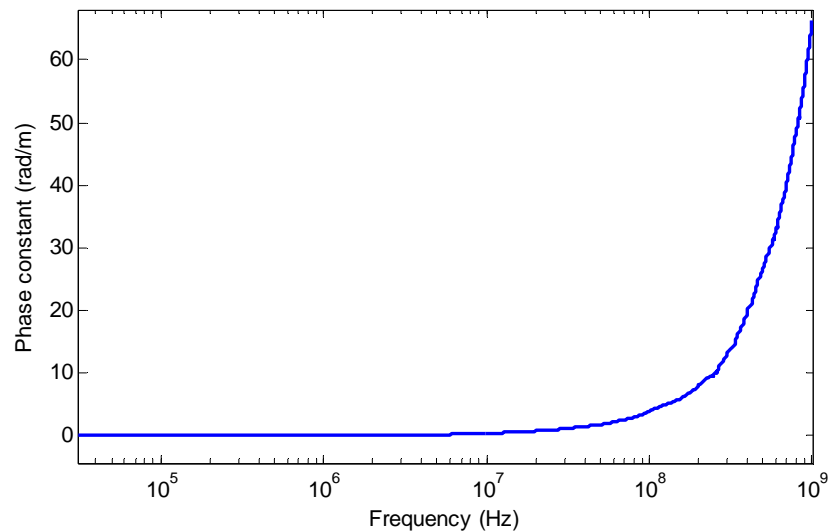


Fig. 4.10 Phase constant versus signal frequency after "unwrapping"

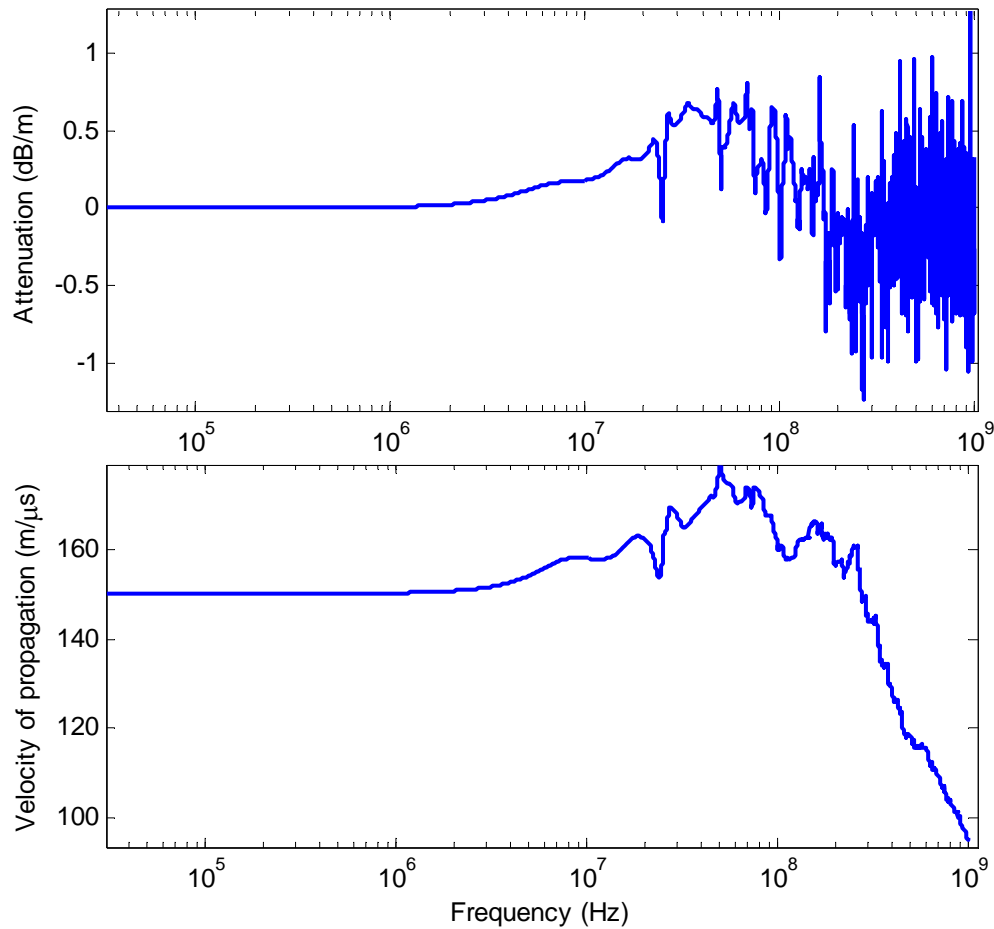


Fig. 4.11 Measured attenuation constant and wave propagation velocity

One possible way to explain the noise level at higher frequencies is to have a look at the FFTs of the measured pulses as shown in Fig. 4.12. It is revealed that FFTs of incident and reflected pulses, after using the correction factor, remain constant up to 0.2 MHz. Therefore, the attenuation is also constant up to this range of frequency. Beyond this frequency, the FFT of reflected pulse starts to decrease at a higher rate, resulting in a linear increase in the attenuation. Later, beyond 25 MHz, FFTs suffer from noise that has different values from the actual function. The noise level has some peaks, the values of which are taken into account instead of those of the actual function, resulting in the noisy peaks in the attenuation curve.

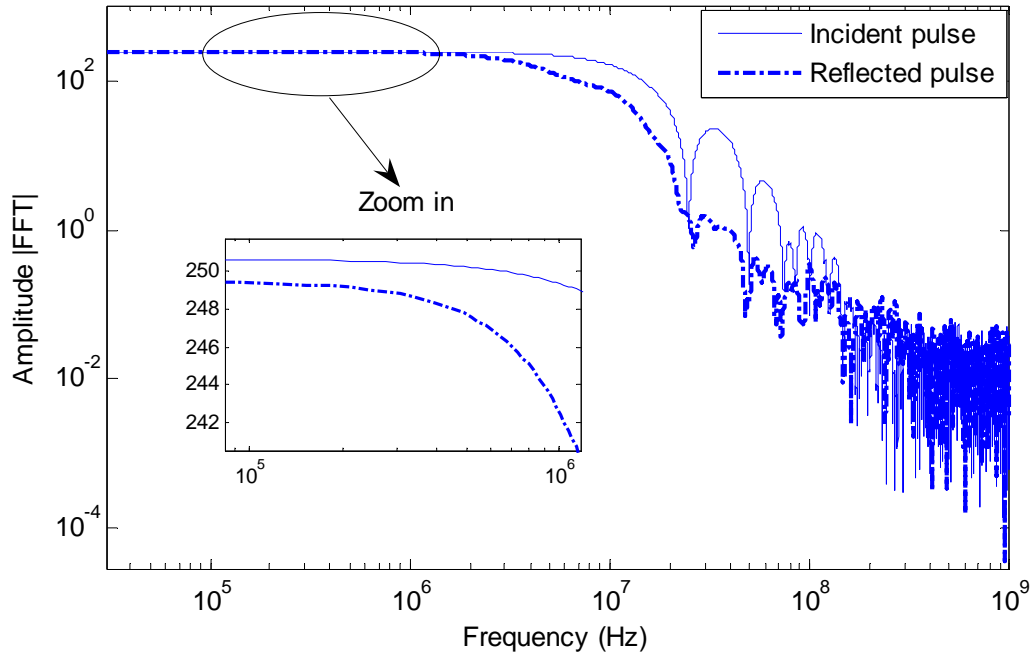


Fig. 4.12 FFTs of the incident and reflected pulses

Another mathematical interpretation is on the basis of the Fourier transform function. For an ideal square pulse as:

$$f(t) = \begin{cases} 1, & |t| < a \\ 0, & |t| > a \end{cases} \quad (4.29)$$

The analytical Fourier transform function is in the form:

$$F[f(t)] = \frac{2 \sin a\omega}{\omega}, \omega > 0 \quad (4.30)$$

It can be concluded that the Fourier transform function would periodically equal to zero and the zero crossings can be defined as [72]:

$$f_0 = \frac{k}{2a} \quad (4.31)$$

where  $k=1,2,3,\dots,N$  and  $f_0$  is the frequency at which the Fourier function equals to zero. In the presented case, the pulse width for the incident signal is  $2a=40$  ns (see Fig. 4.7). Therefore, it can be expected that zero crossings and the respective numerical artifacts to be in the vicinity of  $f_0=25$  MHz (for  $k=1$ ).

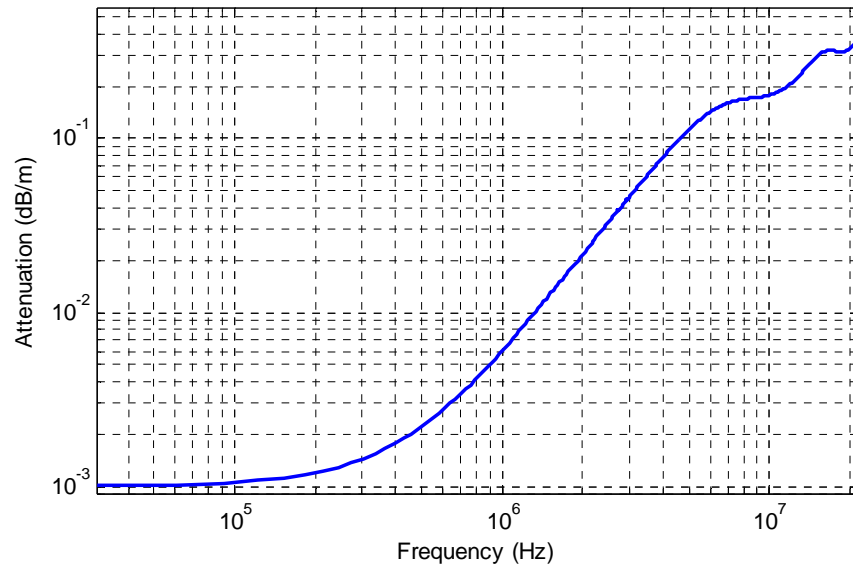


Fig. 4.13 The measured attenuation constant

The reliability of the measurements can also be roughly verified by looking at the pulses shown in Fig. 4.5 [69]. The ratio between the two response pulses is  $0.24/0.63$  V, which is 8.3 dB. This gives an attenuation of 0.2 dB/m (due to the distance there and back for a 20 m long CC line). The pulse-width is 40 ns, which yields a dominant frequency component of approximately 12.5 MHz. In Fig. 4.13, it can be seen that the measured attenuation is also approximately 0.2 dB/m at this specific frequency.

The major parameter which defines the frequency band of the PD signals due to falling trees on CC line is the attenuation of the PD signals propagating over the CC line. The attenuation is frequency-dependent and it increases by increasing the frequency of the propagated signals. As the PD pulses travel along the CC line, the higher frequency components of the pulses are heavily attenuated. The frequency-dependent attenuation of the CC line implies a PD pulse bandwidth that depends on the length of CC line through which the pulse has propagated. If a wide detection bandwidth is employed, the sources close to the detection end of the CC line will be measured with high sensitivity; however, sensitivity is compromised for PD pulses that are generated further from away. Also, the shape of measured pulses will be highly sensitive to PD source location. For a source close to the measurement end of the CC line, the pulse will be very sharp while the PD pulse which propagates down to the far end of the CC line will be much broader due to the dispersion effect. A narrow detection bandwidth limits pulse “sharpness” and thereby limits PD location accuracy. Obviously a detection bandwidth must be selected that represents a good compromise, given typical CC line frequency-dependent attenuation characteristics and typical test lengths [42], [70].

## 4.9 Comparing wave propagation characteristics of XLPE cable and CC line

The attenuation constant and propagation velocity can be easily evaluated because the impedance and admittance formulas of an XLPE cable including the semi conducting layer are well-known [73], [74]. However, the wave propagation characteristics of a single-phase MV XLPE power cable has been determined using TDR measurements and its details are given in [75]. Fig. 4.14 shows a comparison of measured wave propagation characteristics of a single-phase MV XLPE power cable and a CC overhead distribution line. It is revealed from Fig. 4.14 (a) that the CC line has much lower attenuation as compared to XLPE power cable. In MV power cables, the semi-conducting layers have a significant contribution to the wave propagation characteristics and the attenuation is higher due to the presence of these layers [76]. High frequency attenuation in shielded cables is generally considered as a negative attribute, but can be used positively in certain situations. In the CC overhead distribution lines used in Finland, semi conductive layers are absent; therefore, attenuation is lower as compared to power cables [60].

It is clear from Fig. 4.14 (b) that the measured propagation velocity in the CC line seems to be lower than in power cables; however, practical CC lines have comparatively higher propagation velocities [14]. This lower value of propagation velocity is due to the location of the CC line (laying near ground level at a height of 7 cm) in the experimental set-up. The propagation velocity increases by increasing the height of the CC line above ground level. The practical CC lines (generally at a height of more than 10 m) have higher propagation velocities than power cables. Attenuation also depends upon the height of the CC line and it decreases by increasing its height. The practical CC lines have lower attenuation than the measured value in this work.

The measured wave propagation characteristics of CC line suffer in repetitive disturbances or noise at lower frequency as compared to the characteristics of XLPE power cable (see Fig. 4.14). The measurement limitation at varying frequencies for different conductors is due to the different sampling times for XLPE cable and CC line TDR measurements. XLPE cable measurements are sampled at 0.2 ns, while CC line measurements are sampled at 0.5 ns. Therefore, the resolutions of wave propagation characteristics of XLPE cable and CC line are good up to 81 MHz and 25 MHz, respectively.

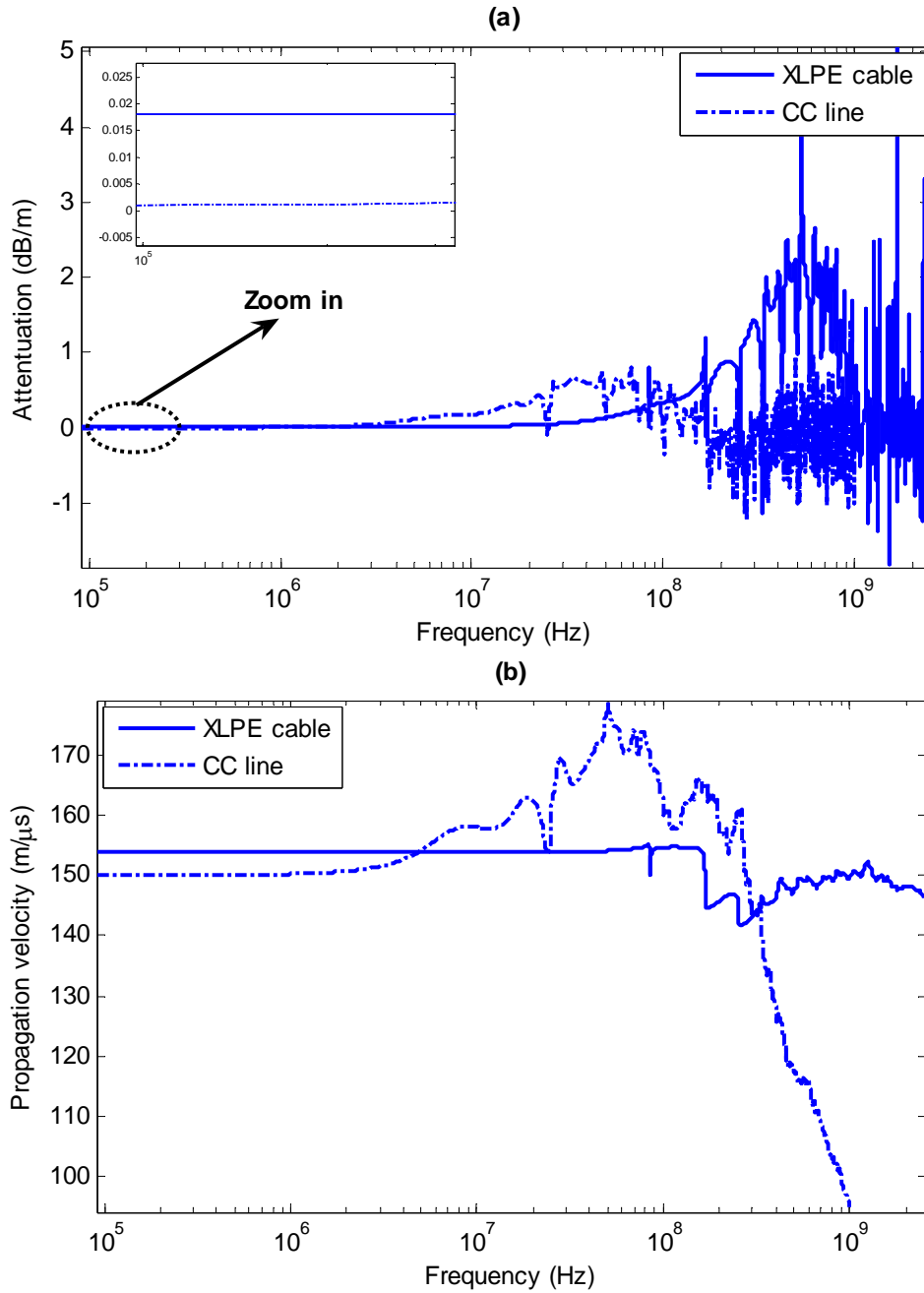


Fig. 4.14. Measured wave propagation characteristics comparison of single-phase MV XLPE power cable and CC overhead distribution line; (a) attenuation constant, and (b) propagation velocity

## 4.10 Discussion

The TDR measurement technique has been presented to extract the frequency-dependent wave propagation characteristics of CC overhead distribution lines. These measurements can be applied for designing and deploying PD sensors over the entire length of the CC line for detecting PDs produced by falling trees. The wave propagation characteristics of single-phase XLPE power cable and CC overhead distribution line are also compared. It is revealed that the signal attenuation and propagation velocity are fairly constant at lower frequencies, but these parameters are frequency-dependent at higher frequencies i.e., their values increase by increasing the frequency. Attenuation in a CC line is much lower than power cables. However, the situation is opposite in case of propagation velocity i.e., signals propagate faster in a CC line. The TDR measurement results on power cable can be used to localize the discontinuities as well as the design of communication through distribution power cables. On the other hand, TDR measurement results on the CC line can be used to decide the number and positioning of PD sensors for the monitoring of falling trees over a specific length of CC overhead distribution line.

The Rogowski coil measurements have shown that PD signals produced due to the leaning trees on the CC line lie in the frequency range of 1-6 MHz [57]. Therefore, the attenuation and propagation velocity of the PD signals in this frequency range are important for designing and positioning of PD sensors over the entire length of CC line.

The approximate attenuation of the PD signals has already been determined using a Rogowski coil sensor measurements at different points on the DUT (section 3.7). The previous measurement results show that at lower frequencies, the attenuation is very high (0.21 dB/m). This high attenuation value for CC line does not sound good in practical terms. In practice, the attenuation of the signals should be low at lower frequencies. There are several reasons for those incorrect high attenuation measurements, e.g., the captured voltage waveforms are oscillatory in nature due to the behavior of the Rogowski coil and the sampling time for those measurements is long (20 ns). Therefore, the previous method is not accurate in measuring the attenuation of the signals in the required bandwidth of the PD signals. However, it is clear that TDR measurements are useful for determining the accurate values of the attenuation over a wide range of the frequencies as shown in Fig. 4.11. The TDR measurement results are illustrated in Fig. 4.15 for the frequency range (1-6 MHz) of PD signals captured by the Rogowski coil [71].

In the laboratory, PDs produced due to a leaning pine tree on 20 kV CC line are of magnitude around 3 nC [57]. This amount could be of several hundred nC in a real situation, where many trees fall on the line due to heavy storms. The minimum detectable magnitude of the PD using a Rogowski coil sensor is 100 pC [57]. Therefore, the measured value of the attenuation can help in estimating the distance from the fault location (point of a leaning tree on the CC line) to the point of measurement. However, the detectable range of the distance could be longer if the magnitude of PDs produced will increase due to the falling of many trees in heavy storms on practical CC lines having lower attenuation than the measured value.

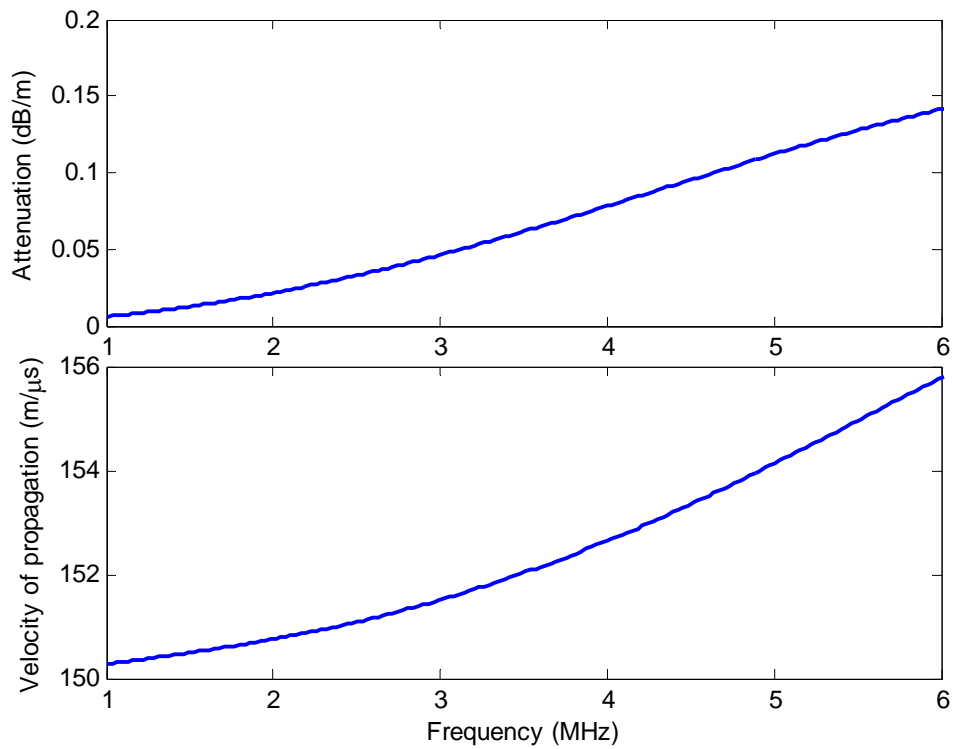


Fig. 4.15 TDR measurement results for PD sensor applications

Due to variations in the attenuation and propagation velocity of the CC line, the knowledge of the frequency-dependent CC line parameters at different heights is necessary for increasing the reliability of PD detection and quantification. Therefore, theoretical modeling of the CC line should be carried out to determine its frequency-dependent line characteristics at different heights.

## Chapter 5

### Theoretical Modeling and Experimental Verification of CC Line

*This chapter presents a theoretical model of the CC overhead distribution line and the frequency-dependent distributed TL parameters, wave propagation characteristics, and characteristic impedance are calculated using the developed model. The derived wave propagation characteristics are compared with those obtained from the TDR measurements to validate the theoretical model of the CC line. The TDR measuring system is also simulated in EMTP-ATP as time domain verification of the measurements. An accurate determination of the TL characteristics for practical CC lines can be used as a design aid for the modeling of PD measuring system in EMTP-ATP.*

#### 5.1 Motivation for developing CC line model

TDR measurements have already been taken on CC lines to determine its frequency-dependent wave propagation characteristics. In the case of power cables, wave propagation characteristics are independent of the cable height above or below the ground level; however, these are strongly influenced by the conductor height in case of CC lines. Therefore, TDR results extracted from the laboratory measurements can not be implemented for practical CC lines, which are located at higher levels above the ground. Due to variations in the attenuation and propagation velocity of the CC line when varying its height above ground level, knowledge of the frequency-dependent TL parameters at different heights is necessary to increase the reliability of PD detection and quantification. Therefore, the theoretical modeling of the CC line should be carried out to determine its frequency-dependent line characteristics at different heights.

Extracting the features of PDs from the Rogowski coil measurements to detect and locate falling trees on a complicated TL network is a challenging task. The challenge for on-line PD measurements is to find the optimal locations for these sensors with respect to their sensitivity, interference level, signal distinction, and universal applicability [61]. To work

with these design aspects of a sensor and in order to relate a measured signal to specific PD amplitude, the wave propagation characteristics of the CC line should be accurately determined. Attenuation is an important parameter in order to estimate the maximum length of the line that can be monitored with a PD sensor. The measurement of the attenuation can give an idea about the length of the conductor at which the PD signal dies, so that the sensor location can be assured of getting the required signals. Therefore, attenuation of the PD pulse is an important consideration while deciding the number of sensors and their positioning. In this way, CC lines will be more reliable and the costs related to visual inspection work will also be reduced.

The modeling of the measuring system in a time domain digital simulator program, such as EMTP-ATP, poses many challenges. One of the main difficulties is the correct representation of the TL dealing with transient simulation studies [77]. The TL parameters are function of the line length, and the per-unit parameters vary with frequency. To develop a theoretical model, the CC line is approximated as a two-wire TL and its characteristics (TL parameters, wave propagation characteristics, and characteristic impedance) are derived. The frequency-dependent distributed TL parameters, which are needed to accurately characterize lossy lines, are derived based on the radial geometry and the electrical properties of the CC material. The wave propagation characteristics and characteristic impedance of the CC line are determined based on the calculated TL parameters. TDR is a measuring technique to accurately determine the wave propagation characteristics of a cable or a conductor [71], [72], [78]. The calculated wave propagation characteristics are compared with those obtained from TDR measurements for experimental verification of the theoretical model of the CC line.

## 5.2 Developing theoretical model of a CC line

When a signal travels along the CC line segment of a certain length, it will be subjected to attenuation losses which depend on the physical properties of the CC material. For a MV line with a propagation constant  $\gamma$ , these losses are fully determined by the TL parameters (i.e.,  $R$ ,  $L$ ,  $G$ , and  $C$ ) and the frequency of the propagated signal  $\omega$ , as given in (4.17). The cross-sectional view of the CC under investigation is shown in Fig. 5.1. As in TDR measurements, the line is kept at a height of 7 cm above the ground level, the same height is first considered in theoretical modeling. The equivalent electrical model of the CC line is shown in Fig. 5.2

The line model per-unit length consists of series impedance  $Z$  and shunt admittance  $Y$ . The stranded aluminum conductor and the ground return path constitutes  $Z$ . For simplicity, the effect of number of strands upon the impedance is not included in this research work. The internal impedance  $Z_i$  of the conductor including the skin effect can be easily derived as follows [79]:

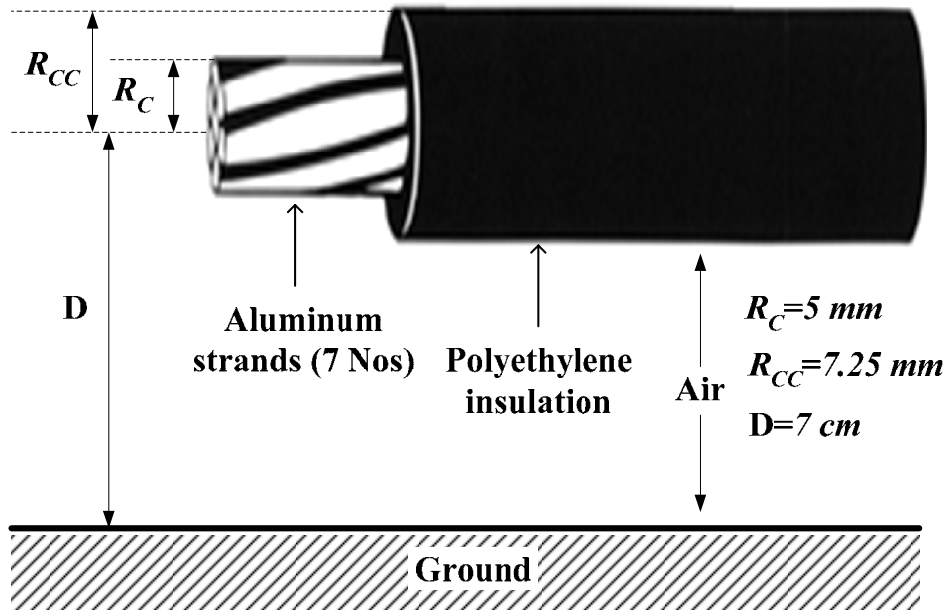


Fig. 5.1 Cross-sectional view of the CC line (in laboratory tests)

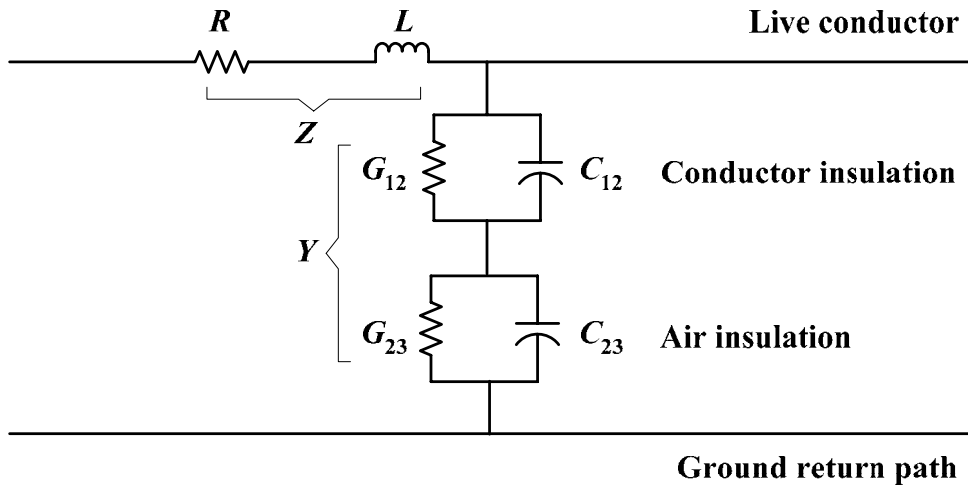


Fig. 5.2 Equivalent electrical model of the CC line

$$Z_i = \frac{\rho_{al}}{S} = \frac{\rho_{al}}{\pi [R_C^2 - (R_C - h_c)^2]} \quad (5.1)$$

where  $\rho_{al}$  is the resistivity of aluminum,  $S$  is the cross-sectional area of the conductor core,  $R_C$  is the radius of aluminum conductor-core, and  $h_c$  is the penetration depth in the conductor-core given as:

$$h_C = \sqrt{\frac{\rho_{al}}{j\omega\mu_{al}}} = \frac{1}{\sqrt{j\omega\mu_0\sigma_{al}}} \quad (5.2)$$

where  $\mu_{al}$  is the permeability of aluminum (equal to  $\mu_0$  due to its non-ferromagnetic behavior),  $\mu_0$  is the permeability of free space, and  $\sigma_{al}$  is the conductivity of aluminum.

By assuming  $R_C \gg h_C$ , equation (5.1) can be approximated as:

$$Z_i \approx \frac{\rho_{al}}{2\pi R_C h_C} = \frac{1}{2\pi R_C} \sqrt{\frac{j\omega\mu_0}{\sigma_{al}}} \quad (5.3)$$

The original accurate formula of the conductor internal impedance was derived by Schelknoff in 1926 [80]. Equation (5.3) is a well-known approximation in a high frequency region and was originally derived by Carson [81] and Sunde [82].

The external impedance  $Z_e$  due to geometrical inductance of the CC line at a height  $D$  above ground level is given as:

$$Z_e = \frac{j\omega\mu_0}{2\pi} \ln\left(\frac{R_{CC}}{R_C}\right) + \frac{j\omega\mu_0}{2\pi} \ln\left(\frac{D}{R_{CC}}\right) \quad (5.4)$$

where  $R_{CC}$  is radius of the CC line with insulating cover. Several expressions for the ground-return path impedance  $Z_g$  have been presented by many researchers; however, one simpler form is given by the following logarithmic function as [83]:

$$Z_g = \frac{j\omega\mu_0}{2\pi} \cdot \ln\left(\frac{1 + \gamma_g D}{\gamma_g D}\right) \quad (5.5)$$

In the above expression,  $\gamma_g$  can be calculated from the following expression as:

$$\gamma_g = \sqrt{j\omega\mu_0(\sigma_g + j\omega\epsilon_0\epsilon_{rg})} \quad (5.6)$$

where  $\sigma_g$  is the ground conductivity (0.001 S/m),  $\epsilon_0$  is the permittivity of free space, and  $\epsilon_{rg}$  is the relative permittivity of ground (taken as 10). After summing up above three impedances, the total series impedance of the CC line is given as:

$$Z = Z_i + Z_e + Z_g \quad (5.7)$$

The shunt admittance in the model is made up of the dielectric losses and the capacitances of the conductor and air insulation as:

$$Y_{12} = G_{12} + j\omega C_{12} \quad (5.8)$$

$$Y_{23} = G_{23} + j\omega C_{23} \quad (5.9)$$

The parameters  $G_{12}=\omega C_{12}\tan\Delta$ ,  $G_{23}=2\pi\sigma_{air}/\ln(D/R_{CC})$ ,  $C_{12}=2\pi\epsilon_c/\ln(R_{CC}/R_C)$ , and  $C_{23}=2\pi\epsilon_0/\ln(D/R_{CC})$  are given and can be calculated. The loss tangent  $\tan\Delta$  for the CC insulation is taken as 0.0003. The permittivity of CC material  $\epsilon_c$  is equal to  $\epsilon_0\epsilon_{rc}$ , where  $\epsilon_0$  is the permittivity of free space and  $\epsilon_{rc}$  is the relative permittivity of CC polyethylene insulation taken as 2.26.  $\sigma_{air}$  is the conductivity of air. The total shunt admittance of the CC line is given as:

$$Y = \frac{1}{\left(\frac{1}{Y_{12}} + \frac{1}{Y_{23}}\right)} \quad (5.10)$$

Using (5.1)-(5.10), it is possible to calculate the frequency-dependent TL parameters. The propagation constant and characteristic impedance of the CC line can be calculated using (4.18) and (4.19), respectively. The frequency-dependent attenuation (dB/m) can be calculated as:

$$\alpha(\omega) = 8.686 * \text{real}[\gamma(\omega)] \quad (5.11)$$

The propagation velocity of the signal  $v$  (m/s) can be determined using phase constant in (4.24). The aforementioned equations can be used in MATLAB to derive TL characteristics from the theoretical model. This model is verified experimentally by taking TDR measurements on the CC line sample of a certain length as described in next section.

### 5.3 Theoretical model verification

The wave propagation characteristics of the CC line have already been determined using TDR measurements (section 4.8). The proposed theoretical model of the CC line can be verified by comparing its calculated wave propagation characteristics with those extracted from TDR measurements. The TDR response of the measuring set-up is also verified using EMTP-ATP.

### 5.3.1 Model parameters verification

The theoretical model of the CC line is verified experimentally using TDR measurements and the wave propagation characteristics extracted from both techniques are compared. The CC is considered by placing it at the same height above the ground level (7 cm) while extracting its frequency-dependent wave propagation characteristic from both techniques.

The attenuation curve obtained theoretically from the CC geometry data is plotted against the attenuation curve obtained from TDR measurements as shown in Fig. 5.3. It is revealed that attenuation curves obtained from both techniques have a good agreement until few MHz (see Fig. 5.4). However, the curve obtained from TDR measurements suffer in noise at higher frequencies due to measuring limitations, which has already been explained in section 4.8.

The propagation velocity curves obtained from the theoretical model and TDR measurements are drawn in Fig. 5.5. It is clear that these curves have a good agreement at lower frequencies; however, the curve obtained from TDR measurements suffer in noise at higher frequencies. From Fig. 5.3 and Fig. 5.5, it can be deduced that the proposed theoretical model of the CC line is valid at higher frequencies as well, where TDR technique fails to extract the wave propagation characteristics from the measurements at higher frequencies due to measuring limitations.

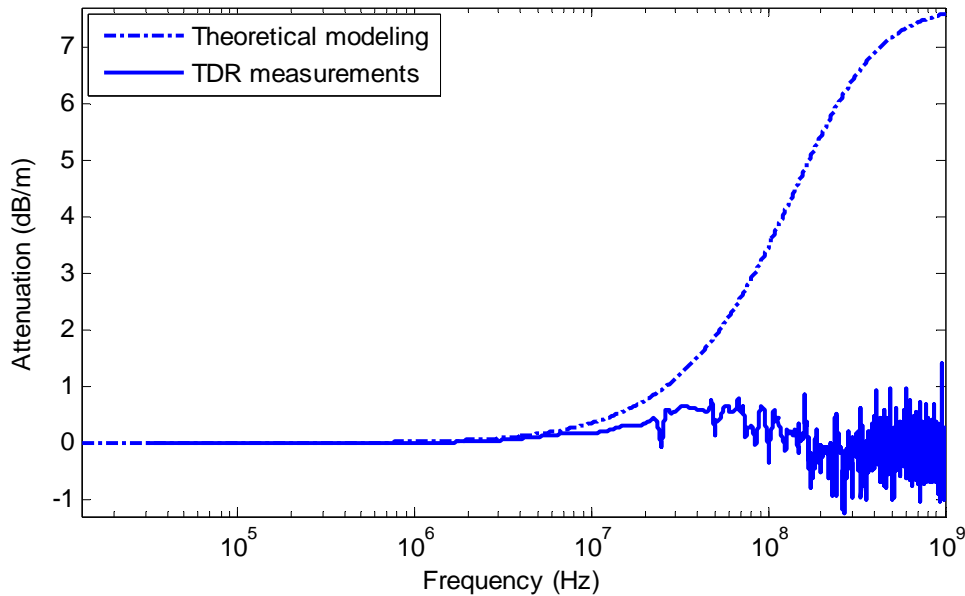


Fig. 5.3 Attenuation curves obtained from different techniques

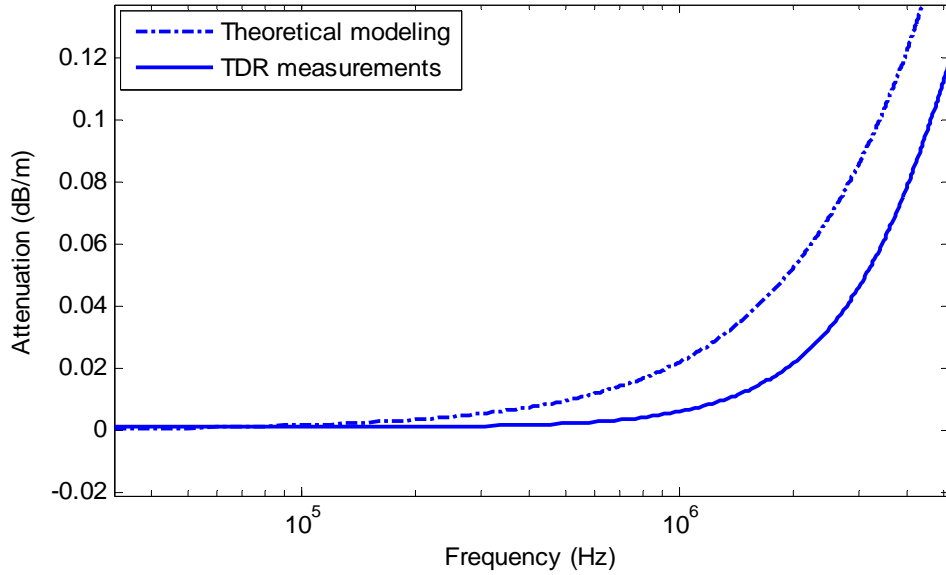


Fig. 5.4 Attenuation curves enlarged in the lower frequency region

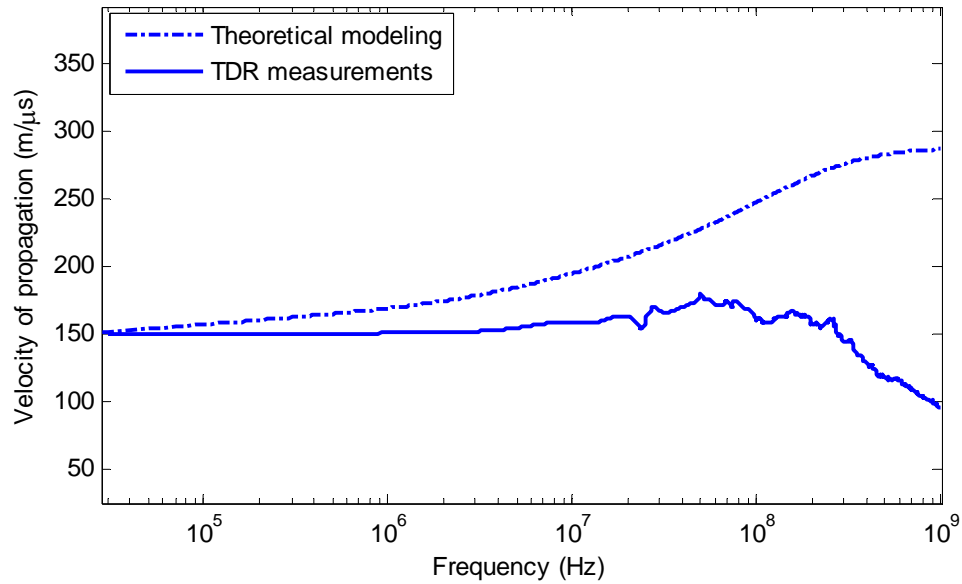


Fig. 5.5 Propagation velocity curves obtained from different techniques

### **5.3.2 Time domain verification using EMTP-ATP**

#### **A. Short description of EMTP-ATP program**

The ATP program is considered to be one of the most widely used software for digital simulation of transient phenomena of electromagnetic, as well as electromechanical nature in electric power systems. It has been continuously developed through international contributions over the past 20 years, coordinated by the Canadian/American EMTP user Group [84].

The ATP program calculates variables of interest within electric power networks as functions of time, typically initiated by some disturbances. Basically, the trapezoidal rule of integration is used to solve the differential equations of system components in the time domain. Non-zero initial conditions can be determined either automatically by a steady-state phasor solution or they can be entered by the user for some components. With this digital program, complex networks of arbitrary structures can be simulated. Analysis of control systems, power electronics equipment, and components with nonlinear characteristics such as arcs and corona are also possible. Symmetric or unsymmetrical disturbances are allowed, such as faults, lightning surges, and any kind of switching operations including commutation of valves. Calculation of the frequency response of phasor networks is also supported.

ATPDraw for windows is a graphical mouse-driven preprocessor to the ATP version of the EMTP. It assists to create and edit the model of the electrical network to be simulated, interactively. It is developed by SINTEF Energy Research (formerly EFI), Norway [85]. In the program, the user can construct an electric circuit by selecting predefined components from an extensive palette. The preprocessor then creates the corresponding ATP input file, automatically in correct format. Circuit node naming is administrated by ATPDraw and the user only needs to give name to “key” nodes. ATPDraw is most valuable to new users of ATP and is an excellent tool for educational purposes. It is to be hoped, however, that even experienced users of ATP will find the program useful for documentation of circuits and exchanging data cases with other users. The possibility of building up libraries of circuits and sub-circuits makes ATPDraw a powerful tool in transient analysis of electric power systems.

## **B. ATP model of TDR measuring system**

In the above sub-section, a theoretical model of the CC line has been verified using TDR measurements. The accuracy of the theoretical model for determining its line characteristics is assured by analyzing the time domain model of the TDR measuring system in EMTP-ATP simulation environment. The ATPDraw is used as a graphical interface and the corresponding network of the TDR measuring system (see Fig. 4.4) is drawn in Fig. 5.6.

The TLs are represented using distributed parameters Clark model. The coaxial cables are considered as lossless lines having zero resistance (due to shorter lengths of 1 m) and  $50 \Omega$  characteristic impedance. As the high frequency signals propagation is being investigated, the average values of the line characteristics at MHz frequency range are used for ATP simulations. The calculated CC line characteristics using the theoretical model are used in simulation as: resistance,  $3.5 \Omega/\text{m}$ ; propagation velocity,  $155 \text{ m}/\mu\text{s}$ ; and characteristic impedance,  $160 \Omega$ . The low propagation velocity of CC line is due to its location near the ground level. The calculated characteristic impedance value can also be verified using various formulae proposed in [48], [82], [86]. The transient response of the CC line for TDR measurements and its ATP simulation response are drawn in Fig. 5.7.

The experimental and the simulated time domain amplitudes and phases of the reflected pulses from the open end of the CC line have a good match. It verifies that attenuation and propagation velocity have the same values in both responses. It shows that TDR measuring system has successfully been modeled, which proves the accuracy of the measuring system. However, the reflected pulses obtained from TDR measurements are distorted. This pulse distortion results as the incident and the reflected pulses travel unequal lengths of line. Therefore, the shapes of the waves will differ as a result of the frequency-dependent attenuation.

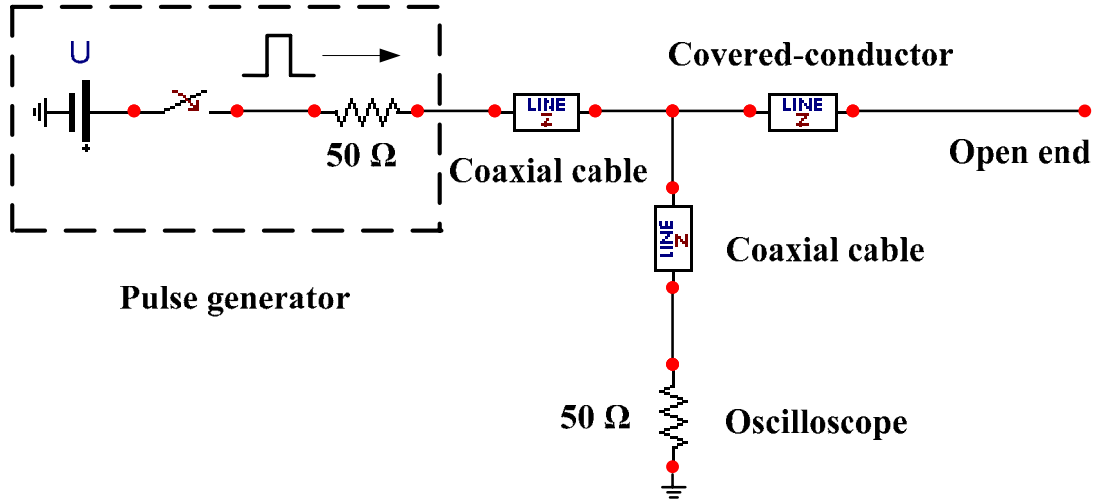


Fig. 5.6 ATP Draw circuit for the TDR measuring system

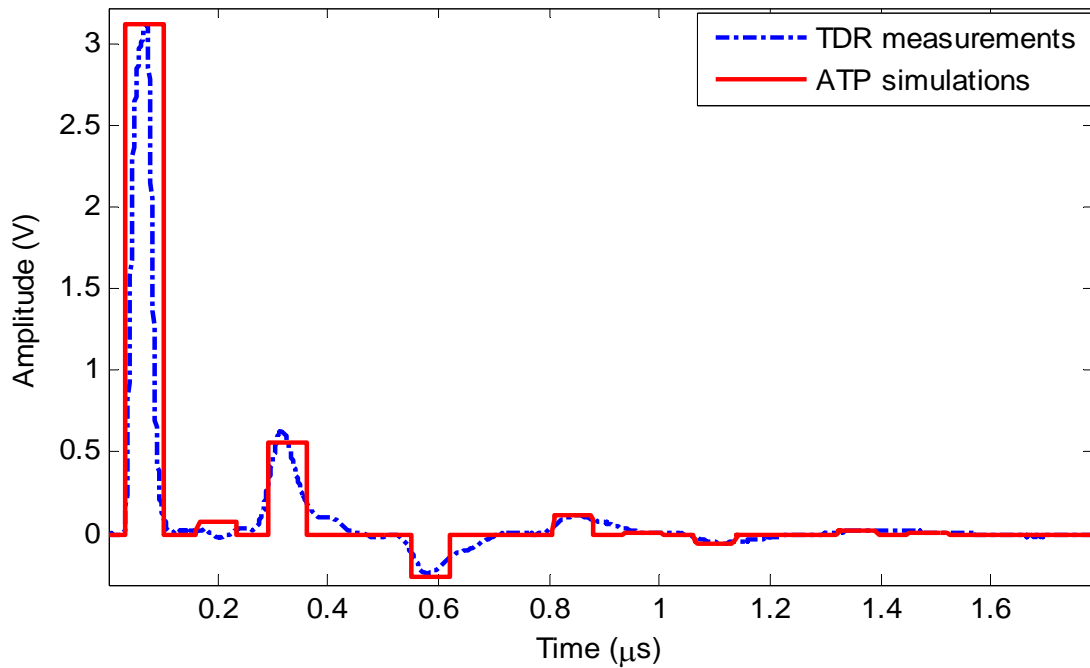
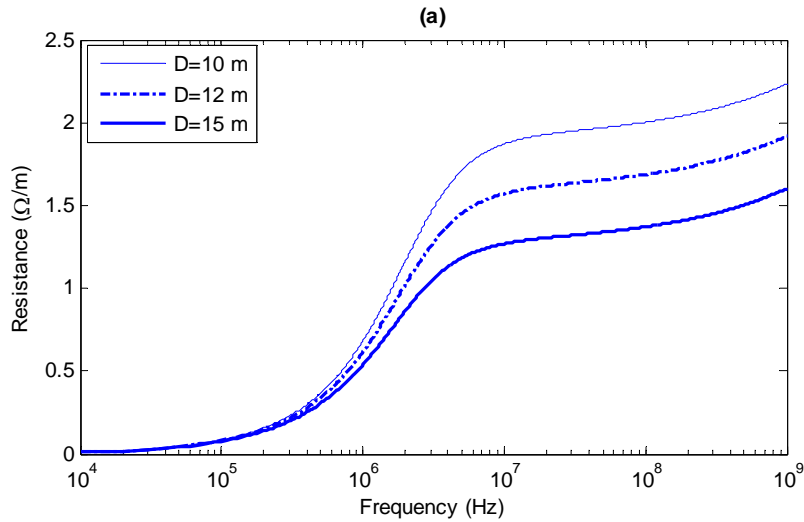


Fig. 5.7 Transient response verification for TDR measurements

## 5.4 Theoretical model results

The CC lines in MV networks are located at different heights above the ground level (e.g., 10, 12, and 15 m) in different regions, depending upon the number of customers, distribution network topologies, and the prevailing environmental conditions. Moreover, the conductor height depends upon the design of the insulators, clamps, and the poles on which they are mounted. The frequency-dependent TL parameters can be derived from the proposed theoretical model for the practical CC lines located at different heights above ground level. The results are obtained by assuming CC lines placed at a fixed height above ground level. However, distribution lines inevitably have sags, which are not taken into account when calculating equations (5.1)-(5.11). The derived frequency-dependent TL parameters for practical CC lines are shown in Fig. 5.8 [87].

It is revealed that  $R$  and  $G$  are frequency-dependent; however,  $L$  and  $C$  are more or less independent of the frequency of the propagated signals. The increase in  $R$  and  $G$  is due to skin effect which is dominant at higher frequencies.  $R$ ,  $G$ , and  $C$  decrease as the height of the conductor above ground level ( $D$ ) is increased; however,  $L$  increases by increasing the conductor height. The effect of conductor height upon the value of  $G$  is not significant as can be seen in the case of other line parameters.



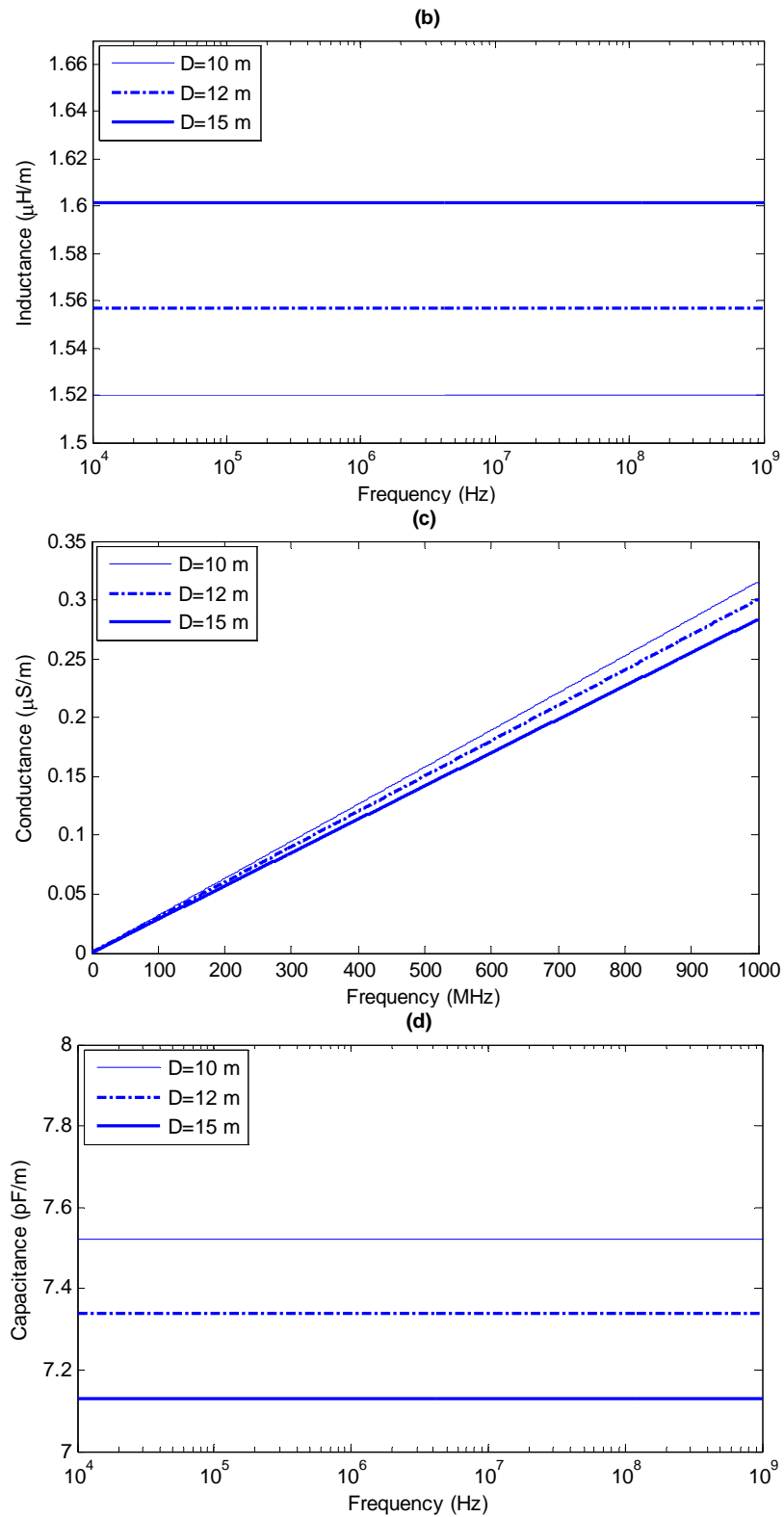


Fig. 5.8 The per-unit length TL parameters of CC overhead distribution line located at different heights for  $\epsilon_{rg}=10$ ; (a) resistance, (b) inductance, (c) conductance, and (d) capacitance

The dependency of the wave propagation characteristics and characteristic impedance upon the height of the conductor above ground level ( $D$ ) is shown in Fig. 5.9 [87]. The attenuation and propagation velocity are frequency-dependent and these parameters increase by increasing the frequency of the propagated signals. The characteristic impedance is more or less constant at all signal frequencies. The attenuation decreases by increasing the conductor height above the ground level, and conversely, propagation velocity and characteristic impedance increase by increasing the conductor height. These results have a good agreement with the values given in reference [14] that also verify the accuracy of the proposed theoretical model. The results given in Fig 5.9 are drawn for  $\epsilon_{rg}=10$ . In general, the ground permittivity is not clear and  $\epsilon_{rg}=1, 10, \text{ and } 20$  are often used. The wave propagation characteristics and characteristic impedance of CC line for different values of ground permittivity at  $D=15$  m are drawn in Fig. 5.10. It is revealed that attenuation decreases and propagation velocity increases by increasing the ground permittivity, however, the effect is not significant in lower frequency range. The characteristic impedance of the CC line is more or less independent of the value of ground permittivity.

The results drawn in Fig. 5.9 and Fig. 5.10 are useful for the wave propagation analysis of PD signals produced due to falling trees on the CC line. The attenuation of the CC line can be used as a design aid for the sensor location to get the required signal, so that it can be processed for detecting the presence of falling trees.

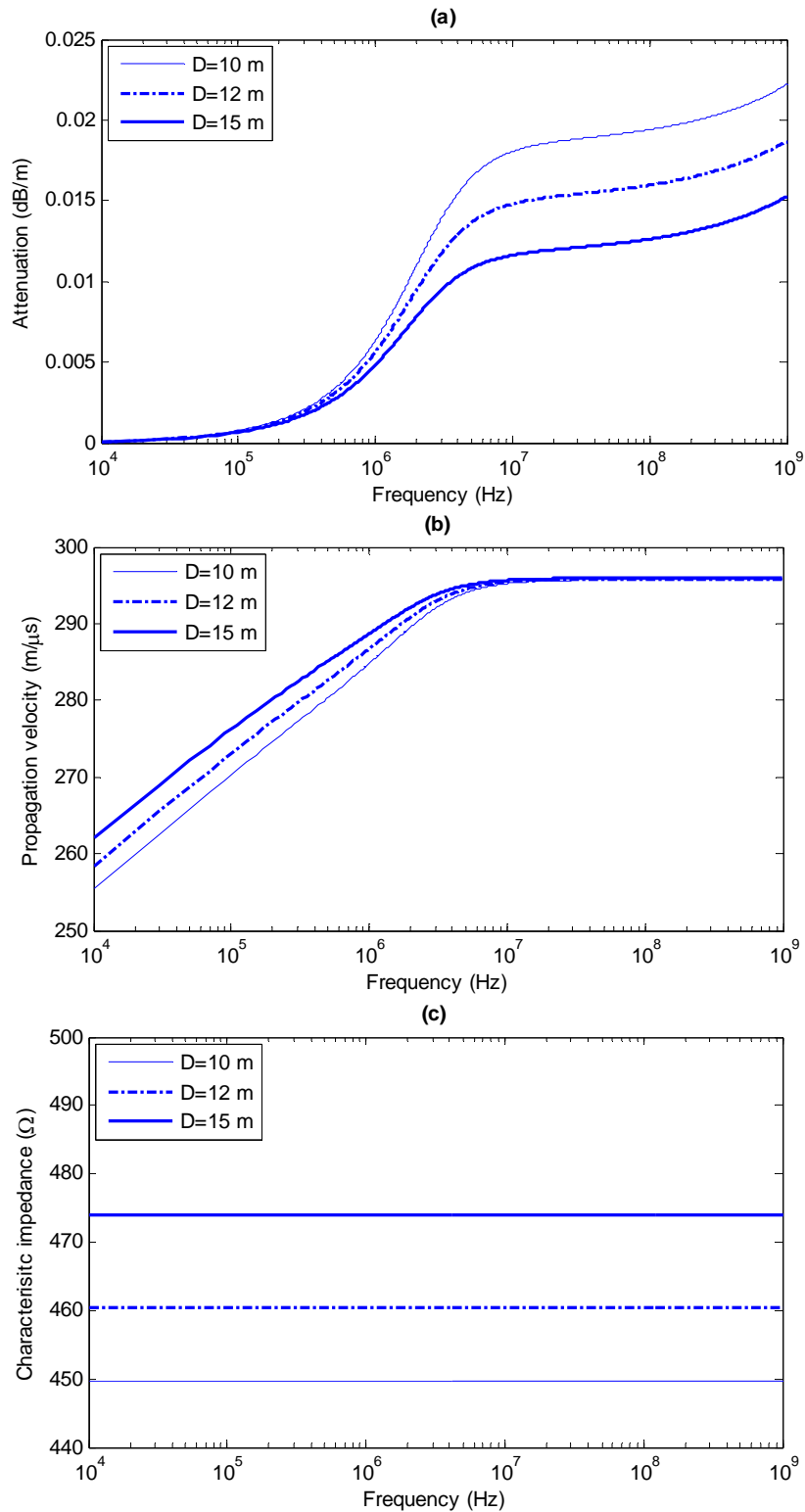


Fig. 5.9 Wave propagation characteristics of MV overhead CC line located at different heights for  $\epsilon_{rg}=10$ ; (a) attenuation, (b) propagation velocity, and (c) characteristic impedance

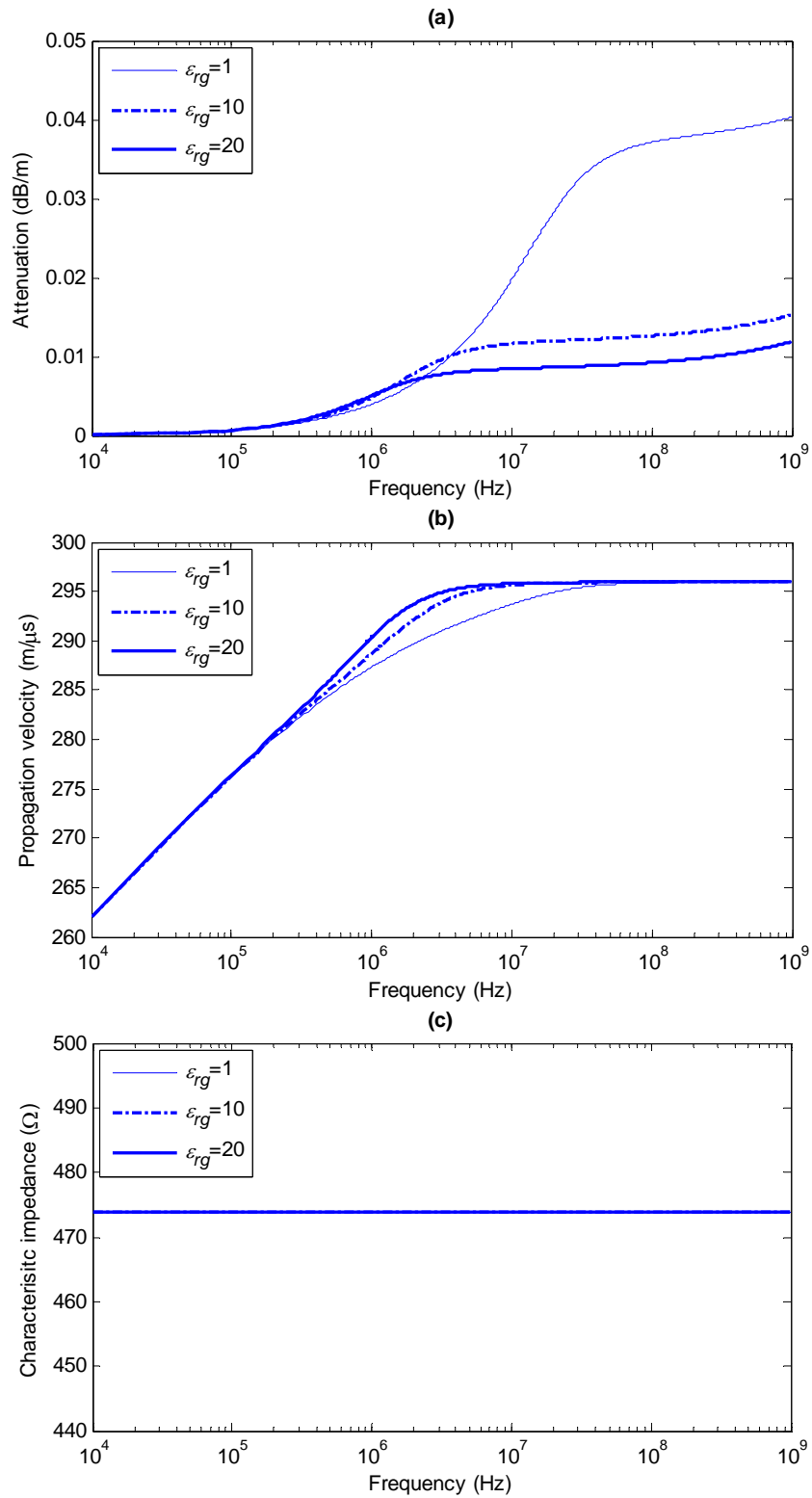


Fig. 5.10 Wave propagation characteristics of MV overhead CC line for different ground permittivities located at  $D=15$  m; (a) attenuation, (b) propagation velocity, and (c) characteristic impedance

## 5.5 Discussion

The theoretical modeling of the CC line based on its geometry has been presented using two-wire TL theory and its frequency-dependent line characteristics have successfully been derived. It is proved that the model does not only give correct values of the wave propagation characteristics at lower frequencies, but it also works well at higher frequencies, where TDR measurements fail to extract these characteristics due to measuring limitations.

The frequency-dependent TL characteristics are extracted from the proposed theoretical model for the practical CC lines in MV networks located at different heights above the ground level. The attenuation of the CC line can be determined for a specific frequency band at which the PD signals produced due to falling trees propagate along the line. Depending upon the severity of fault, this quantity can assure the placing of a sensor to detect falling trees on the CC line. In this way, the safety and reliability of the CC lines will improve; this will also result in reduced costs for inspection work.

The results drawn from the model show that attenuation and propagation velocity in the CC line is strongly influenced by its location i.e., the height  $D$  of the conductor-core above the ground level. The attenuation decreases and propagation velocity increases by increasing the height of the practical CC line above ground level. However, the location of the power cable does not have any effect on the propagation velocity as the distance between the conductor-core and grounding wire remains constant anywhere (for coaxial mode only). Fig. 5.11 shows a comparison of measured attenuation of single-phase MV XLPE power cable (using TDR) and calculated attenuation (using the theoretical model) of the practical CC lines at different heights. It is revealed from Fig. 5.11 that practical CC lines have lower attenuation than power cables. The practical CC lines have higher propagation velocities than power cables and this fact is revealed from Fig. 5.12 [75].

The effect of snow on the wave propagation characteristics of the bare conductor has already been investigated [88]. It is revealed that the admittance is increased by the snow. The difference from the case of no-snow becomes smaller as the frequency becomes higher, because the permittivity of the snow reaches unity as the frequency increases. The increase of the admittance is roughly proportional to the depth, density, and temperature of the snow. The effect of snow on the attenuation constant increases and that on the propagation velocity and characteristic impedance decreases, as the frequency increases. The difference from the no-snow case in the attenuation constant, the velocity, and the step response of wave deformation increases as the snow depth, the density, and the temperature increase. The characteristic impedance depends on the snow depth but not on the density and temperature [88]. In the presented theoretical model, the effect of snow on the wave propagation characteristics of a CC line has not been included. However, the same effects of snow are expected for CC line as mentioned for bare conductor.

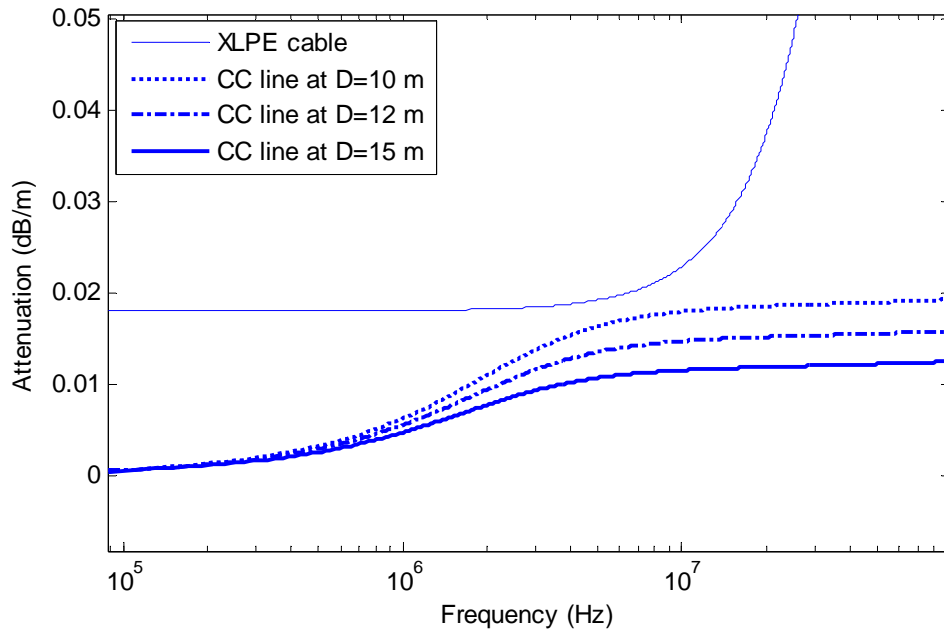


Fig. 5.11 Comparison of measured attenuation for single-phase MV XLPE power cable (for coaxial mode) and calculated attenuation for practical CC lines at different heights above ground level

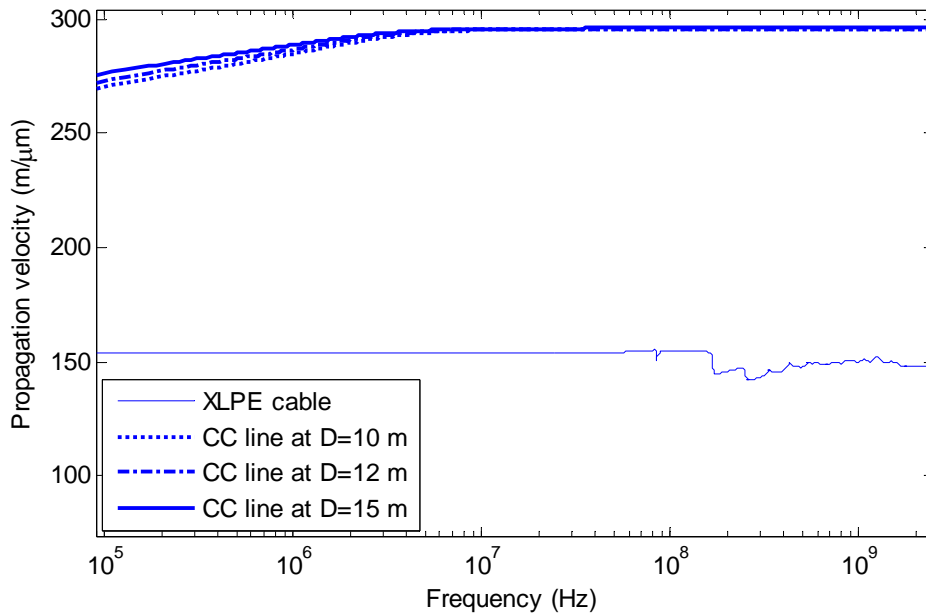


Fig. 5.12 Comparison of measured propagation velocity for single-phase MV XLPE power cable (for coaxial mode) and calculated propagation velocities for practical CC lines at different heights above ground level

The lower value of signal attenuation in the CC line is an attribute to monitor falling trees on it using PD sensors, e.g., a Rogowski coil. Attenuation is an important parameter in order to estimate the maximum length of the line that can be monitored with a PD sensor. The measurement of the attenuation can give an idea about the length of the CC at which the PD signal dies, so that the sensor location can be relied on to get the required signal. Therefore, the attenuation of the PD pulses is an important consideration while deciding the number of the sensors and their positioning over the entire length of the CC line.

The wave propagation characteristics obtained from the theoretical model can be used for the accurate modeling of the CC line in EMTP-ATP simulation environment. The simulated PD measuring system will help in deciding the number and positioning of the sensors to monitor the falling trees over a specific length of the CC overhead distribution lines in an integrated network.

## Chapter 6

### On-line PD Measuring System Modeling and Experimental Verification

*This chapter presents EMTP-ATP simulations to model an on-line single-phase PD measuring system including CC line and Rogowski coil for the monitoring of falling trees on the CC overhead distribution lines. The CC is modeled as a distributed parameters line and the Rogowski coil is modeled based on its equivalent circuit as a saturable current transformer having linear magnetizing characteristics. The simulation results are compared with those obtained from the laboratory measurements. The effect of the Rogowski coil terminating impedance is analyzed for the performance of the PD measuring system. The proposed model can be used to estimate the length of the CC line at which PDs due to falling trees can be detected; thus deciding the number and positioning of the sensors over a particular length of the CC overhead distribution line. The wired Rogowski coil used in this research work would be converted into a wireless one in future. The challenges in on-line condition monitoring of falling trees on the CC overhead distribution lines using wireless sensors are also discussed.*

#### 6.1 High frequency distributed parameters model of Rogowski coil

The attenuation of the CC line approximated from the Rogowski coil measurements is much higher than measured using TDR method or calculated from the theoretical model of the line [57], [71], [87]. As the theoretical model of the CC line has already been experimentally verified using TDR measurements [87], the higher attenuation in the Rogowski coil measurements is an issue that needs a deeper analysis. To resolve this matter, the PD measuring system is modeled in EMTP-ATP simulation environment to investigate the source of high attenuation.

The Rogowski coil used in this research project is a commercial model, therefore its parameters cannot be changed easily. The PD wave propagation due to falling trees on CC lines can be thoroughly investigated by changing the parameters of the Rogowski

coil, and their effect on the PD detection phenomenon in terms of coil bandwidth and sensitivity. This can be done by modeling the PD measuring system and optimizing the Rogowski coil parameters for reliable PD detection in this specific application. The low-cost Rogowski coil can be manufactured in the laboratory on the basis of results drawn from the modeling for real system analysis in the field.

In this research work, the Rogowski coil is used to measure PDs, which typically last a few nanoseconds; therefore, the high frequency behavior of the Rogowski coil is of paramount importance. Up to now, two different models of the Rogowski coil have been developed; the distributed parameters and the lumped parameters model [89]-[91]. The distributed parameters model can help in calculating the sensitivity  $H$  (V/A) of the Rogowski coil used in ATP simulations, and the transfer function has been extracted from the lumped parameters model (see Fig. 3.4) to analyze its bandwidth [55].

A model of the distributed parameters to analyze the high frequency behavior of the Rogowski coil has already been developed [92]. In this model, the system is considered as a distributed line with per-unit length parameters; resistance  $R_d$  ( $\Omega/\text{m}$ ), inductance  $L_d$  (H/m), and capacitance  $C_d$  (F/m). For a Rogowski coil of length  $l_{rc}$  (m), characteristic impedance  $Z_{0rc}$  ( $\Omega$ ), propagation constant  $\gamma_{rc}$ , and terminating with an impedance  $Z_{out}$  ( $\Omega$ ), the transfer function that relates the induced voltage  $V_{rc}$  (V) with the output voltage per-unit length  $V_{outd}$  (V/m) measured at the terminating impedance is given as [55], [92]:

$$V_{outd} = \frac{\frac{Z_{out}}{sL_d + R_d}}{1 + \frac{Z_{out}}{Z_{0rc}} + \frac{1 + e^{-2\gamma_{rc}l_{rc}}}{1 - e^{-2\gamma_{rc}l_{rc}}}} \cdot V_{rc} \quad (6.1)$$

where  $s$  is the Laplace variable.  $Z_{0rc}$  and  $\gamma_{rc}$  are given as:

$$Z_{0rc} = \sqrt{(sL_d + R_d) / sC_d} \quad (6.2)$$

$$\gamma_{rc} = \sqrt{sC_d(sL_d + R_d)} \quad (6.3)$$

The output voltage can be expressed as [55]:

$$V_{outd} = \frac{Z_{out}}{L_d} \cdot MI \quad (6.4)$$

where  $I$  is the current flowing in the CC line. The coil sensitivity can be calculated using the aforementioned equation as:

$$H = \frac{V_{outd} \cdot l_{rc}}{I} \quad (6.5)$$

## 6.2 ATP simulation parameters calculation

### 6.2.1 Rogowski coil parameters

The geometric characteristics of the circular cross-section Rogowski coil are given in Table 6.1 (see Fig. 3.3). For toroidal coils having a circular cross-section, the lumped parameters can be calculated as follow [55]:

$$R_l = \rho_c \cdot \frac{l_w}{\pi r^2} \quad (6.6)$$

$$L_l = \frac{\mu_0 N_{rc}^2 d_{rc}}{2\pi} \log \frac{d_2}{d_1} \quad (6.7)$$

$$C_l = \frac{4\pi^2 \varepsilon_0 (d_2 + d_1)}{\log \left( \frac{d_2 + d_1}{d_2 - d_1} \right)} \quad (6.8)$$

where  $\rho_c$  is copper resistivity and  $\varepsilon_0$  is air permittivity. In order to provide the coil with appropriate damping, the approximate value of the  $Z_{out}$  can be determined as [89]:

$$Z_{out} = \frac{\pi}{2} \sqrt{\frac{L_l}{C_l}} \quad (6.9)$$

The number of turns of the coil  $N_{rc}$  can be calculated using the approximate value of  $M$  as:

$$N_{rc} = \frac{2\pi M}{\mu_0 d_{rc} \log \frac{d_2}{d_1}} \quad (6.10)$$

The measured parameters of the Rogowski coil lumped model are given in Table 6.2. The Rogowski coil parameters are measured at a frequency of 1 KHz with the help of Agilent 4263B LCR Meter. As the high frequency behavior of the Rogowski coil is being investigated, the measured lumped parameters are preferred for reliable simulation results. The frequency response of the Rogowski coil can be investigated by drawing bode plots from the transfer function using (3.7), and is given in Fig. 6.1. The resonance frequency calculated using the Rogowski coil measured lumped parameters model is 29

MHz. This can also be verified in Fig. 6.1, where the maximum gain is obtained at resonance frequency.

The distributed parameters can be calculated dividing the lumped parameters by the length of the coil  $l_{rc}$ . Using the distributed parameters values in (6.5), the sensitivity of the coil can be calculated.  $H$  is taken as 0.001 (V/A) from the manufacturer's data sheet [56]. In ATP simulations,  $H$  and  $N$  are used to model the Rogowski coil as a saturable current transformer having linear magnetizing characteristics [77]. These characteristics will simulate the behavior of an air-cored Rogowski coil. As the value of  $M$  is not given by the manufacturer, it is assumed to be 200 nH in this work, and  $N$  comes out to be 431 using (6.10).

TABLE 6.1  
GEOMETRY OF THE ROGOWSKI COIL

Geometrical parameters	Specifications
Inner diameter $d_1$	162.4 mm
Outer diameter $d_2$	191 mm
Transducer diameter $d_{rc}$	14.3 mm
Length of the wire $l_w$	25 m
Radius of the wire $r$	1 mm
Length of coil $l_{rc}$	600 mm

TABLE 6.2  
MEASURED LUMPED MODEL PARAMETERS OF THE ROGOWSKI COIL

Lumped model parameters	Measured values
Resistance $R_l$	0.11 $\Omega$
Inductance $L_l$	0.6 $\mu\text{H}$
Capacitance $C_l$	50.3 pF
Terminating impedance $Z_{out}$	2 k $\Omega$

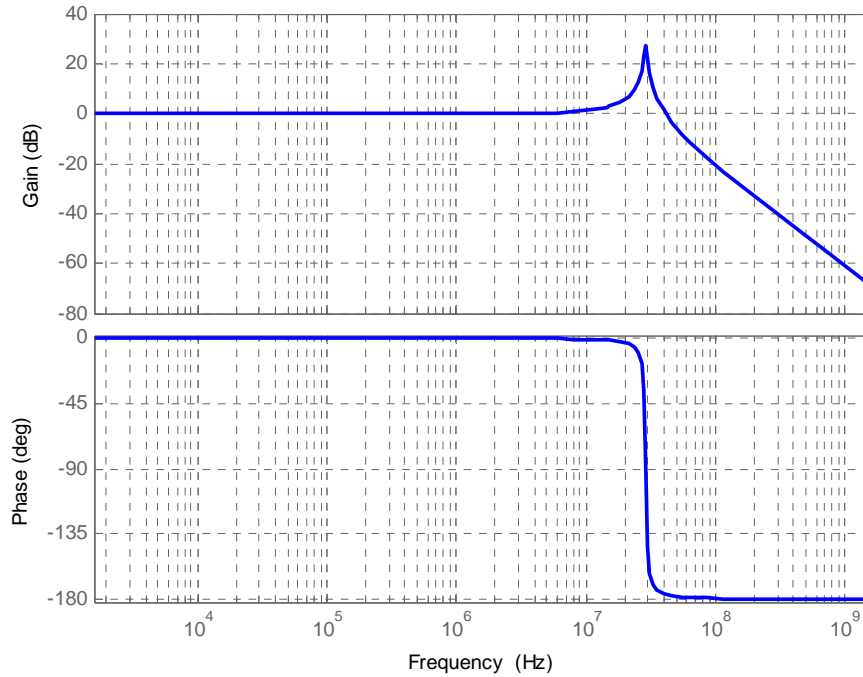


Fig. 6.1 Bode plots for measured lumped parameters model of the Rogowski coil

### 6.2.2 Covered-conductor line parameters

The CC line is mounted at an approximate height of 3 m above ground level in the experimental set-up. The frequency-dependent CC line characteristics can be calculated theoretically [87]. As the high frequency PD signals propagation is being investigated, the average values of the line characteristics at MHz frequency range are selected. The calculated CC line characteristics using the theoretical model are used in simulation as: resistance, 2  $\Omega$ /m; characteristic impedance, 350  $\Omega$ ; and propagation velocity, 230 m/ $\mu$ s. The lengths of coaxial cable and Rogowski coil cable are 1 and 2.3 m, respectively. These lines are considered as lossless lines having zero resistance (due to shorter lengths) and 50  $\Omega$  characteristic impedance. All the TLs are represented using a distributed parameters Clarke model.

## 6.3 ATP simulation results for PD measuring system

### 6.3.1 Modeling of on-line PD measuring system

The on-line single-phase PD measuring system is drawn using ATPDraw and the corresponding network of the PD measuring system including CC line and Rogowski coil is shown in Fig. 6.2. The calibrator pulse produces a simulated PD signal which is traveling down the CC line and is captured by the Rogowski coil at a certain distance over the line.

It has already been determined that PD magnitude produced due to the leaning of a pine tree on the CC line is around 3 nC. This amount can vary depending upon the size, weight, and the species of the leaning tree as well as the prevailing environmental conditions. A 3 nC pulse produced due to a leaning tree propagates in both directions on the CC line; however, 1.5 nC pulse propagating unidirectionally is equivalent to 3 nC pulse discharge in a real system.

When a PD signal is traveling from the pulse calibrator towards the CC line through coaxial cable, there is a mismatch between the characteristic impedances of coaxial cable ( $50 \Omega$ ) and CC line ( $350 \Omega$ ) at the point of their connection (see Fig. 6.2). The signal is not totally transmitted to the CC line and a part of it is reflected back into the coaxial cable. Using equation (4.1), the reflection coefficient  $\Gamma$  in this case is 0.75. Therefore, only 25% of the PD signal amplitude will reach the CC line and propagate inside it. If a 5 nC pulse is injected from the pulse calibrator, only 1.25 nC pulse will reach the CC line for further propagation; this amount is approximately equal to PD magnitude produced and propagating unidirectionally due to a leaning tree. Keeping in view above fact, an average value of 5 nC calibrator pulse is simulated in the PD measuring system to make the real analysis of a single pine tree leaning on the CC line. The measured and the simulated 5 nC calibrator pulses are shown in Fig. 6.3 [93]-[95].

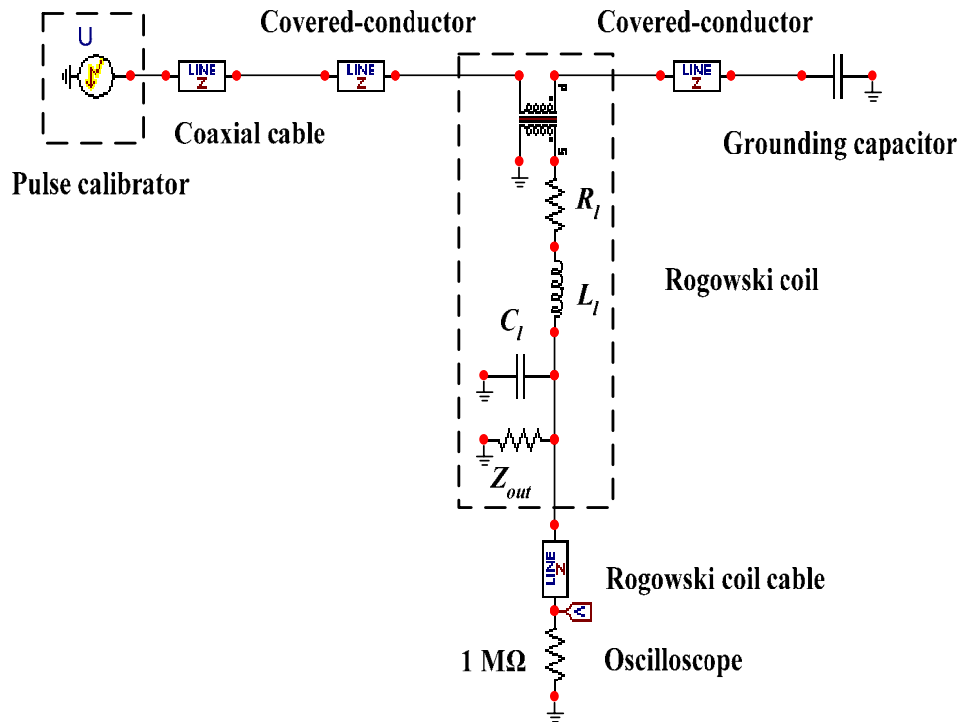


Fig. 6.2 ATPDraw circuit for on-line single-phase PD measuring system

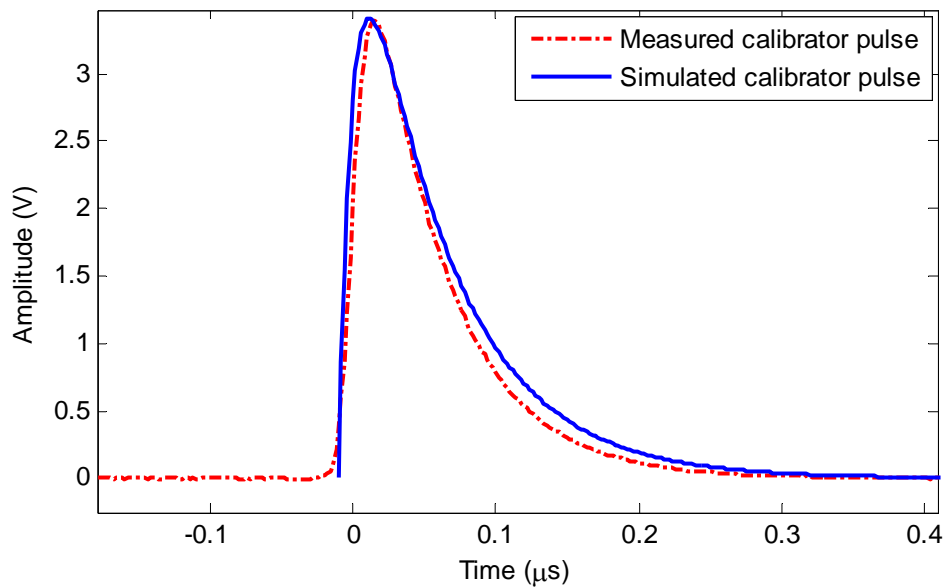


Fig. 6.3 Measured and simulated 5 nC calibrator pulses

A comparison of the measured and simulated voltage pulses captured by the Rogowski coil at point  $P_2$ , as shown in Fig. 3.9 (a), is given in Fig. 6.4. The comparison is carried out considering the time domain performance and FFT analysis. From Fig. 6.4, it is clear

that simulated PD measuring system response has a close match with the measurements, both in the time and frequency domain. It is revealed that resonance occurs at 5 MHz. The resonance frequency of the Rogowski coil is 29 MHz; however, due to the effect of cabling, stray inductances are introduced into the system. This results in the lower value of the resonance frequency of the coil (see Fig. 6.4). The resonance effect can also be verified by determining the simulated transfer impedance of the Rogowski coil as show in Fig. 6.5.

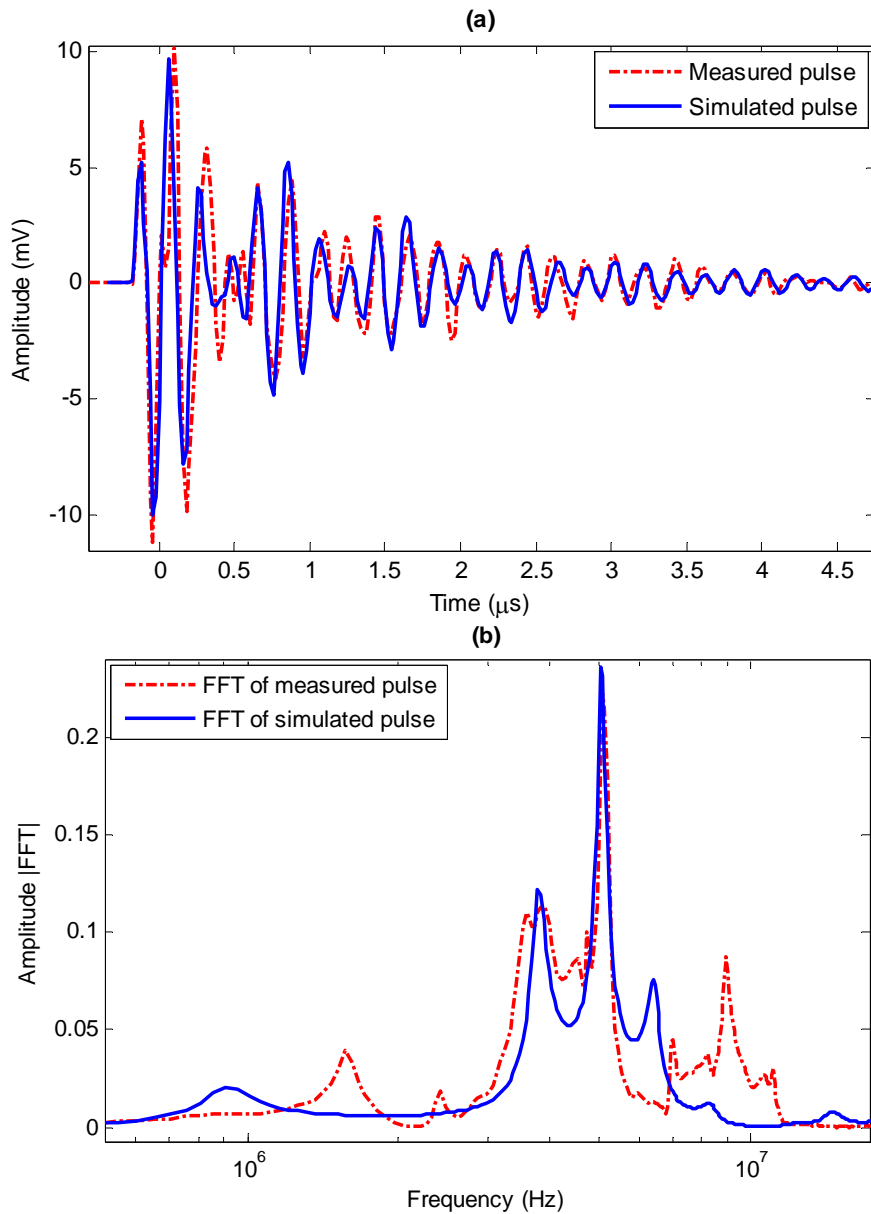


Fig. 6.4 The Rogowski coil response for 5 nC calibrator pulse at point  $P_2$  in (a) time domain, and (b) frequency domain

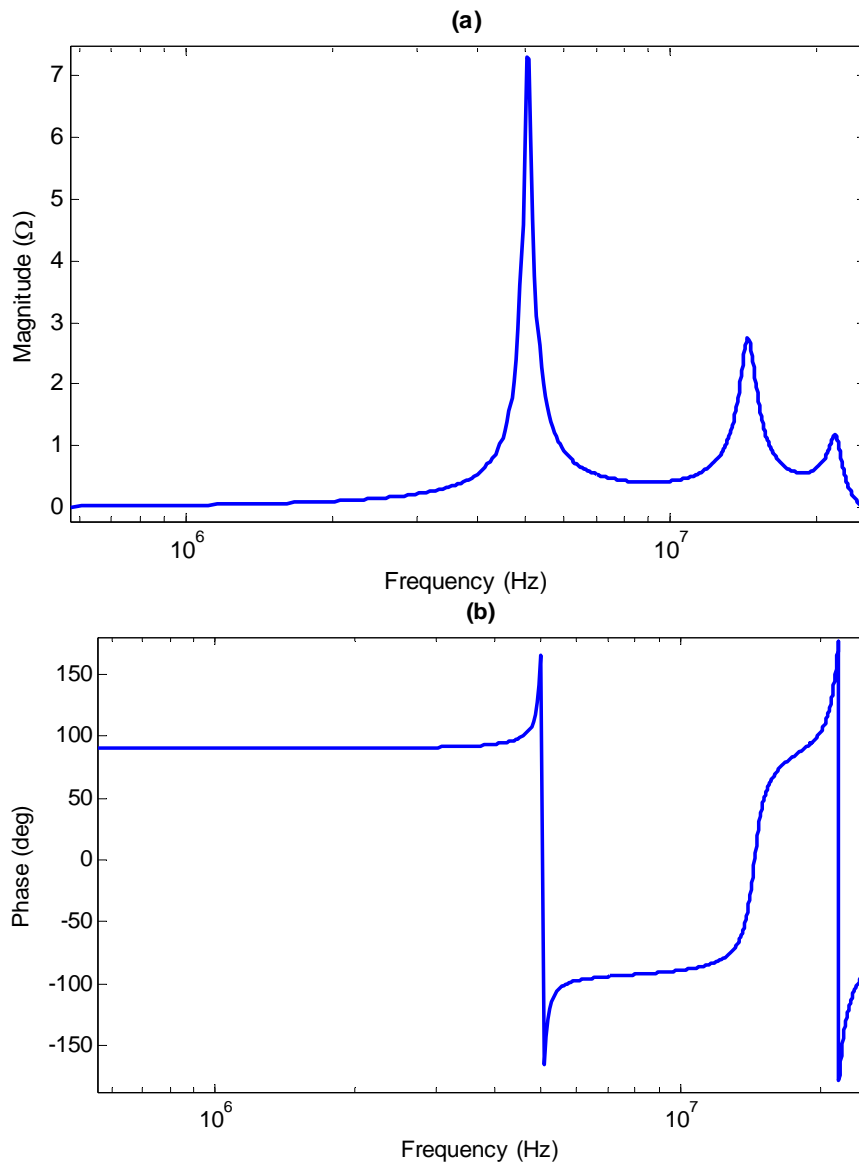


Fig. 6.5 Simulated transfer impedance of the Rogowski coil; (a) magnitude, and (b) phase

The measured and the simulated voltage pulses captured by the Rogowski coil at point  $P_1$ , as shown in Fig. 3.9 (a), are given in time and frequency domain as shown in Fig. 6.6. The amplitudes of the measured and the simulated pulses are not closely matched in the first few cycles, and the pulses are also distorted in phase. This can be explained by the fact that the resonance frequency of the Rogowski coil has different values (in measurements) at different locations along the CC line. This can be due to the effect of stray capacitances, introduced during the measurements taken at point  $P_1$ , which is nearer to the exposed metal components lying in the HV laboratory.

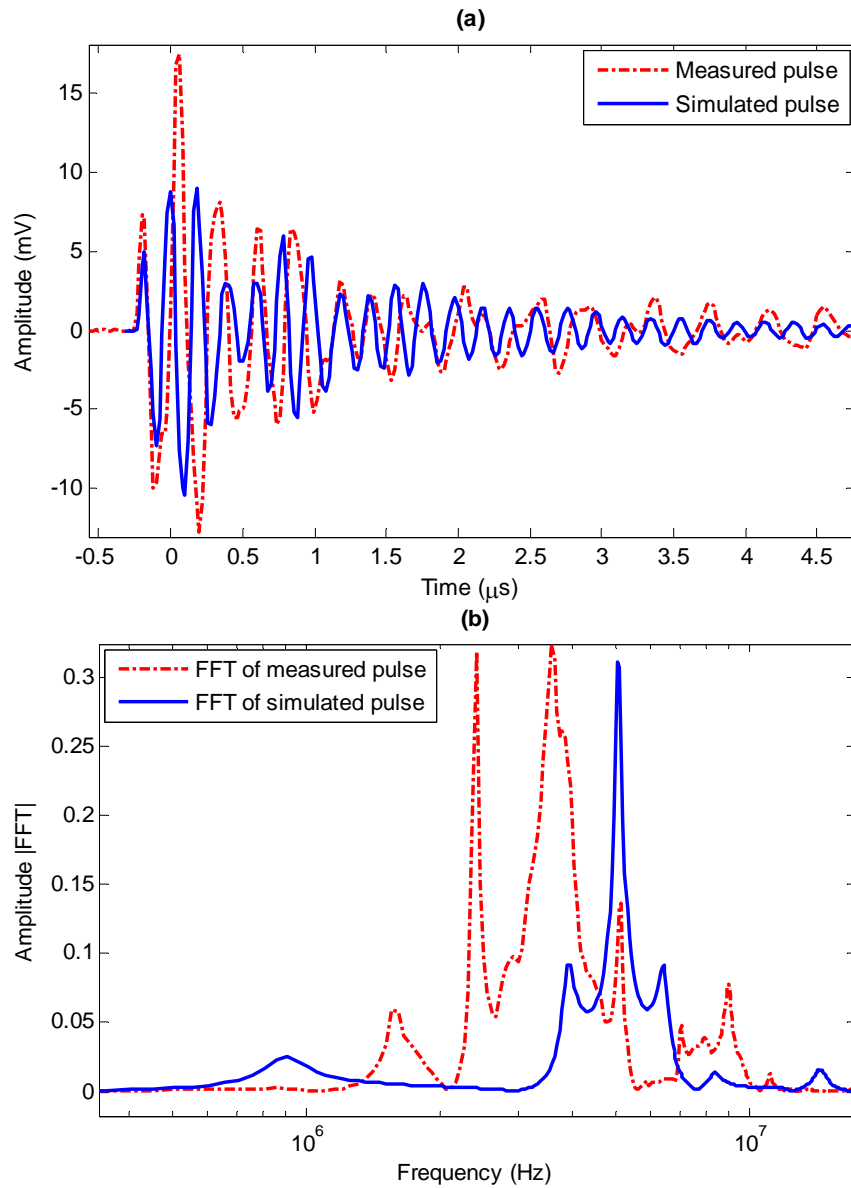


Fig. 6.6 The Rogowski coil response for 5 nC calibrator pulse at point  $P_1$  in (a) time domain, and (b) frequency domain

Another reason which explains the odd behavior of the Rogowski coil measurements can be the unequal clearance of the CC above ground at different locations, resulting in different values of the line capacitances. The higher attenuation calculated from the Rogowski coil measurements can be due to the effect of its varying resonance frequencies at different distances from the pulse calibrator [57]. An on-site PD measuring system can be more reliable in terms of its fixed geometrical parameters.

### 6.3.2 Effect of Rogowski coil terminating impedance

The Rogowski coil terminating impedance  $Z_{out}$  has a significant effect on the performance of PD measurements in terms of the coil's bandwidth and sensitivity. The sensitivity of the Rogowski coil decreases by decreasing the terminating impedance; however, bandwidth increases by decreasing the terminating impedance as shown in Fig. 6.7.

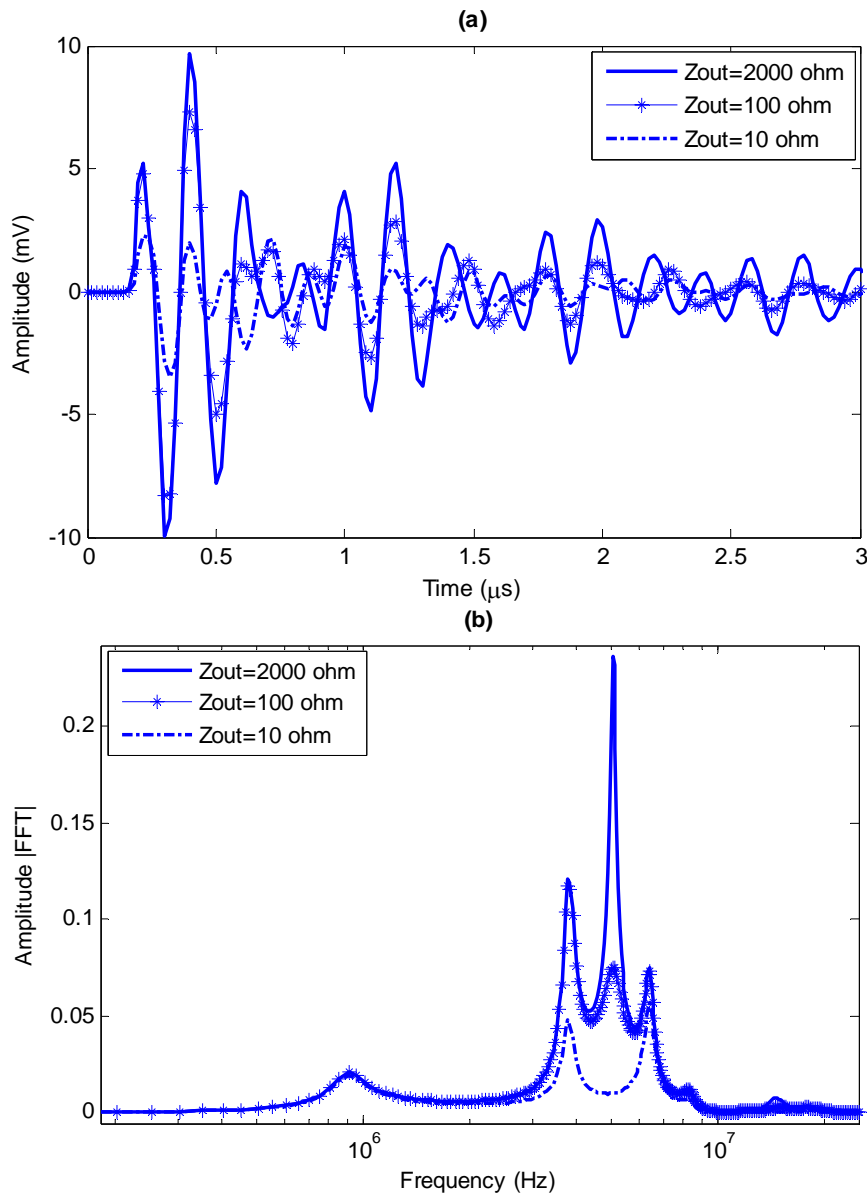


Fig. 6.7 Effect of the Rogowski coil terminating impedance  $Z_{out}$  on the PD measurements (a) time domain, and (b) frequency domain

There is a trade-off between the bandwidth and the sensitivity of the coil by selecting a suitable value of terminating impedance for the required signals. Fig. 6.7 shows the simulated voltage amplitudes captured by the Rogowski coil (at point  $P_2$ ) on CC line in the laboratory for different values of terminating impedances. The number of turns of the coil  $N$  has also a similar effect on the sensitivity and bandwidth of the coil; the sensitivity increases and bandwidth decreases by increasing the number of turns of the coil. The Rogowski coil used in this research work has higher values of  $N$  and  $Z_{out}$ ; therefore it has higher sensitivity.

### 6.3.3 Simulation results for practical CC lines

In section 6.3.1, the PD measuring system is modeled for CC line mounted at an approximate height of 3 m above ground level (the same height in the experimental setup). It would be interesting to analyse the PD measurements for practical CC lines which are normally mounted at a height of more than 10 m. For this purpose, the CC line characteristics for a real situation (line at a height of 15 m above ground level) can be calculated from the theoretical model, and are used in simulation as: resistance, 0.54  $\Omega$ /m; propagation velocity, 288 m/ $\mu$ s; and characteristic impedance, 475  $\Omega$  [87].

Fig. 6.8 depicts the simulated PD measurements for a CC line in the laboratory (at 3 m height) as well as for a practical line (at 15 m height) in real system. However, the comparison is made by keeping  $S_2=23.7$  m and  $S_3=5.5$  m in each case (see Fig. 3.9). It is revealed from Fig. 6.8 that the Rogowski coil measurement has higher voltage amplitude for practical CC line as compared to CC line in laboratory. Therefore, the sensitivity of the measurements increases for practical CC lines due to higher height, which results in reduced signal attenuation and higher propagation velocity.

The simulated model can be used in order to estimate the maximum length of the real CC line that can be monitored with a PD sensor. As the PD source (calibrator pulse) is of 5 nC, which is approximately equivalent to a pine tree leaning on the CC line, the maximum distance at which the falling tree can be detected on the CC line from the point of measurement, can be determined. In these simulations, the distance  $S_3$  (see Fig. 3.9) is kept at 3.5 km to avoid the interference of any signal reflections from the termination of the CC line into the actual PD measurements. The PD measurements are taken at different locations on the CC line as shown in Fig. 6.9.

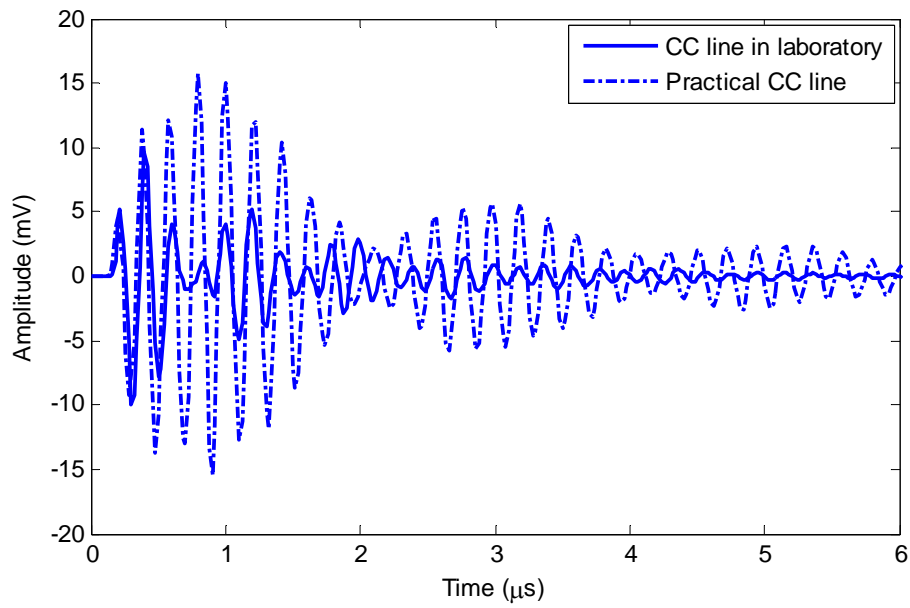


Fig. 6.8 The Rogowski coil PD measurements for CC lines at different distances ( $S_2=23.7$  m and  $S_3=5.5$  m)

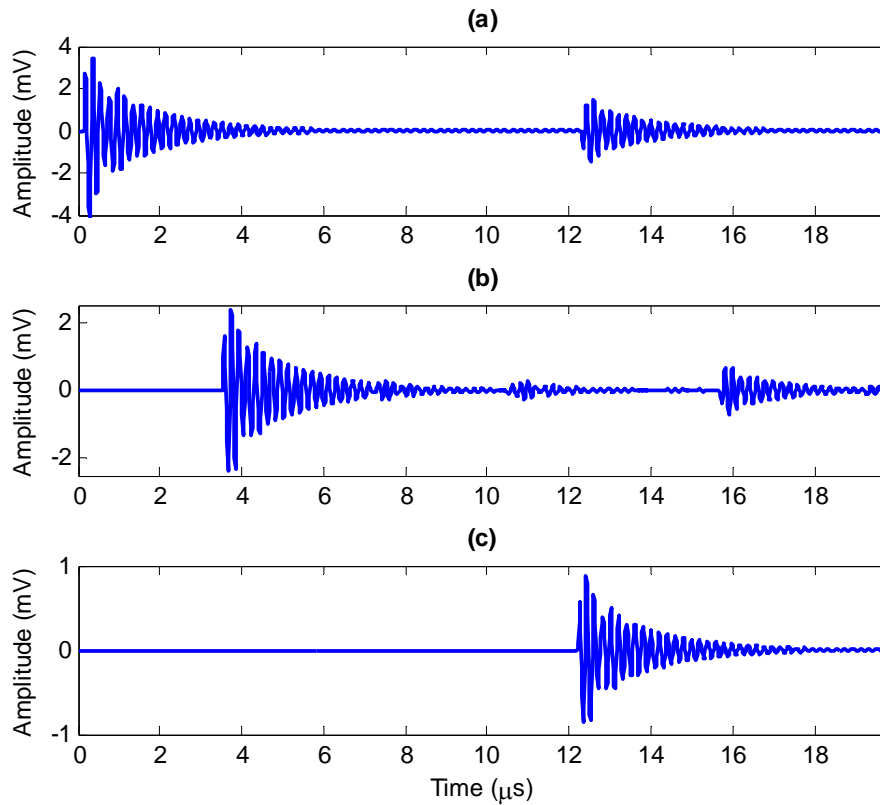


Fig. 6.9 The Rogowski coil PD measurements due to leaning of a single tree on practical CC lines (keeping  $S_3=3.5$  km) at different locations; (a)  $S_2=23.7$  m, (b)  $S_2=1$  km, and (c)  $S_2=3.5$  km

The PD pulse captured by the Rogowski coil in Fig. 6.9 (a) initiates at  $t=0.08 \mu\text{s}$ . The value of propagation velocity  $v$  used in simulations is  $288 \text{ m}/\mu\text{s}$ ; therefore, the distance traveled by the signal until it reaches the point of insertion of the Rogowski coil is  $S_2=vt=23.04 \text{ m}$ , which is in good agreement with the value used in simulation ( $23.7 \text{ m}$ ). Similarly, the initiation times for the signals in Figure 6.9 (b) and (c) are  $3.5$  and  $12.2 \mu\text{s}$ , and the distances covered by these signals are  $1.008$  and  $3.513 \text{ km}$ , respectively (the values used in simulations are  $1$  and  $3.5 \text{ km}$ , respectively). This reveals that the simulated PD measuring system can be used to detect the PDs due to falling trees as well as localizing the falling trees on the CC lines.

The interference of signal reflections from the CC termination has a dominant effect on the PD measurements. The signal captured by the Rogowski coil for practical CC line ( $S_2=23.7 \text{ m}$  and  $S_3=5.5 \text{ m}$ ) has a voltage amplitude of  $15 \text{ mV}$  (see Fig. 6.8). However, if the distance between the measurement point and CC line termination is increased ( $S_2=23.7 \text{ m}$  and  $S_3=3.5 \text{ km}$ ), the voltage amplitude decreases to  $3.5 \text{ mV}$  (see Fig. 6.9). This reveals that the laboratory measurements would also have the effect of interferences in the actual PD measurements due to the reflections from the nearby CC line termination. The simulated Rogowski coil measurement results shown in Fig. 6.9 seem free of interferences as the measurement point is at a distance of  $3.5 \text{ km}$  away from the CC line termination.

## 6.4 Wireless sensors concept for on-line PD measurements

### 6.4.1 Motivation for wireless sensors

The rapid development in electronics, microcontroller performance, digital signal processing, and wireless communication has opened up possibilities to implement new industrial sensor solutions on the process level. One such promising concept is the wireless sensor [96]. Wireless sensors can be used in several applications like environmental monitoring, medical diagnosis, and different industrial condition monitoring applications. The wireless sensors may become a key technology, especially in on-line condition monitoring, as they are cheap and can easily be embedded in the processes (also as retrofit). They do not need wiring, which is a source of noise and unreliability [97].

The motivation for using wireless sensors in power system instrumentation is generally twofold: economy and safety. From a system operation perspective, wireless sensors give an opportunity to safely and cost efficiently increase measurement coverage of the network, including locations where wiring is impossible. Hence, more extensive and accurate real-time information regarding the state of the system becomes available to the operator. This means that the components and the network can safely be run closer to their technical limits and that vital information for condition based maintenance of the network assets can be elicited.

Today, one of the biggest shortcomings in distribution automation is the lack of simple and cheap instrumentation solutions that are easy to implement and are applicable in system refurbishment. The cost of instrumentation in a distribution automation system with a high degree of automation is approximately 25% [98]. The overall cost of installing and wiring a sensor exceeds the cost of the sensor by more than ten times [99]. Using wireless communication, installation costs are significantly reduced; no problems appear with damaged signaling cables that would need maintenance, and instrumentation is possible in applications where wiring is unfeasible [97]. Typically these relate to rotating machines as well as medium and HV environments. In these environments, isolation becomes a problem and maintenance activities can be dangerous [99]. In addition, refurbishment and installation without de-energizing the power network is possible. This favors wireless over power line communications (PLC), although PLC has similar advantages to wireless technologies for sensor communication in industrial environments [100].

#### ***6.4.2 Challenges in on-line condition monitoring using wireless sensors***

Wireless sensor networks in general pose considerable technical problems in data processing, communication and system management. These problems are typically caused by a harsh and dynamic environment; combined with bandwidth and energy constraints that affect the communication, data, and signal processing that can be done. One of the biggest limitations is the fact that the wireless sensors are self-powered (the power is drawn from a battery or from energy harvested from the environment). This means that the energy resources are scarce (especially as the sensors should be small, easy to embed in components and economical); only very low frequency sampling and limited data processing can be done in the sensor [97], [101], [102].

For on-line monitoring, especially of fast phenomena like PDs, this means that the sensor has many design challenges. For example, the design of the signal processing filters must be very energy efficient and the designer must know which frequency component are the important ones for the application (to reduce the impact of noise). Also the analogue-to-digital (A/D) conversion is difficult to implement because the A/D converters working at high frequencies have rather high energy dissipation. The samples received from the conversion must be processed by the microcontroller, which means that the requirements on processing and memory capabilities are high.

Minimizing the power consumption is the most important design aspect for wireless sensors. In addition to optimized components and functionality, “shut-down” and power management strategies are used. In wireless sensors for power systems, minimized energy dissipation is essential for the feasibility of integrating the sensor within equipment and components. A light, small sensor is easy to integrate and thus minimizes the impact the sensors have on the power system reliability and operability. To achieve this goal, wireless sensors in power systems should not operate continuously. They instead need properly designed “shut-down” strategies and the means to minimize the

pre-processing done by the sensor. However, they must preserve functionality, i.e., the capability to participate in, for example, state estimation and fault management [96].

Hence, it is clear that the design of a wireless sensor for the measurements of PDs in CC overhead lines needs a totally new design philosophy. To be able to find the right solutions for the design of the critical sensor components, and to be able to find the trade-off that must be made between energy dissipation and functionality, a generic model of the sensor and the PD behavior should be created.

## 6.5 Discussion

ATP simulations are performed to model the Rogowski coil based on its lumped parameters equivalent circuit. The results confirm that ATP can effectively be used to simulate the Rogowski coil transient behavior for PD measurements. The on-line single-phase PD monitoring system is simulated in ATP. The ATP simulation results are verified by comparison with experimental results, which prove that PD measuring system has successfully been modeled that can be used to detect and localize the falling trees on the CC overhead distribution lines. The simulation results show that CC line has very low attenuation, and the higher amplitude pulse measured by the Rogowski coil near the source of PD is due to the effect of its varying resonance frequencies (in the over-damped resonant circuit of the Rogowski coil) at different locations. Moreover, the Rogowski coil measurements in the laboratory are corrupted due to reflections from the nearby CC line termination. Therefore, PD measurements must be de-noised before processing for accurate results. The model can be used to estimate the length of the CC line at which the PDs due to falling trees can be detected; thus deciding the number and positioning of the sensors over a particular length of the CC line. This model can also be applied to determine the design trade-offs that must be made and the data processing algorithms that will be developed for the sensors.

The amplitude of PD signal captured by the Rogowski coil due to the leaning of a pine tree on CC line at a distance of 3.5 km is less than 1 mV. It is quite possible to detect PD signals beyond 4 km distance from the Rogowski coil, provided there are a few trees leaning on the line or the knife scratches are impressed on the CC insulation due to leaning of tree. As the PD pulse is propagating in both directions from the source, it is suggested to monitor 3.5-7 km CC line using one Rogowski coil when deploying several sensors to monitor the full length of the line. In case of leaning trees at more than one location on the CC line within a radius of 3.5 km monitored by one Rogowski coil, it is possible to detect them. However, it would be challenging to localize them. The advanced signal processing techniques can be used in this specific situation to avoid any misinterpretation of the PD detection results.

The Rogowski coil used in this research work is not good for high frequency measurements beyond 5 MHz. Therefore, a higher bandwidth Rogowski coil should be used for real time analysis of PD signals produced by falling trees on the CC overhead distribution lines. The proposed model should also be used for different bandwidth Rogowski coils to validate it for higher frequency applications.

## Chapter 7

### De-noising of On-line PD Signals using Wavelet Transform

*PD measurements conducted in the HV laboratory are less affected by electromagnetic disturbances (EMD). However, on the other hand, online/on-site PD measurements are often affected by several EMD sources. Extracting low level PD signal from noisy backgrounds is a major challenge for on-line condition monitoring. In this chapter, WT technique is proposed as a powerful tool to de-noise the on-line PD signals in CC overhead distribution lines, which are completely buried by EMI. The PD signals are captured in the laboratory environment and on-site measurements are simulated in MATLAB. The principle of de-noising based on MSD is implemented. The proposed method should be implemented in a real system environment to get more stable and reliable on-line/on-site PD detection results for the monitoring of falling trees on the CC distribution lines.*

#### 7.1 Significance of de-noising on-line PD signals

It is well known that PD measurements are widely employed in testing power apparatus after manufacturing [103]. However, there is a recent trend to extend them to on-site measurements, where the major problem encountered is the strong coupling of external noise. In the case of development and routine tests, the PD measurements are carried out in the manufacturer's shielded laboratories, with filtered mains, to reach the demanded measurement sensitivity. However, the problem faced in PD measurements performed in unshielded laboratories as well as on-site conditions is the strong coupling of external noise. This noise can be suppressed by applying several analogue and digital techniques [104]-[109].

A PD measurement has to be performed in an environment free from EMD; therefore, up to now the PD measurements usually have been a HV laboratory technique. On the other hand, monitoring of falling trees on the CC lines need on-site PD measurements and the existence of excessive interferences will significantly influence the measurement sensitivity. The on-site PD measurement is often affected by strong coupled EMI that makes such insulation assessment very difficult [110]. Noise rejection is an important

part of a wider setting of on-line/on-site condition monitoring activities. A schematic diagram of a proposed on-line/on-site condition monitoring system is shown in Fig. 7.1 [111]. Initially, on-site test system calibration has to be undertaken followed by data acquisition. The process of data acquisition essentially consists of the PD sensing stage using the Rogowski coils. Following sensing, the analysis of the corrupted PD signals is necessary. Noise rejection and PD database comparison are essential before reaching a decision on the integrity of the system and the actions that needed to remove the falling trees on the CC lines.

As the PD signal magnitude normally is very low, the on-site PD measurement signal picked up by the sensor is completely buried by EMI and cannot be distinguished by simple visual inspection. In such circumstances, applying noise reduction techniques is required for better SNR. Fortunately, advances in A/D conversion technology and recent developments in digital signal processing (DSP) have enabled an easy extraction of PD signals. The traditional de-noising techniques can only focus on either time or frequency domain resolution. For non-stationary and short transient PD pulses, which occur randomly, the WT is more suitable than the traditional Fourier transform as it provides information in both time and frequency domains.

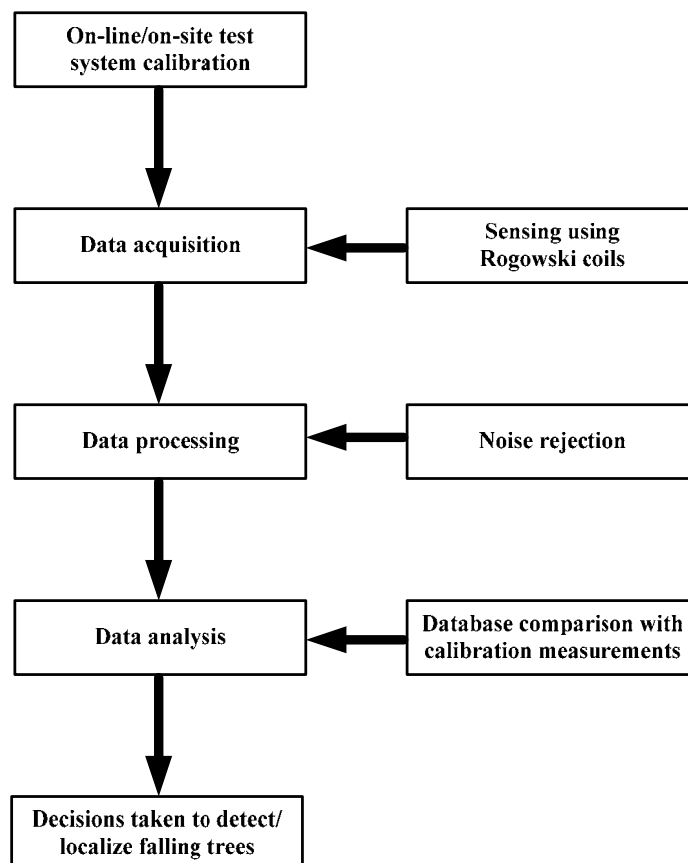


Fig. 7.1 On-line/on-site condition monitoring system philosophy to detect falling trees on CC lines

## 7.2 EMD sources corrupting on-line PD measurements

A major bottleneck encountered with on-line/on-site PD measurements is the ingress of external interferences (usually of very high amplitude comparable to PD signal) that directly affects the sensitivity and reliability of acquired PD data. Digital signal processing techniques must be applied to on-line PD measurements to recognize PD pulses within the EMI background, which often swamps the PD signal on-site. The ability to discriminate the PD signal from the noise requires knowledge of both the PDs and the noise. In general, noise sources may be divided into the following [112], [113]:

- i) Discrete spectral interference (DSI), narrowband interference caused by e.g., radio broadcasts due to amplitude modulation/frequency modulation (AM/FM) radio emissions and communication networks
- ii) Periodical pulse shaped disturbances, repetitive pulses caused by e.g., corona discharges, other discharges due to transformers or power electronics
- iii) Stochastic pulse shaped disturbances, random pulses caused by e.g., lightning or switching operations, PD and corona from the power system which can get coupled to the apparatus under test; and
- iv) White noise, broadband interference caused by e.g., the measuring instrument itself.

Generally, DSI has a narrowband spectrum centered around dominant frequencies. PD signals, however, have a relatively broad spectrum. This difference in spectrum characteristic is utilized to implement notch filters to block that specific band interference. Periodical pulses could be removed by implementing a gating circuit. But for the other two types of disturbances listed above, it is difficult to implement filtering techniques to discriminate PD signals because these types of noise can be either pulses (like PDs) or have a broad spectrum content (also like PDs) [114].

Various methods for post-processing of PD signals have been reported with the advancement in DSP techniques during the last two decades. These methods include the designing of suitable filters e.g., finite impulse response (FIR) and infinite impulse response (IIR) filters, FFT based approaches, moving averages, adaptive filtering as well as wavelet analysis. Among them, wavelet analysis has recently been found to be an extremely efficient tool to de-noise the PD signals under such a harsh environment where PD signal is interacted with various interferences [104], [110], [113], [115], [116].

## 7.3 Wavelet transform analysis

### 7.3.1 *Brief introduction to the wavelet*

A wavelet is small waveform with limited duration and a zero mean value. It oscillates in amplitude and decays to zero quickly on both sides of the central position of the waveform. It is a tool meant for analysis of transients and non-stationary or time varying signals. Similar to the Fourier transform, which breaks up a signal into sine waves of

various frequencies, the WT breaks up a signal into shifted and scaled versions of the original (or mother) wavelet. For a mathematical viewpoint, if a wavelet is defined as  $\psi(t)$ , it has the property of equation (7.1) as:

$$\int_R \psi(t) dt = 0 \quad (7.1)$$

It has to satisfy the admissibility condition  $C_\psi (0 < C_\psi < \infty)$  in equation (7.2) so that a signal can be decomposed and then reconstructed perfectly through the WT.

$$C_\psi = 2\pi \int_R \frac{|\psi(\omega)|^2}{\omega} d\omega \quad (7.2)$$

where  $\psi(\omega)$  is the Fourier transform of  $\psi(t)$  and  $R$  means the sets of real numbers. In wavelet terms,  $\psi(t)$  is referred to as the mother wavelet.

### 7.3.2 Continuous wavelet transform (CWT)

The CWT of a signal  $x(t)$ , consisting of a family of shifted and scaled wavelets associated with  $\psi(t)$  can be described as [117]:

$$CWT_x^\psi(\tau, s) = \frac{1}{\sqrt{|s|}} \int_{-\infty}^{+\infty} x(t) \psi^* \left( \frac{t-\tau}{s} \right) dt \quad (7.3)$$

where  $\tau$  is shift operator (translation),  $s$  is the scaling function, and  $*$  stands for complex conjugation. The value of CWT represents the similarity extent between the examined section of  $x(t)$  and the scaled and shifted wavelets. The greater the CWT, the more energetic it is, and greater the similarity between the wavelets and the original signal.

### 7.3.3 Discrete wavelet transform (DWT)

The CWT is computationally expensive and also generates a lot of redundant data. To overcome these drawbacks, an effective implementation applicable to discrete signals, called the DWT is formulated as [118]:

$$DWT_\psi f(m, k) = \frac{1}{\sqrt{a_o^m}} \sum_n x(n) \psi \left( \frac{k - nb_o a_o^m}{a_o^m} \right) \quad (7.4)$$

The mother wavelet in the above equation is discretely dilated by the scale parameter  $a_o^m$  and translated using the translation parameter  $nb_o a_o^m$ , where  $a_o$  and  $b_o$  are fixed values with  $a_o > 1$  and  $b_o > 0$ , while  $m$  and  $n$  are positive integer values [119]. In case of dyadic

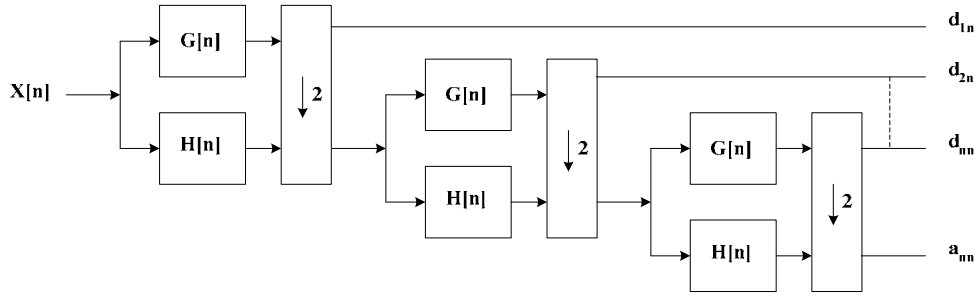
transform, which can be viewed as a special kind of the DWT spectral analyzer,  $a_0=2$  and  $b_0=1$  are taken and the DWT is realized by characterizing the scale variable  $s$  in  $s=2^m$  and assuming the time variable as  $\tau=n2^m$ .

The DWT can be obtained through the use of MSD. A time-scale representation of a digital signal is obtained using digital filtering technique. Filters of different cut-off frequencies are used to analyze the signal at different scales. The time domain signal is passed through a series of high-pass filters and down-sampled by two to analyze the high frequencies (referred to as details). It is also passed through a series of low-pass filters followed by down-sampling by two, to analyze the low frequencies (referred to as approximations). These filters (high-pass and low-pass) are called quadrature mirror filters (QMF), and are exactly halfband filters, thus enabling a perfect error-free reconstruction of the original signal. DWT is implemented using a multistage filter with down-sampling of the low-pass filter output. For reconstruction, the above procedure is followed in reverse order using an inverse discrete wavelet transform (IDWT). The final reconstructed signal is the sum of the approximation and multi-level details [113].

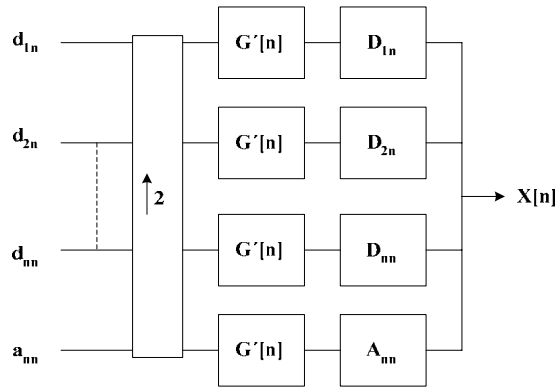
### ***7.3.4 Wavelet-based de-noising procedure based on MSD***

As the PD signals are non-stationary and transients of very short time having broadband frequency spectrum, therefore DWT techniques are viable and superior in rejecting different kinds of inferences from the noisy signal. The principle of de-noising based on MSD wavelet analysis is implemented in this work [113], [115]. The original signal is decomposed into approximation and detail components up to the desired number of levels. This is done by first choosing a suitable mother wavelet according to the signal and noise characteristics. The components corresponding to PD signals, interference, and random noise are identified at each level by visual inspection and knowledge of frequency characteristics. Finally, the de-noised signal is obtained by discarding components corresponding to interference and random noise from the summation process. The reconstruction of the signal based on the selected components gives an interference-free signal. The analysis and synthesis trees of the MSD technique are depicted in Fig. 7.2, where,  $G[n]$  and  $H[n]$  are the high-pass and low-pass filters respectively,  $d_{1n}, d_{2n}, \dots, d_{nn}$  are the details, and  $a_{nn}$  is the approximation.

The selection of “mother wavelet” is an important consideration when using WT. The mother wavelet having the closest resemblance to the original signal is preferred for de-noising it from interferences that have similar frequencies to that of it. Higher compression is achieved when more correlation exists between the mother wavelet and the transformed signal into wavelet coefficients. Among the wavelets available, the Daubechies wavelet family has almost all of the required properties such as compactness, limited duration, orthogonality, and asymmetry for the analysis of fast transient and irregular pulses [116]. Therefore, the Daubechies wavelet family is selected to de-noise the PD measurements in this research work.



Decomposition of signal-Analysis



Reconstruction of signal-Synthesis

Fig. 7.2 Analysis and synthesis trees of MSD technique [113]

## 7.4 On-Line PD de-noising results

### 7.4.1 Processing of laboratory measurements

The PD signals have been captured by the Rogowski coil in the laboratory environment and MSD technique is applied to de-noise these noisy signals. The two signals are:

**Signal-1:** PD signal produced by 50 nC calibrator pulse

**Signal-2:** PD signal produced by leaning two trees on the CC line, while energizing it with 20 kV distribution line voltage.

For signal-1, a 50 nC calibrator pulse is sent from one end of the conductor and the Rogowski coil measurements are taken at a distance of 23.7 m from the point of insertion of the calibrator pulse [57]. This voltage pulse is shown in Fig. 7.3. This pulse is taken and padded with zeros up to the length  $N=2^n$ , for  $n=16$  ( $N=65536$  points) and its FFT is shown in Fig. 7.4. A time step of  $\Delta T=20$  ns is used in the Fourier analysis. From the FFT, it is clear that the dominant frequency contents of the signal-1 lie in the frequency range from 1-4 MHz and the noise could also be seen in the higher frequency ranges.

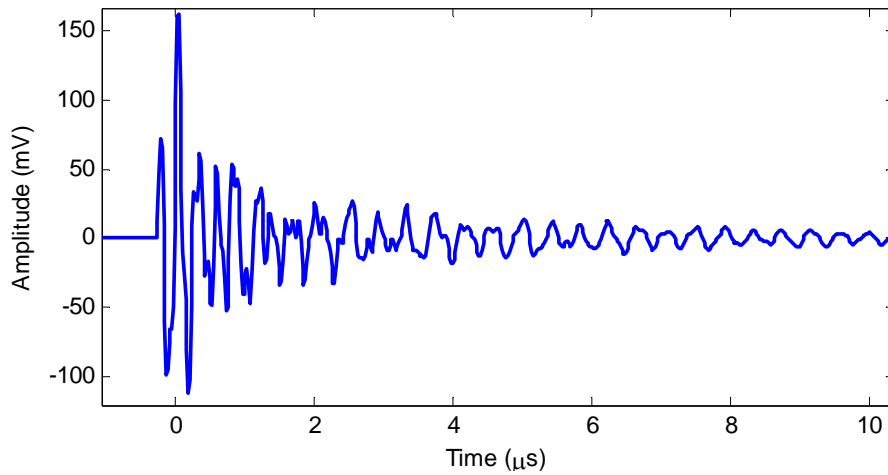


Fig. 7.3 The Rogowski coil voltage response for signal-1

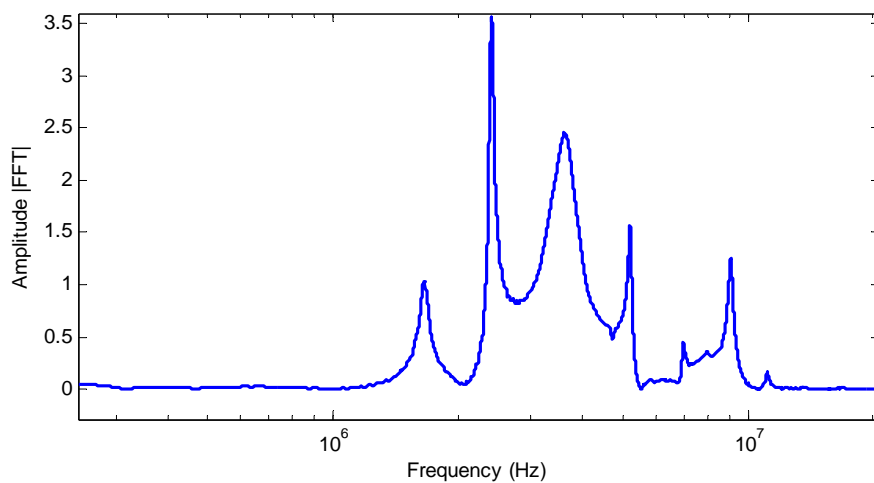


Fig. 7.4 FFT of the Rogowski coil voltage for signal-1

For the processing of signal-1 using MSD, it is decomposed up to level 7 using “Daubechies 7” as a mother wavelet. Fig. 7.5 shows the reconstructed detail components ( $D_1$ - $D_7$ ) up to level 7. The de-noised signal is obtained by selecting the detail component at level 3 only and the others are discarded.

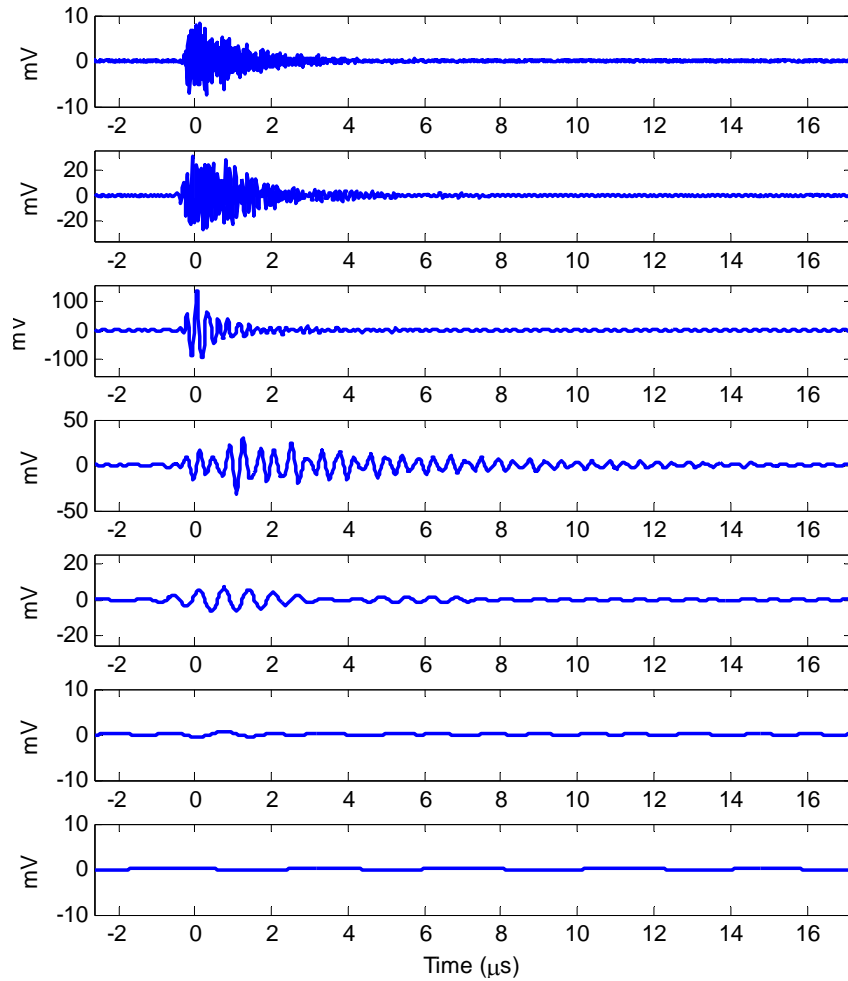


Fig. 7.5 Reconstructed detail components ( $D_1$ - $D_7$ ) up to level 7 for signal-1

In the frequency or time domain, there are some differences between the PD and the external interference characteristics. These differences can be used to implement filtering techniques to discriminate the PD signal from the noise. For comparison, an IIR band-pass filter (Butterworth type) of order 16 having frequency band 1-4 MHz is applied for noise elimination. The pulse becomes smoother after noise suppression. The de-noised pulse is processed in the Simulink model to determine the quantity of the PDs as described in section 3.7. The de-noised signal-1 using WT and IIR filtering techniques is shown in Fig. 7.6.

It is clear from the time domain comparison shown in Fig. 7.6 that the WT technique is faster than IIR filtering. The multi-resolution feature helps in obtaining higher amplitude, better recovery of pulse shape, and a fine frequency separation. The FFT of the de-noised signal-1 using WT technique (see Fig. 7.7) shows the actual broadband frequency spectrum of PD signals, which is better than obtained using IIR filter. It confirms that the

WT technique has successfully de-noised the actual PD signal-1 from the electric and magnetic field coupling between the CC line and the Rogowski coil cabling, which can induce undesirable effects in the latter [120]. Another source of noise inside the laboratory environment could be the reflections induced in the measurements due to the mismatching effects from the CC line termination, as explained in section 6.3.

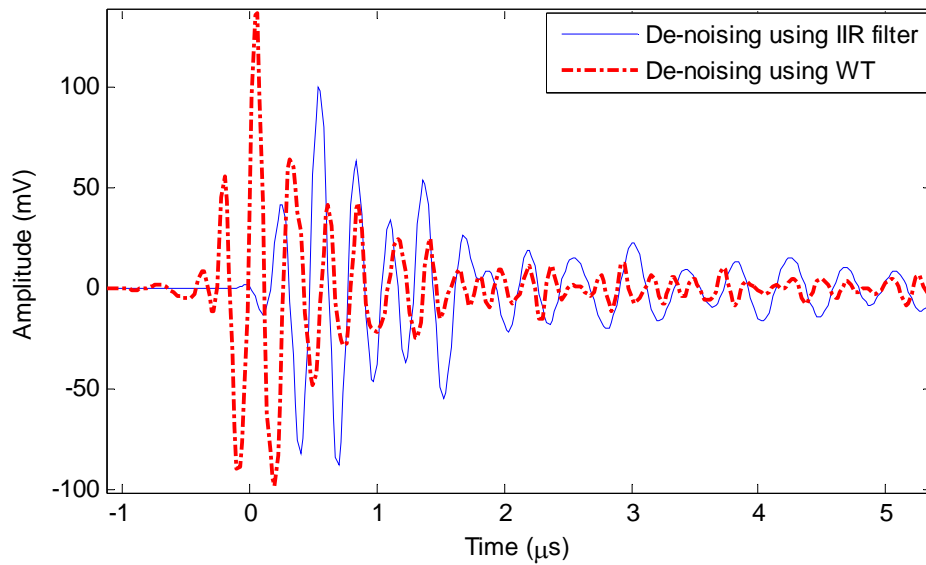


Fig. 7.6 De-noised signal-1 using different techniques

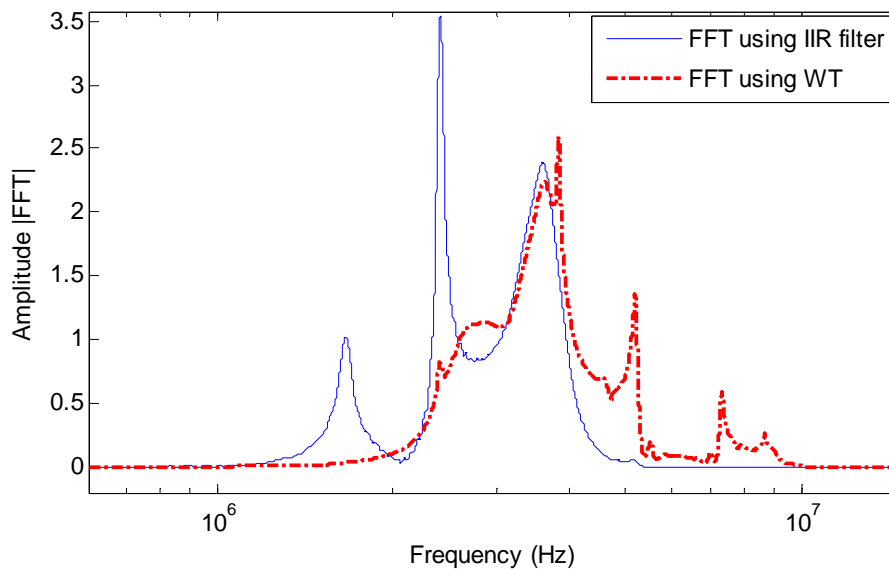


Fig. 7.7 FFTs of de-noised signal-1 using different techniques

For capturing signal-2, the Rogowski coil is placed at a distance of 20.2 m from the leaning trees (see Fig. 3.9). In order to process signal-2 by MSD, “Daubechies 8” is used as a mother wavelet and the signal is decomposed up to level 6. Due to lower sampling frequency (12.5 MHz) of PD signal-2 obtained in this case, higher number of detail components is not possible. Fig. 7.8 shows the decomposition detail components ( $D_1$ - $D_6$ ). After inspecting all the components, the de-noised signal is obtained by selecting the detail component 2 only. The actual and the de-noised signal-2 are shown in Fig. 7.9.

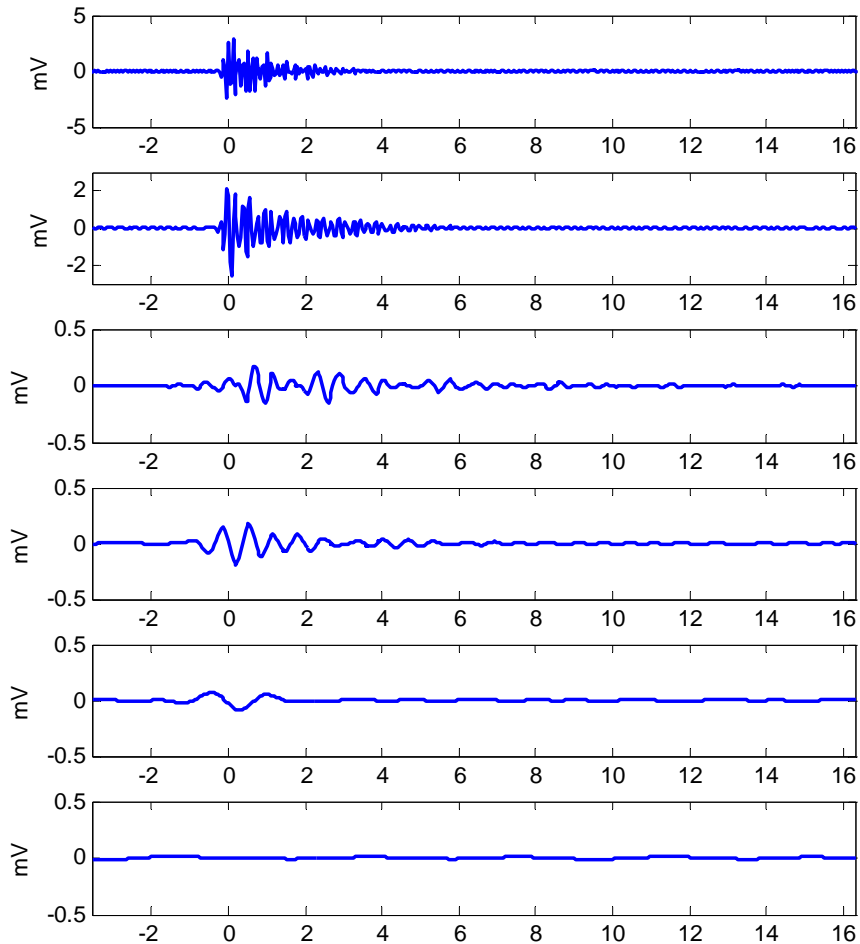


Fig. 7.8 Reconstructed detail components ( $D_1$ - $D_6$ ) up to level 6 for signal-2

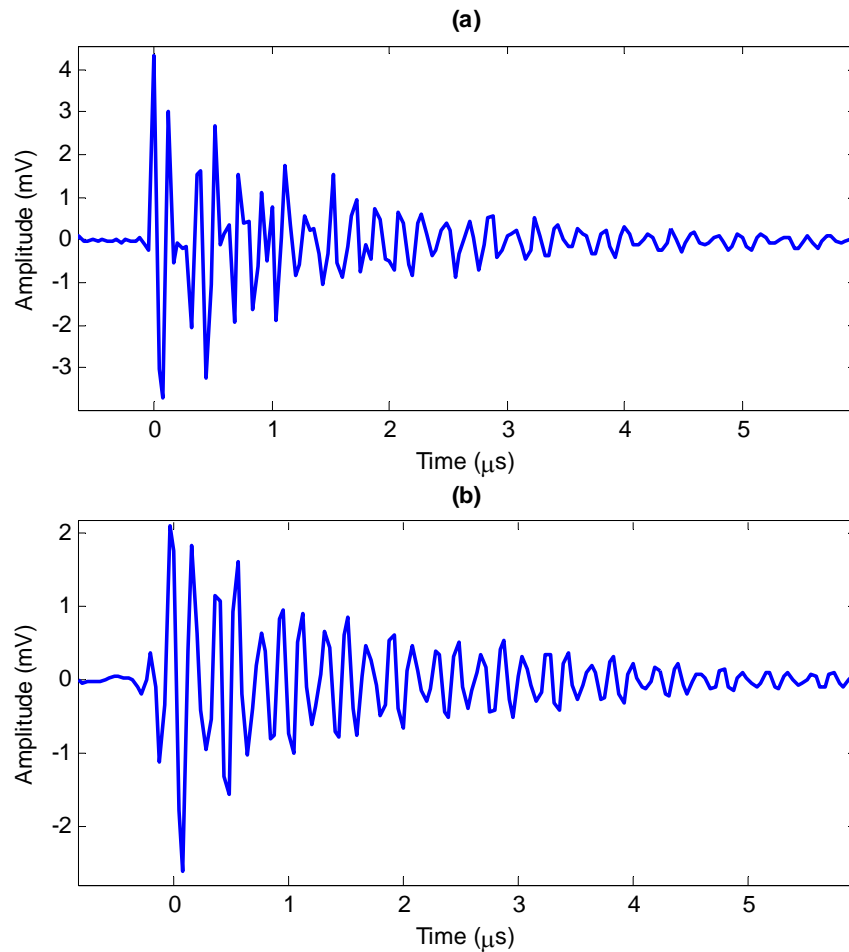


Fig. 7.9 The signal-2; (a) before de-noising, (b) after de-noising

### 7.4.2 Processing of on-site measurements

The on-line/on-site PD monitoring has the major problem of EMI, which often subsumes completely the very low level PD signals picked up by the PD sensors. For the processing of on-site measurements, the PD signal produced by the pulse calibrator (signal-1) is mixed with different types of simulated (in MATLAB) on-site disturbances in the following three patterns [121], [122]:

**Signal-3:** Signal-1 is mixed with simulated random noise

**Signal-4:** Signal-1 is mixed with simulated DSI (sinusoidal signal having 100 mV amplitude with AM radio frequency of 98 KHz)

**Signal-5:** Signal-1 is mixed with a mixture of simulated random noise and DSI (signal-3+signal-4)

For the processing of signal-3 using WT technique, it is decomposed up to level 8 using “Daubechies 7” as a mother wavelet. Fig. 7.10 shows the reconstructed detail components ( $D_1$ - $D_8$ ) up to level 8.

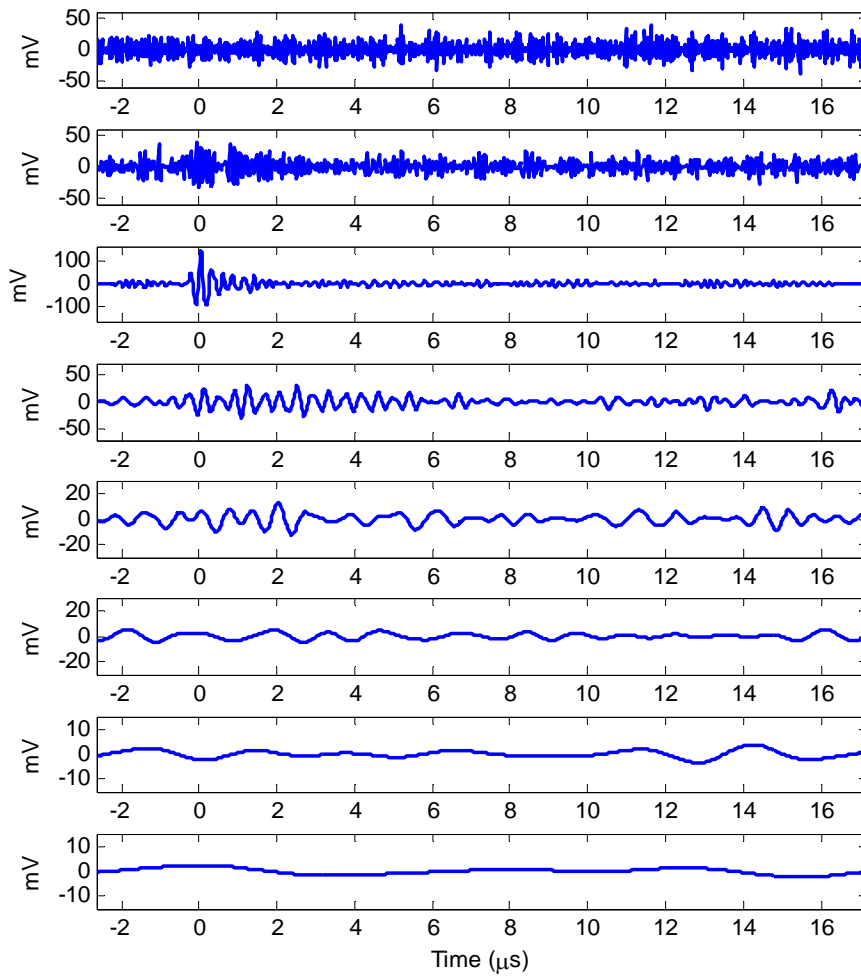


Fig. 7.10 Reconstructed detail components ( $D_1$ - $D_8$ ) up to level 8 for signal-3

The de-noised signal is obtained by selecting the detail component at level 3 only and the rest are discarded. The actual and the de-noised signal-3 are shown in Fig. 7.11. It is clear

that the WT technique has de-noised PD signal mixed with random noise. Although some reflections of smaller amplitude are seen, the overall signal is successfully de-noised.

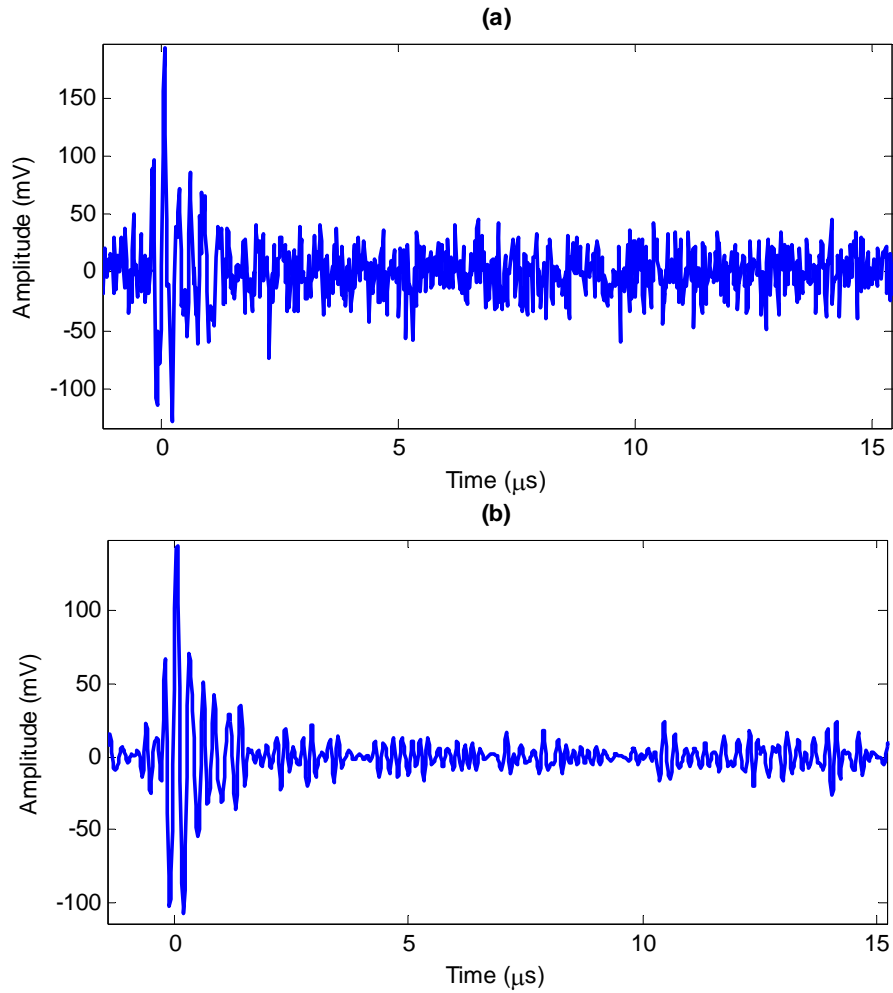


Fig. 7.11 The signal-3; (a) before de-noising, (b) after de-noising

In order to process signal-4 using MSD, “Daubechies 7” is used as a mother wavelet and signal-4 is decomposed up to level 8. The Fig. 7.12 shows the decomposition detail components (D1-D8) up to 8 levels.

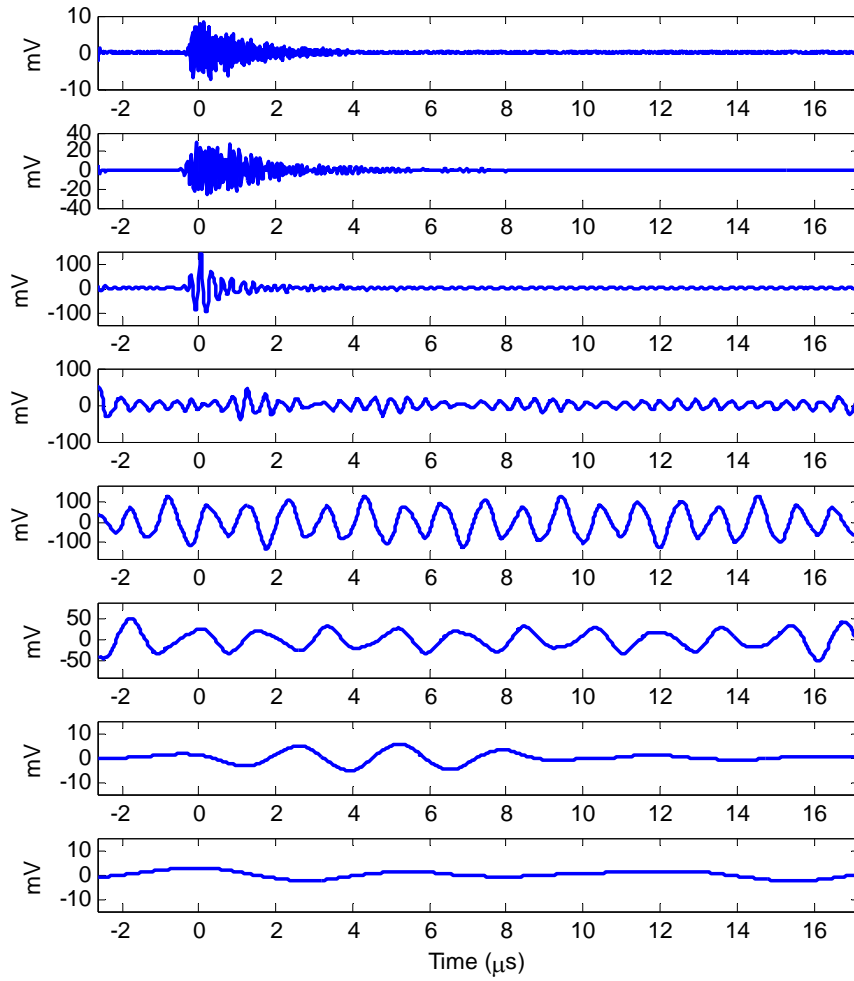


Fig. 7.12 Reconstructed detail components ( $D_1$ - $D_8$ ) up to level 8 for signal-4

After inspection of all components in Fig. 7.12, the de-noised signal is obtained by selecting the detail component 3 only. The actual and the de-noised signal-4 are shown in Fig. 7.13. It is clear that the WT technique has effectively de-noised the PD signal superimposed by AM radio interference of comparable magnitude. In this case, a single AM radio frequency interference is taken into account for DSI. However, various AM/FM radio frequencies interferences with PD measurements are possible in the real on-site environment

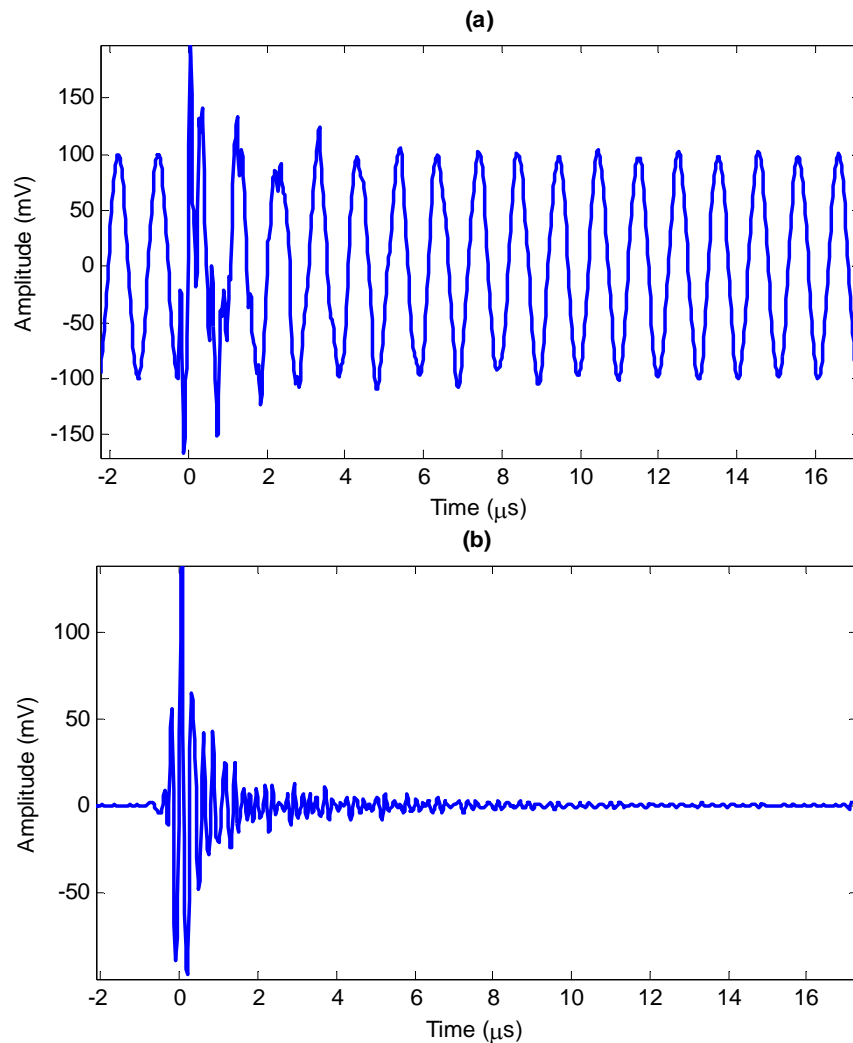


Fig. 7.13 The signal-4; (a) before de-noising, (b) after de-noising

Another possibility is the additive interference due to random noise and AM/FM radio frequency with PD measurements in a harsh environment and this scenario is simulated as signal-5. This signal is processed using MSD where "Daubechies 7" is used as a mother wavelet for analysis. Fig. 7.14 shows the decomposition detail components ( $D_1$ - $D_8$ ) up to 8 levels. The actual and the de-noised signals (by selecting the detail component 3 only) are shown in Fig. 7.15.

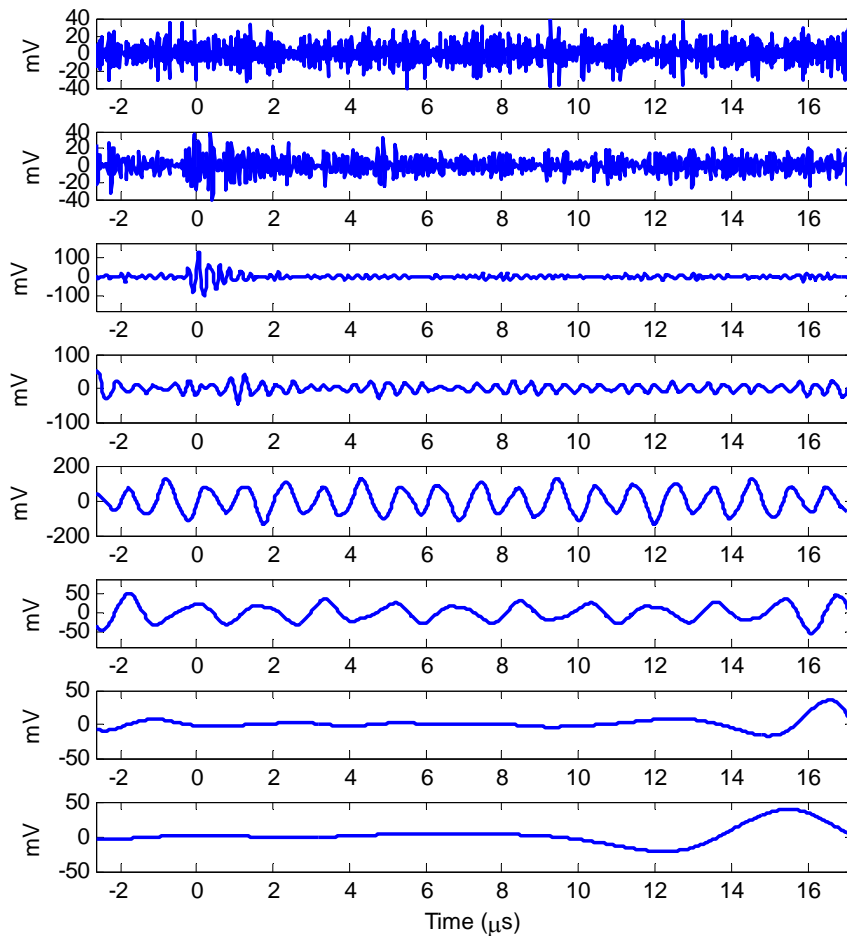


Fig. 7.14 Reconstructed detail components ( $D_1$ - $D_8$ ) up to level 8 for signal-5

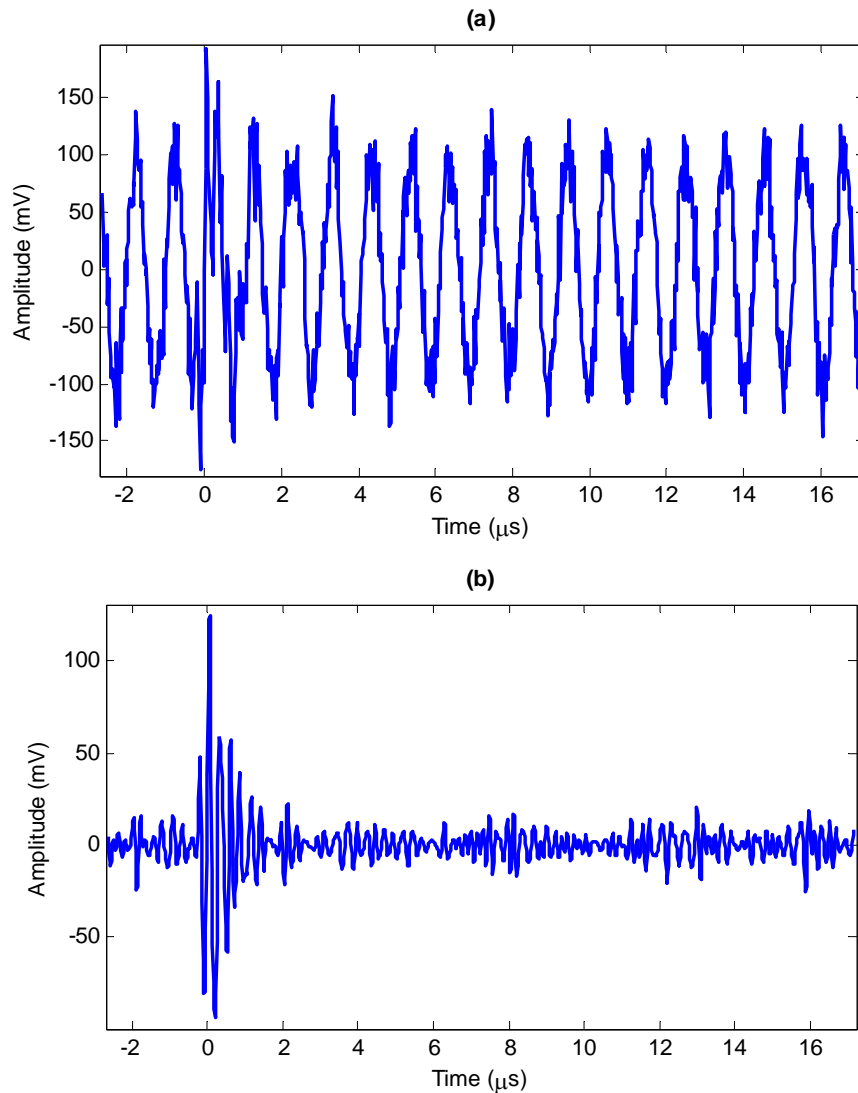


Fig. 7.15 The signal-5; (a) before de-noising, (b) after de-noising

It is revealed from Fig. 7.15 that the WT technique has effectively de-noised the PD signal superimposed by a mixture of random noise and AM radio frequency interference of comparable magnitude. The more practical situation can be simulated by mixing random noise with various combinations of AM/FM frequencies in the measured PD signal and applying de-noising technique.

## 7.5 Discussion

Noise and disturbances are always present in on-line PD measurement, regardless of the technique or system is used. Noise rejection can be achieved at different stages, e.g., sensor design, data acquisition, data processing, by any of them or any combination [123]. A differential system can suppress common-mode interferences effectively, either impulse or periodical interferences, coming from a TL. The noise rejection technique using a balanced circuit or two sensors in differential mode has been well developed and widely used in off-line PD measurement. Apart from its inapplicability to on-line use, it also suffers from the problems, e.g., balance over a wide frequency range and identical apparatuses or dielectric characteristic requirements. These limitations mean the balanced circuit and the hardware differential technique are very hard to implement in practice and successful cases are quite rare in medium/long length cable PD measurement [124].

A novel software based differential technique has been developed and applied for the investigation of cable PD activities in a 33 kV substation [123]. In that fully automatic software, a lot of noise rejection techniques using signal processing rely on the right triggering, where the triggered signal must contain both the PD signal and noise. Then the noise part will be removed by the signal processing technique. This requires experienced staff to perform manual triggering on the “right” signal. Therefore, it is revealed that on-line differential techniques are not sufficient to de-noise PD signals completely. By combining on-line differential technique with WT signal processing, the white noise can be removed, which would eventually increase the measurement sensitivity. In this research work, a single sensor is preferred rather than the two sensors required for the differential technique, keeping in view the challenges faced and the limitations of the latter technique.

Processing of signal-1 and signal-2 reveals the effectiveness of MSD technique for the laboratory measurements. For signal-1, the results of MSD technique are compared with those obtained from IIR filtering approach and found more effective than the latter. From the processing of signal-3, it can be concluded that wavelet method can be equally applied for the on-site measurements corrupted with random noise. The processing of signal-4 and signal-5 reveals that the wavelet method can easily de-noise PD pulses superimposed by DSI or mixture of DSI with random noise. During the processing of above mentioned signals, the minimum loss of pulse magnitude and distortion of pulse shape is obtained, which is a significant consideration for on-line PD measurements and further quantification of the measured results.

## Chapter 8

### Conclusions and Future Developments

*This chapter contains the summary and conclusions of the research work. The future developments of the present research work are also discussed.*

#### 8.1 Conclusions

The use of CC lines has been expanding in MV networks throughout the world over the last 30 years. CC systems are developed to reduce failure rates compared to bare wire MV networks and hence, to improve the security of the supplies. One compelling reason to use CC lines is that they are more compact and environment-friendly than bare conductors. The additional investment cost is often fully compensated by savings in line spacing, reduced maintenance, and a better quality of network. A drawback of CC lines is that falling trees on the line cause a very high impedance fault which cannot be detected with normal or advanced protection relays. However, these leaning trees produce PDs in the insulation of the CC lines, which may rupture after the passage of a certain time, thus introducing different kinds of faults in the network.

A relatively new and challenging application is conducting on-line high frequency PD measurements for the monitoring of falling trees on CC lines. The advantage of on-line PD monitoring allows for conductor insulation diagnostics during normal operation, and specifically, when the trees are leaning on the conductors. By monitoring these PDs on-line, progressive deterioration of the insulation can be indicated. Early detection of developing faults leads to better power quality and increased customer satisfaction. PD monitoring involves the analysis of materials, electric fields, arcing characteristics, pulse wave propagation and attenuation, sensor spatial sensitivity, frequency response, calibration, noise, and data interpretation.

A new on-line PD detection technique for the monitoring of falling trees on the CC lines has been presented. The Rogowski coil has been used as a PD sensor for this application. An experimental set-up was arranged for on-line single-phase PD monitoring system in the HV laboratory at TKK. The PD measurement methodology is based on acquiring

voltage signals captured by the Rogowski coil and processing those in Simulink environment. The measurements have shown that no significant effect has practically been found in time or frequency domain behavior measurements of the Rogowski coil, if the coil geometry is not symmetrically positioned around the CC line. The calibration of the PD measuring system has been carried out using pulse calibrator. The test results have shown that PD magnitudes produced are 2.9, 3, and 3.7 nC when a pine tree without knife scratches, a pine tree with knife scratches, and two pine trees with knife scratches, respectively, are falling on the CC line. It reveals that by increasing the numbers of falling trees, the PD quantities also increase. In addition, knife traces produce PDs. The PD signals initiated by different sources have different frequency ranges and this observation is important for the design of a wireless PD sensor to detect falling trees on CC lines; especially for the development of a low-power signal processing algorithm inside it.

The TDR measurement technique has been presented to extract the frequency-dependent wave propagation characteristics of CC overhead distribution lines. TDR measuring set-up was arranged in the HV laboratory at TKK. In practice, a narrow electric pulse was applied to the CC and the incident and reflected waves were measured by means of a digital oscilloscope. The parameters extraction technique is based on electromagnetic theory. The amplitude of the reflected pulse has been corrected by calibrating the TDR measuring set-up. The wave propagation characteristics (propagation constants, i.e., attenuation and phase constants, and propagation velocity) of a single-phase CC overhead distribution line have been determined. It is revealed that the signal attenuation and propagation velocity are fairly constant at lower frequencies, but these parameters are frequency-dependent at higher frequencies, i.e., their values increase by increasing the frequency. The wave propagation characteristics of a single-phase XLPE power cable and a CC overhead distribution line are also compared. Attenuation in a CC line is much lower than in power cables; however, the situation is the opposite in the case of propagation velocity, i.e., signals propagate faster in CC lines. In the CC overhead distribution lines used in Finland, semi conductive layers are absent; therefore, attenuation is lower as compared to power cables. These measurements can be used for the design and deployment of PD sensors over the entire length of a CC line in order to detect PDs produced by falling trees.

The theoretical modeling of a CC line based on its geometry has been presented using two-wire TL theory and its frequency-dependent line characteristics have successfully been derived. The derived wave propagation characteristics are compared with those obtained from the TDR measurements to validate the theoretical model of the CC line. The TDR measuring system is also simulated in EMTP-ATP as time domain verification of the measurements. It is proved that the proposed model does not only give correct values of the wave propagation characteristics at lower frequencies, but it also works well at higher frequencies, where TDR measurements fail to extract these characteristics due to measuring limitations. It is revealed that resistance and conductance of the practical CC line are frequency-dependent; however, inductance and capacitance are more or less independent of the frequency of the propagated signals. The increase in resistance and

conductance is due to skin effect which is dominant at higher frequencies. The resistance, conductance, and capacitance decrease as the height of the conductor above ground level is increased; however, inductance increases by increasing the conductor height. The effect of conductor height upon the value of conductance is not significant. The results drawn from the model show that attenuation and propagation velocity of the practical CC line are frequency-dependent and these parameters increase by increasing the frequency of the propagated signals. The characteristic impedance of the CC line is more or less constant at all signal frequencies. The attenuation decreases and propagation velocity increases by increasing the height of the practical CC line above ground level. However, the location of power cable does not have any effect on the propagation velocity as the distance between the conductor-core and grounding wire remains constant anywhere. The effect of ground permittivity on the wave propagation characteristics of the practical CC line has also been investigated. It is revealed that attenuation decreases and propagation velocity increases by increasing the ground permittivity, however, the effect is not significant in lower frequency range. The characteristic impedance of the CC line is more or less independent of the value of ground permittivity.

The lower value of signal attenuation in a CC line is an attribute that enables the monitoring of falling trees using PD sensors. Attenuation is an important parameter in order to estimate the maximum length of the line that can be monitored with a PD sensor; it is an important consideration when deciding the number of the sensors and their positioning over the entire length of a CC line.

The on-line single-phase PD monitoring system is modeled in EMTP-ATP simulation environment. The ATP simulation results are verified by comparison with experimental results, which prove that PD measuring system has successfully been modeled that can be used to detect and localize the falling trees on the CC lines. The proposed model can be used to estimate the length of the line at which the PDs due to falling trees can be detected; thus deciding the number and positioning of the sensors over a particular length of the CC line, the design trade-offs that must be made, and the data processing algorithms that will be developed. The amplitude of PD signal captured by the Rogowski coil due to the leaning of a pine tree on CC line at a distance of 3.5 km is less than 1 mV. It is quite possible to detect PD signals beyond 4 km distance from the Rogowski coil, provided there are a few trees leaning on the line or the knife scratches are impressed on the CC insulation due to leaning of tree. As the PD pulse is propagating in both directions from the source, it is suggested to monitor 3.5-7 km CC line using one Rogowski coil when deploying several sensors to monitor the full length of the line. Automatic detection of the falling trees will reduce visual inspection work after storms and it will improve reliability and safety of the distribution system. The proposed on-line PD monitoring system can be planned to be integrated into the distribution automation system in order to reduce the overall costs of the CC lines.

The on-line/on-site PD measurements are strongly influenced by external interferences. The PD signal is non-stationary and can not be processed using Fourier analysis. The WT techniques can provide a powerful tool to detect transient PD signals obscured in very high levels of noise with multi-resolution analysis, keeping both the time and frequency

domain resolution. Through appropriate selection of the wavelet family and the number of decomposition levels, the wavelet analysis technique can effectively discriminate real PD pulses among external interferences for enhancing PD detection. The Daubechies wavelet family has almost all of the properties to analyze the fast transient and irregular PD pulses, therefore, it has been selected to de-noise the PD measurements in this research work.

## 8.2 Future developments

The PD magnitude caused by a leaning tree on a CC line in different environmental conditions has not been thoroughly investigated in this research; rather some preliminary tests have been performed to verify the occurrence of PD activity in a CC line due to leaning of pine trees on it. The measurements conducted in the laboratory environment show that PD magnitude due to the leaning of a single pine tree is around 3 nC; however, this magnitude may vary between 3-10 nC. This amount can vary depending upon the size, weight, and the species of the leaning tree. The variation of PD magnitude as a function of various environmental parameters should also be deeply investigated in order to detect the leaning trees on CC lines using the proposed technique.

The Rogowski coil used in this research work is not good for high frequency measurements beyond 5 MHz. Therefore, a higher bandwidth Rogowski coil should be constructed for the real time analysis of PD signals produced by falling trees on CC overhead distribution lines. The PD measurements have only been taken in the laboratory; however, in the next stage of this work, this concept should be verified in a real system environment. In addition, the WT method should be implemented practically in a real system to get more stable and reliable PD detection results.

The effect of snow on the wave propagation characteristics of the bare conductor has already been investigated. The effect of snow on the wave propagation characteristics of a CC line has not been taken into account in the present work. It would be interesting to consider this factor and developing a theoretical model of the CC line including the effect of snow on it.

The measurements are taken using a wired Rogowski coil, which can be converted into a wireless sensor in the future. Due to limited computation capacity and energy constraints in wireless sensors, signal processing techniques can not be implemented as is possible in the case of the wired Rogowski coil. We must collect PD energy over a long period of time at a specific bandwidth. This PD energy will be sensed by the sensor to detect the intensity of PDs.

An on-line single-phase ATP model of the PD measuring system has been developed in this research work. However, it would be more practical and demanding if an on-line three-phase PD measuring system can be modeled; thus investigating the PD wave propagation in an integral network to analyze and resolve the real problems faced by local utilities. With those results, we would have the basis to develop requirements for wireless sensors used in this specific application. Wireless technology is fairly

inexpensive and it can be integrated into modern protection relays and to the distribution automation systems for detecting falling trees on CC lines. The proposed system will improve the safety of CC lines and make them more attractive to utilities due to reduced maintenance costs and visual inspection work.



## References

- [1] H. Lehtinen, I. Lehtinen, and A. Hinkkuri, "Research on Covered Medium-Voltage Overhead Lines in Finland", *CIREC 1989*, pp.179-184.
- [2] S. Hanninen, M. Lehtonen, and T. Hakola, "Earth Faults and Related Disturbances in Distribution Networks", *IEE Proceedings on Generation, Transmission, and Distribution*, vol. 149, No. 3, May 2002, pp.283-288.
- [3] M. Aro, J. Seppälä, and M. Toikka, "PAS-johtoon syntyneen vian ilmaisemismahdollisuudet sähköasemalla (The possibilities of detecting CC line faults at substations)", *Research report (in Finnish), Helsinki University of Technology*, Espoo, 1991, pp.24-52.
- [4] K. Noponen, I. Lehtinen, and A. Hinkkuri, "On the Design and Experience with High Voltage Covered Conductor System", *Distribution 2000 Conference*, Melbourne, Australia, November 9-12, 1993.
- [5] T. Yamashita, H. Matsuo, and H. Oshima, "The Characteristics of the Surface Discharge on the Covered Conductor for Distribution Systems", *4<sup>th</sup> International Conference on Properties and Applications of Dielectric Materials*, Brisbane, Australia, July 3-8, 1994.
- [6] B. Hart, "HV Overhead Line – The Scandinavian Experience" *Power Engineering Journal*, Vol. 8, Issue 3, June 1994, pp.119-123.
- [7] L. Voldhaug and C. Robertson, "MV Overhead Line using XLPE Covered Conductors – Scandinavian Experience and NORWEB Developments" *IEE Colloquium on review of options for overhead rural distribution*, UK, March 2, 1995.
- [8] W. Pinheiro, E. E. Nachvalger, J. J. S. Oliveira, L. E. Caron, A. Ruvolo F., A. F. Castro, R. M. Faria, R. B. L. Oliveira, E. A. T. Dirani, F. J. Fonseca, and A. M. Andrade, "Study of Polymeric Material Characteristics on Covered Conductors used in Brazil", *1996 IEEE Annual Report – Conference on Electrical Insulation and Dielectric Phenomena*, San Francisco, October 20-23, 1996, pp.416-419.
- [9] Y. Ojala, T. Leskinen, M. Lehtinen, and A. Hinkkuri "110 kV Overhead Transmission Line with Covered Conductors", *CIGRE 1998*, Paris.
- [10] W. Panosch, K. Schongrundner, and K. Kominek, "20 kV Overhead Lines with Covered Conductors", *CIREC 2001, IEE Conference Publication No. 482*, 18-21 June 2001.
- [11] J. Brunnsberg, *Second Forest – SAX Project Report*, September 2003, <http://www.forest-sax.com/>.
- [12] J. Pihler and I. Ticar, "Design of Systems of Covered Overhead Conductors by Means of Electric Field Calculation", *IEEE Transactions on Power Delivery*, Vol. 20, No. 2, April 2005, pp.807-814.

- 
- [13] *Accessories for Medium Voltage Distribution Networks – Ensto Overhead*, a report by Utility Networks, Ensto Sekko Oy, Finland, 2006.
- [14] W. Skomudek, “Computer Analysis of Over voltage Hazard due to Lightning Discharges in Medium Voltage Overhead Lines with Covered Conductors”, *Journal of Electrical Engineering*, Vol. 55, No. 5-6, pp.161-164,2004.
- [15] I. Ticar, J. Pihler, O. Bíró, and Kurt Preis, “Partial Discharges in Insulation of Medium Voltage Systems”, *The international Journal for Computation and Mathematics in Electrical and Electronics Engineering*, Vol. 20, No.2, 2001, pp.473-481.
- [16] T. Babnik, R. K. Aggarwal, P. J. Moore, and Z. D. Wang, “Radio Frequency Measurement of Different Discharges”, *IEEE PowerTech Conference*, Bologna, Italy, June 23-26, 2003.
- [17] P. Heine, J. Pitkänen, and M. Lehtonen, “Voltage Sag Characteristics of Covered Conductor Feeders”, *38<sup>th</sup> International Universities Power Engineering Conference (UPEC 2003)*, Thessaloniki, Greece, September 1-3, 2003.
- [18] D. König and R. Y. Narayana, *Partial Discharges in Power Apparatus*, Berlin: Vde-Verlag GmbH, 1993. 316p.
- [19] G. C. Stone, “The Use of Partial Discharge Measurements to Asses the Condition of Rotating Machine Insulation”, *IEEE Electrical Insulation Magazine*, Vol. 12, No. 4, July-August 1996.
- [20] E. Gulski, B. R. Hammerling, F. J. Wester, J. J. Smit, E. Groot, and P. Schikarski, “Insulation Condition Assessment of Medium Voltage Power Cables using On-site PD Detection and Analysis Techniques”, *CIGRE 2001 Conference Publication*.
- [21] G. Kane, B. Lease, and A. Golubev, “Practical Experiences of On-line Partial Discharge Measurements on a Variety of Medium-voltage Electrical Equipment”, *IEEE Transaction on Industry Applications*, Vol. 35, No. 6, November-December 1999.
- [22] K. Fukunaga, M. Tan, H. Takehana, T. Takahashi, and S. Yoshida, “New Partial Discharge Detection Method for Live Power Cable Systems”, *3<sup>rd</sup> International Conference on Properties and Applications of Dielectric Materials*, Tokyo, Japan, July 8-12, 1991, pp.1218-1220.
- [23] H. Maekawa, T. Ito, and E. Yajima, “GIS Monitoring Sensors”, *4<sup>th</sup> International Conference on Advances in Power System Control, Operation and Management (APSCOM-97)*, Hong Kong, November 1997, pp.773-778.
- [24] P. C. J. M. van der Wielen, J. Veen, P. A. A. F. Wouters, and E. F. Steennis, “Sensors for On-line PD Detection in MV Power Cables and their Locations in Substations”, *7<sup>th</sup> International Conference on Properties and Applications of Dielectric Materials*, Nagoya, June 1-5, 2003.

- 
- [25] P. C. J. M. van der Wielen, P. A. A. F. Wouters, J. Veen and D. M. van Aartrijk, "Synchronization of On-line PD Detection and Localization Setups using Pulse Injection", *7<sup>th</sup> International Conference on Properties and Applications of Dielectric Materials*, Nagoya, June 1-5, 2003.
- [26] K. Nousiainen and K. Tuominen, "Instrument Transformers as Sensors in Partial Discharge Measurements", *Nordic Insulation Symposium*, Stockholm, Sweden, 2001.
- [27] P. Pakonen, V. Latva-Pukkila, M. Björkqvist, and T. Hakola, "Condition Monitoring and Fault Detection of Medium Voltage Covered Conductor Lines", *4<sup>th</sup> Nordic Distribution Automation Conference (NORDAC)*, Trondheim, Norway, May 22-23, 2000.
- [28] P. Pakonen, "Detection of Incipient Tree Faults on High Voltage Covered Conductor Lines", *Doctoral dissertation, Tampere University of Technology (TUT)*, Tampere, Finland, November 2007.
- [29] K. Nousiainen and P. Nevalainen, "Implementation of Partial Discharge Measurements in a Noisy Environment", TTKK, 2002.
- [30] L. A. Kojovic, "Rogowski Coil Transient Performance and ATP Simulations for Applications in Protective Relaying", *International Conference on Power Systems Transients (IPST'05)*, Montreal, Canada, June 19-23, 2005.
- [31] D. A. Ward and J. La T. Exon, "Using Rogowski Coils for Transient Current Measurements", *Engineering Science and Education Journal*, June 1993.
- [32] P. Heine, "Voltage Sags in Power Distribution Networks", *Doctoral dissertation, Helsinki University of Technology (TKK)*, Espoo, Finland, November 2005.
- [33] M. Washino, A. Fukuyama, K. Kito, and K. Kato, "Development of Current Limiting Arcing Horn for Prevention of Lightning Faults on Distribution Lines", *IEEE Transactions on Power Delivery*, Vol. 3, No. 1, January 1988, pp.138-152.
- [34] G. M. Hashmi, R. J. Millar, and M. Lehtonen, "Cable Ampacity Analysis for MV Underground Networks Laid in Thermally Unstable Environment", *International Conference on Electrical and Control Technologies, (ECT07)*, Kaunas, Lithuania, May 3-4, 2007.
- [35] F. Shahina, A. M. Kashtiban, K. R. Milani, and M. T. Haque, "Insulation Effects and Characteristics of XLPE Covered Overhead Conductors in Low and Medium Voltage Power Distribution Systems in Iran", *IEEE International Symposium on Electrical Insulation*, Toronto, Canada, 11-14 June 2006.
- [36] S. A. Boggs and J. Densley, "Fundamentals of Partial Discharge in the Context of Field Cable Testing", *IEEE Electrical Insulation Magazine*, Vol. 16, No.5, September-October 2000, pp.13-18.
- [37] F. H. Kreuger, *Partial Discharge Detection in High-Voltage Equipment*, Butterworths, 1989.
- [38] R. Bartnikas and E. J. MsMahon (eds.), *Engineering Dielectrics Volume 1: Corona Measurement and Interpretation*, ASTM STP 669, 1979.

- 
- [39] E. Kuffel, W. S. Zaengl, and J. Kuffel, *High Voltage Engineering: Fundamentals*: 2<sup>nd</sup> ed. Newnes, Butterworth-Heinemann, 2000.
- [40] H. Edin, "Partial Discharge Studied with Variable Frequency of the Applied Voltages", *Doctoral dissertation, Kungl Tekniska Hogskolan (KTH)*, Stockholm, Sweden, 2001.
- [41] Y. Qiu, A. Sun, and Z. Zhang, "Factors Affecting Partial Discharges in SF<sub>6</sub> Gas Impregnated Polymer Film Insulation", *2<sup>nd</sup> International Conference on Properties and Applications of Dielectric Materials*, Beijing, China, September 12-16, 1988.
- [42] F.H. Kreuger, M.G. Wezelenburg, A.G. Wiemer, and W.A. Sonneveld, "Partial Discharge Part XVIII: Errors in the Location of Partial Discharges in High Voltage Solid Dielectric Cables", *IEEE Electrical Insulation Magazine*, Vol. 9, No.6, November-December 1993, pp.15-25.
- [43] P. J. Moore, I. Portugues, and I. A. Glover, "A Non-Intrusive Partial Discharge Measurement System based on RF Technology" *2003 IEEE Power Engineering Society General Meeting*, Toronto, Canada, 13-17 July 2003.
- [44] G. C. Stone and S. A. Boggs, "Propagation of Partial Discharge Pulses in Shielded Power Cable", *Annual report of the conference on electrical insulation and dielectric phenomenon*, National Academy of Science, Washington, DC, 1982, pp. 275-280.
- [45] S. A. Boggs and G. C. Stone, "Fundamental Limitations to the Measurement of Corona and Partial Discharge," *1981 Annual Report of the Conference on Electrical Insulation and Dielectric Phenomena and reprinted in the IEEE Trans. EI-17*, April, 1982, p.143.
- [46] S. Sakaguchi and M. Oyama, "Application of Maxwell Solvers to PD Propagation-Part III: PD Propagation in GIS", *IEEE Electrical Insulation Magazine*, Vol. 19, No. 1, 2003, pp.6-12.
- [47] IEC60270, *High-Voltage Test Techniques – Partial Discharge Measurements, CEI/IEC 60270, third edition*, 2000-12.
- [48] N. H. Ahmed and N. N. Srinivas, "On-line Partial Discharge Detection in Cables", *IEEE Transaction on Dielectrics and Electrical Insulation*, Vol. 5, N0.2, April 1998, pp.181-188.
- [49] P. Pakonen and V. Latva-Pukkila, "On-line Partial Discharge Measurements on Covered Conductor Lines", *Nordic and Baltic Workshop on Power Systems*, Tampere, Finland, February 4-5, 2002.
- [50] B. A. Lloyd, S. R. Campbell, and G. C. Stone, "Continuous On-line Partial Discharge Monitoring of Generator Stator Windings", *IEEE Transaction on Energy Conservation*, Vol. 14, No. 4, December 1999.
- [51] G. Xiaohua, L. Jingsheng, Z. Mingjun, and Y. Miaoyuan, "Improved Performance Rogowski Coils for Power System" *Transmission and Distribution Conference and Exposition, 2003 IEEE PES*, Wuhan, China, 7-12 September 2003.

- 
- [52] D. A. Ward and J. L. T. Exon, "Experience with using Rogowski Coils for Transient Measurements", *Pulsed Power Technology, IEE Colloquium*, February 20, 1992, pp.61-64.
- [53] Z. Mingjuan, D. J. Perreault, and V. Caliskan, "Design and Evaluation of an Active Ripple Filter with Rogowski Coil Current Sensing", *Power Electronics Specialists Conference, PESC99, 30<sup>th</sup> Annual IEEE*, Vol. 2, 1999, pp.874 -880.
- [54] L. A. Kojovic, "Rogowski Coil Suit Relay Protection and Measurement of Power Systems", *IEEE Computer Applications in Power*, Vol. 10, No. 3, July 1988, pp.47-52.
- [55] M. Argueso, G. Robles, and J. Sanz, "Implementation of Rogowski coil for the Measurement of Partial Discharges", *American Institute of Physics, Review of Scientific Instruments*, 76, 065107, June 2005.
- [56] Instruction sheet, FLUKE i2000flex, *Flexible AC Current Probe*.
- [57] G. M. Hashmi, M. Nordman, and M. Lehtonen, "A Partial Discharge Detection Concept for Wireless Sensors in Covered-Conductors Distribution System", *Europe's Premier Conference on Electrical Insulation (INSUCON2006)*, Birmingham, UK, May 24-26, 2006.
- [58] P. C. J. M. van der Wielen, E. F. Steenis, and P. A. A. F. Wouters, "Fundamental Aspects of Excitation and Propagation of On-line Partial Discharge Signals in Three-phase Medium Voltage Cable Systems", *IEEE Transactions on Dielectrics and Electrical Insulation*, Vol. 10, No. 4, August 2003.
- [59] Q. Shaozhen and S. Birlasekaran, "The Study of PD Propagation Phenomenon in Power Network", *IEEE Transactions on Power Delivery*, Vol. 21, No. 3, July 2006.
- [60] G. M. Hashmi, "Determination of Propagation Constants of Three Phase Medium Voltage Cables using Time Domain Reflectometry", *Master thesis work, Kungl Tekniska Hogskolan (KTH)*, Stockholm, Sweden, 2001.
- [61] P. C. J. M. van der Wielen, J. Veen, and P. A. A. F. Wouters, "Evaluation of Different Types of Sensors and Their Positioning for On-line PD Detection and Localisation in Distribution Cables", *Nordic Insulation Symposium*, Tampere, Finland, June 11-13, 2003, pp.367-374.
- [62] W. L. Weeks and Y.M. Diao, "Wave Propagation Characteristics in Underground Power Cable", *IEEE Transaction on Power Apparatus and Systems*, Vol. 103, No. 10, pp.2816-2824, Oct. 1984.
- [63] D. K. Cheng, *Field and Wave Electromagnetics, 2<sup>nd</sup> edition*, Addison Wesley Publishing Company, Inc., 1989.
- [64] A. Ametani, Y. Kasai, J. Sawada, A. Mochizuki, and T. Yamada, "Frequency-Dependent Impedance of Vertical Conductors and a Multiconductor Tower Model", *IEE Proceedings on Generation, Transmission, and Distribution*, Vol. 141, No. 4, July 1994.

- 
- [65] R. Papazyan, "Techniques for Localization of Insulation Degradation along Medium-Voltage Power Cables", *Doctoral dissertation, The Royal Institute of Technology(KTH)*, Stockholm, Sweden, 2005.
- [66] J. W. Cooley, and J. W. Tukey, "An Algorithm for the Machine Computation of the Complex Fourier Series" *Mathematics of Computation*, Vol. 19, pp.297-301, April 1965.
- [67] D. K. Cheng, *Fundamental of Engineering Electromagnetics*, Addison-Wesley Publishing, ISBN 0-201-56611-7.
- [68] H. Meng, S. Chen, Y. L. Guan, C. L. Law, P. L. So, E. Gunawan, and T. T. Lie, "A Transmission Line Model for High-Frequency Power Line Communication Channel", *International Conference on Power System Technology (PowerCon 2002)*, Kunming, China, October 13-17, 2002, pp.1290-1295.
- [69] R. Villefrance, J. T. Holboll, and M. Henriksen, "Estimation of Medium Voltage Cable Parameters for PD-Detection", *IEEE International Symposium on Electrical Insulation*, Arlington, Virginia, USA. June 7-10, 1998.
- [70] S. A. Boggs, A. Pathak, and P. Walker, "Partial Discharge Part XXII; High Frequency Attenuation in Shielded Solid Dielectric Power Cable and Implications thereof for PD Location", *IEEE Electrical Insulation Magazine*, Vol. 12, No. 1, January-February 1996, pp.9-16.
- [71] G. M. Hashmi, M. Nordman, and M. Lehtonen, "Determination of the Wave Propagation Characteristics of Covered-Conductors Distribution System for On-line Partial Discharge Detection", *Modern Electric Power Systems (MEPS06 conference)*, Wroclaw, Poland, September 6-8, 2006.
- [72] R. Papazyan and R. Eriksson, "Calibration for Time Domain Propagation Constant Measurement on Power Cables", *IEEE Transaction on Instrumentation and Measurement, Special Issue*, September 2002.
- [73] A. Ametani, "A General Formulation of Impedance and Admittance of Cables", *IEEE Transactions on Power Apparatus and Systems*, Vol. PAS-99, No. 3, May-June 1980, pp.902-910.
- [74] A. Ametani, Y. Miyamoto, and N. Nagaoka, "Semiconducting Layer Impedance and its Effect on Cable Wave-Propagation and Transient Characteristics", *IEEE Transactions on Power Delivery*, Vol. 19, No. 4, October 2004, pp.1523-1531.
- [75] G. M. Hashmi, R. Papazyan, and M. Lehtonen, "Comparing Wave Propagation Characteristics of MV XLPE Cable and Covered-Conductor Overhead Line using Time Domain Reflectometry Technique" *IEEE International Conference on Electrical Engineering (ICEE07)*, University of Engineering and Technology (UET), Lahore, Pakistan, April 11-12, 2007.
- [76] G. Mugala, R. Papazyan, and P. Navok, "High Frequency Characteristics of Medium Voltage Cables using Time Domain Reflectometry Techniques", *17<sup>th</sup> Nordic Insulation Symposium*, Stockholm, Sweden, June 11-13, 2001, pp.211-218.

- 
- [77] H. W. Dommel, “*Electromagnetic Transients Program (EMTP) – Rule Book*”, Oregon, 1984.
- [78] G. Mugala and R. Eriksson, “High Frequency Characteristics of a Shielded Medium Voltage XLPE cable”, in *CEIDP Annu. Rep.*, 2001, pp.132-136.
- [79] A. Ametani, *Distributed-Parameter Circuit Theory*, Corona Pub. Co., Tokyo, 1990 (in Japanese).
- [80] S. A. Schelkunoff, “The Electromagnetic Theory of Coaxial Transmission Lines and Cylindrical Shields”, *Bell System Technical Journal*, Vol. 13, 1934, pp.532-579.
- [81] J. R. Carson, “Wave Propagation in Overhead Wires with Ground Return”, *Bell System Technical Journal*, Vol. 5, 1926, pp.539-554.
- [82] E. D. Sunde, *Earth Conduction Effects in Transmission Systems*, Dover, N.Y., 1948.
- [83] F. Rachidi, C. A. Nucci, and M. Ianoz, “Transient Analysis of Multiconductor Lines above a Lossy Ground”, *IEEE Transaction on Power Delivery*, Vol. 14, No. 1, January 1999.
- [84] ATP – EMTP Rule Book, Canadian – American EMTP User Group, 1997.
- [85] ATPDRAW version 3, User Manual, TR A4389, EFI, Norway, 1996.
- [86] L.M Wedepohl and D.J. Wilcox, “Transient Analysis of Underground Power Transmission Systems”, *IEE Proceedings*, Vol. 120, No. 2, February 1973, pp.253-260.
- [87] G. M. Hashmi and M. Lehtonen, “Covered-Conductor Overhead Distribution Line Modeling and Experimental Verification for Determining its Line Characteristics”, *IEEE PES PowerAfrica2007 Conference and Exposition*, Johannesburg, South Africa, July 16-20, 2007.
- [88] A. Ametani, R. Koide, and N. Nagaoka, “Effect of Snow on Wave Propagation Characteristics on an Overhead Single Conductor”, *ICEE 1999 Proc., Paper E2-03*, Hong Kong, July 1999.
- [89] W. F. Ray and C. R. Hewson, “High Performance Rogowski Current Transducers”, *Industry Applications Conference*, Rome, Italy, October 8-12, 2000.
- [90] J. D. Ramboz, “Machinable Rogowski Coil, Design, and Calibration”, *IEEE Transaction on Instrumentation and Measurement*, Vol. 45, No. 2, April 1996.
- [91] D. G. Pellinen, M. S. Di Capua, S. E. Sampayan, H. Gerbracht, and M. Wang, “Rogowski coil for Measuring Fast, High-Level Pulsed Currents”, *American Institute of Physics, Review of Scientific Instruments*, Vol. 51, Issue 11, November 1980, pp.1535-1540.
- [92] J. Cooper, “On the High-Frequency Response of a Rogowski coil”, *Plasma Physics (Journal of the Nuclear Energy Part: C)*, Vol. 5, 1963, pp.285-289.

- 
- [93] G. M. Hashmi, M. Lehtonen, and A. Elhaffar, "Modeling of Rogowski Coil for On-line PD Monitoring in Covered-Conductor Overhead Distribution Networks", *19<sup>th</sup> International Conference on Electricity Distribution (CIRED07)*, Vienna, Austria, May 21-24, 2007.
- [94] G. M. Hashmi and M. Lehtonen, "On-line PD Measuring System Modeling and Experimental Verification for Covered-Conductor Overhead Distribution Lines", *IEEE Mediterranean Conference on Control and Automation (MED07)*, Athens, Greece, June 27-29, 2007.
- [95] G. M. Hashmi and M. Lehtonen, "Effects of Rogowski Coil and Covered-Conductor Parameters on the Performance of PD Measurements in Overhead Distribution Networks", *16<sup>th</sup> Power Systems Computation Conference (PSCC08)*, Glasgow, UK, July 14-18, 2008.
- [96] M. Nordman, "An Architecture for Wireless Sensors in Distributed Management of Electrical Distribution Systems", *Doctoral dissertation, Helsinki University of Technology (TKK)*, Finland, November 2004.
- [97] T. Brooks, "Wireless Technology for Industrial Sensor and Control Networks", *Sensors for Industry Conference, Sicon'01*, Rosemount, Illinois, USA, 5-7 November 2001.
- [98] E. Antila, "Developing Distribution Automation in Medium Voltage Networks", *Master's Thesis, Helsinki University of Technology (TKK)*, Finland, February 2003.
- [99] G. Shamble, J. Schutz, and C. Apneseth, "Novel Wireless Power Supply System for Wireless Communication Devices in Industrial Automation Systems", *IEEE Annual Conference of the Industrial Electronics Society (IECON02)*, Sevilla, Spain, 5-8 November, 2002.
- [100] J. Ahola, "Applicability of Power-line Communications to Data Transfer of On-line Condition Monitoring of Electrical Drives", *Doctoral dissertation, Lappeenranta University of Technology (LUT)*, Finland, 2003, ISBN: 951-764-783-2.
- [101] A. Sinha and A. Chandrakasan, "Dynamic Power Management in Wireless Sensor Networks", *IEEE Design & Test of Computers*, Vol. 18, March-April 2001.
- [102] D. Wentzloff, B. Calhoun, R. Min, A. Wang, N. Ickes, and A. Chandrakasan, "Design Considerations for Next Generation Wireless Power-aware Microsensor Nodes", *International Conference on VLSI Design*, Mumbai, India, January 2004.
- [103] G. C. Stone, "Partial Discharge Part XXV; Calibration of PD Measurements for Motor and Generator Windings – why it can't be done", *IEEE Electrical Insulation Magazine*, Vol. 14, No. 1, January-February 1998, pp.9-12.
- [104] X. Zhou, C. Zhou and I. J. Kemp, "An Improved Methodology for Application of Wavelet Transform to Partial Discharge Measurement De-noising" *IEEE Transaction on Dielectrics and Electrical Insulation*, Vol. 12, No. 3, June 2005, pp.586-594.

- 
- [105] U. Kopf and K. Feser, "Rejection of Narrow-band Noise and Repetitive Pulses in On-site PD Measurement", *IEEE Transaction on Dielectrics and Electrical Insulation*, Vol. 2, 1995, pp.1166-1179.
- [106] Z. K. Sher, D. H. Zhu, X. H. Jin, and K. X. Tan, "A New Technique for On-line Partial Discharge Monitoring", *IEEE Transaction on Dielectrics and Electrical Insulation*, Vol. 2, 1995, pp.700-707.
- [107] I. Shim, J. J. Soraghan, and W. H. Siew, "Detection of PD Utilizing Digital Signal Processing Methods Part 3: Open-Loop Noise Reduction", *IEEE Electrical Insulation Magazine*, Vol. 17. No. 1, 2001, pp.6-13.
- [108] G. Strang and T. Nguyen, *Wavelet and Filter Banks*, Wellesley-Cambridge Press, 1996.
- [109] X. Ma, C. Zhou, and I. J. Kemp, "Automated Wavelet Selection and Thresholding for PD Detection", *IEEE Electrical Insulation Magazine*, Vol. 18. No. 2, 2002, pp.37-45.
- [110] H. Zhang, T. R. Blackburn, B. T. Phung, and M. S. Naderi, "A Novel Wavelet De-noising Method for On-site PD Measurements on HV Cables", *International Symposium on Electrical Insulating Materials*, Kitakyushu, Japan, June 5-9, 2005, pp.845-848.
- [111] G. M. Hashmi and M. Lehtonen, "On-line PD Detection for Condition Monitoring of Covered-Conductor Overhead Distribution Networks – A Literature Survey", *IEEE International Conference on Electrical Engineering (ICEE08)*, University of Engineering and Technology (UET), Lahore, Pakistan, March 25-26, 2008.
- [112] V. Nagesh and B. LGururaj, "Evaluation of Digital Filters for Rejecting Discrete Spectral Interference in On-site PD Measurement", *IEEE Transactions on Electrical Insulation* Vol.28, No.1, February 1993, pp.73-85.
- [113] L. Satish and B. Nazneen, "Wavelet-based De-noising of Partial Discharge Signals Buried in Excessive Noise and Interference", *IEEE Transactions on Dielectrics and Electrical Insulation*, Vol.10, No. 2, April 2003, pp.354-367.
- [114] H. Zhang, T. R. Blackburn, B. T. Phung, and Z. Liu, "Application of Signal Processing Techniques to On-line Partial Discharge Detection in Cables", *International Conference on Power Systems Technology (POWERCON04)*, Singapore, November 21-24, 2004.
- [115] P. Wang, P. L. Lewin, Y. Tian, S. J. Sutton, and S. G. Swingler, "Application of Wavelet-based De-noising to On-line Measurement of Partial Discharges", *International Conference on Solid Dielectrics*, Toulouse, France, July 5-9, 2004.
- [116] X. Ma, C. Zhou, and I. J. Kemp, "Interpretation of Wavelet Analysis and Its Application in Partial Discharge Detection", *IEEE Transactions on Dielectrics and Electrical Insulation*, Vol.9, No.3, June 2002, pp.446-457.
- [117] R. K. Young, *Wavelet Theory and its Applications*, Pennsylvania State University, Kluwer Academic Publishers, 1993.

- 
- [118] N. I. Elkalashy, "Modeling and Detection of High Impedance Arcing Fault in Medium Voltage Networks", *Doctoral dissertation, Helsinki University of Technology (TKK)*, Finland, November 2007.
- [119] C. H. Lee, Y. J. Wang, and W. L. Huang, "A Literature Survey of Wavelets in Power Engineering Applications", *Proc. Natl. Sci. Counc. ROC (A)*, Vol. 24, No. 4, 2000, pp.249-258.
- [120] D. Charnock, "Electromagnetic Interference Coupling Between Power Cables and Sensitive Circuits", *IEEE Transactions on Power Delivery*, Vol. 20, No. 2, April 2005, pp.668-673.
- [121] G. M. Hashmi, M. Lehtonen, and M. Nordman, "Application of Wavelet Transform to De-noise Partial Discharge Signals in Covered-Conductor Distribution Networks", *XVI-th International Conference on Electromagnetic Disturbances (EMD06)*, Kaunas, Lithuania, September 27-29, 2006.
- [122] G. M. Hashmi, M. Lehtonen, R. A. Jabbar, and S. A. Qureshi, "Application of Wavelet-based De-noising of Partial Discharge Signals in MV Covered-Conductor Networks", *Australian Universities Power Engineering Conference (AUPEC06)*, Melbourne, Victoria, Australia, December 10-13, 2006.
- [123] H. Zhang, T. R. Blackburn, B. T. Phung, J. Hanlon, and P. Taylor, "A Novel On-line Differential Technique for Partial Discharge Measurement of MV/HV Power Cables", *8<sup>th</sup> International Conference on Properties and Applications of Dielectric Materials*, Bali, Indonesia, June 2006.
- [124] H. Zhang, T. R. Blackburn, B. T. Phung, J. Hanlon, and P. Taylor, "A Software Based Differential Technique of Partial Discharge Detection", *Australasian University Power Engineering Conference (AUPEC05)*, Hobart, Australia, 2005.



ISBN 978-951-22-9446-6  
ISBN 978-951-22-9447-3 (PDF)  
ISSN 1795-2239  
ISSN 1795-4584 (PDF)